Doctoral Dissertation

Studies on C–H Functionalization by Rhodium(III) Complexes Bearing Redox-active Ligands

Daiki Fujita

January 2020

Department of Material and Life Science
Division of Advanced Science and Biotechnology
Graduate School of Engineering
Osaka University

Contents

General Introduction

C–H Functionalization by Late-transition Metal Complexes

C–H functionalization by transition metal complexes is a promising method for efficient synthesis of high-valued organic compounds from abundant hydrocarbons (R-H). The C–H functionalization by transition metal complexes can be divided into two classes based on the mechanism for C–H bond cleavage: (a) inner sphere mechanism and (b) outer sphere mechanism (Scheme 1).[1,2] In the inner sphere mechanism, the metal center directly participates in the C–H bond cleavage of R–H to form the intermediate with the σ-metal-carbon (σ-M–C) bond. By further coordination of the reactant (X) to the metal center and successive reductive elimination, the functionalized product (R–XH) is yielded (Scheme 1a). The inner sphere C–H functionalization by late-transition metal complexes consists of two-electron redox processes, namely, oxidative addition and reductive elimination.[3-5] The metal complexes which enable two-electron redox reactions between the metal centers and R–H substrates are suitable for the inner sphere C–H functionalization and noble metal elements such as Pd, Pt, and Rh have been chosen as the metal center. As the results, numerous examples of stoichiometric and catalytic inner sphere C–H functionalization by using such metal complexes have been reported in the field of organometallic chemistry.[1-16] On the other hand, in the outer sphere mechanism, the metal centers do not directly participate in the C–H bond cleavage. However, the metal complexes can be changed to the active species, such as high-valent metal-oxido (M=O) or -imido (M=NR') species, for the C–H bond cleavage by reactions with the corresponding oxidants. The subsequent C–H bond cleavage by the active species and C–X bond formation proceeds for yielding the products, R–OH and R–NHR' (Scheme 1b). This outer sphere mechanism is found in C–H hydroxylation by cytochrome P450 and models of heme and non-heme metal enzymes.[17-22]

The inner sphere mechanism is dominant to C–H functionalization using rhodium(III) complexes.[23-25] In general, rhodium complexes show two-electron redox reactivity, interchanging between +I and +III oxidation states. However, the ligands for stabilizing the +I oxidation state (e. g. carbon monoxide, alkenes, phosphines, and thiolates) are readily oxidized by the reactants for the outer sphere C–H functionalization. In addition, rhodium complexes in +IV, and +V oxidation states are unstable unless the high-valent rhodium center can be stabilized by strong π-donation from 2-(2-pyridyl)-2-propanoate ligand.[26] Due to these drawbacks, rhodium(III) complexes are not suitable to the catalysts for the outer sphere C–H functionalization .

Scheme 1. (a) Inner sphere mechanism and (b) outer sphere mechanism of C–H functionalization by transition metal complexes.

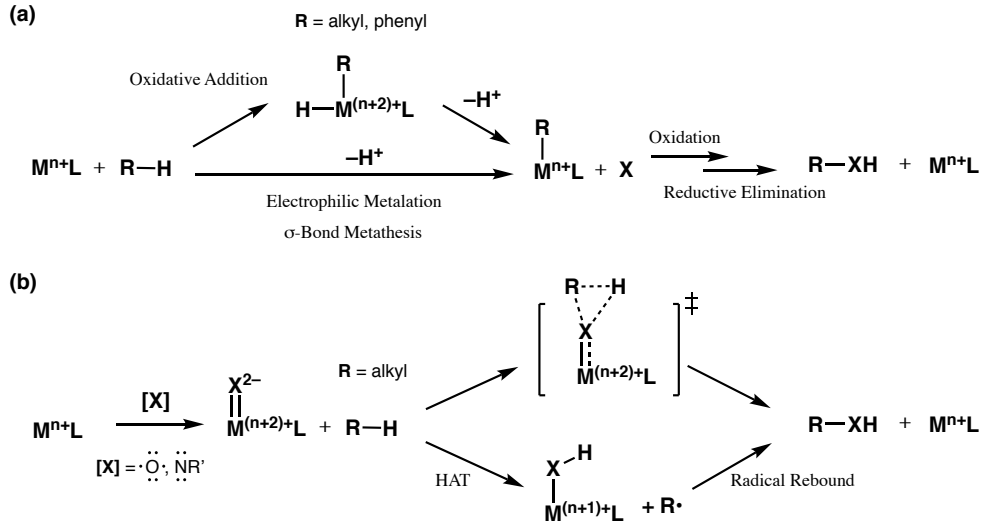

Redox-active Ligands as Electron Reservoirs

Some π-conjugated molecules have suitable π-orbitals in energy for redox reactions. When such molecules coordinate to a metal center, they can work as redox-active ligands, using the filled or empty π-orbitals.[27-35] Since the discovery of nickel-dithiolene systems,[36,37] various core structures of redox-active ligands have been prepared, e.g. dithiolene,[38–40] α-diimine,[41,42] β-diketiminate,[41-44] catechol derivatives,[45-49] diiminopyridine,[50-52] salen,[53-59] porphyrin,[60-64] and others (Figure 1).[65-70]

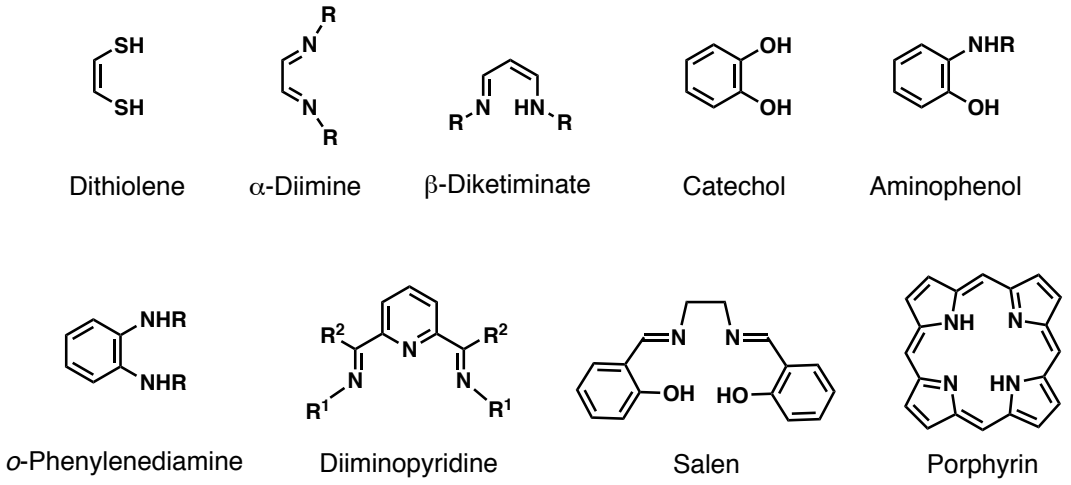

Figure 1. Well known redox-active ligands.

In recent years, stoichiometric and catalytic C–H activation reactions by metal complexes bearing redox-active ligands have been reported.[71-75] In these reactions, redox-active ligands play a role as electron reservoir for the formation of the active species. However, these examples have been limited to hydrogen atom abstraction and intramolecular C–H amination.

In this thesis, the reaction behaviors of rhodium(III) complexes bearing redox-active ligands (Figure 2) in C(sp^3)–H amination and C(sp^2)–H iodination are investigated. These complexes show two-successive one-electron redox behavior (Scheme 2).

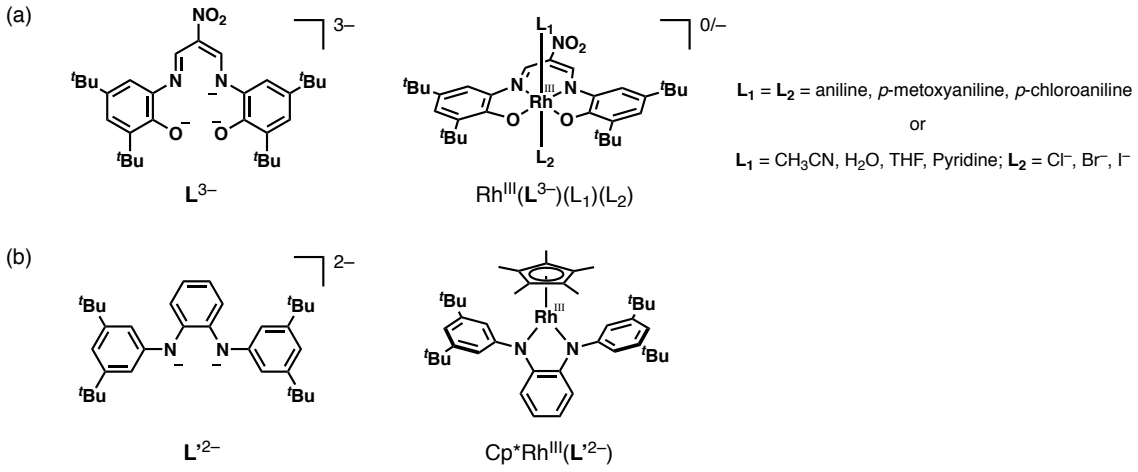

Figure 2. Rhodium(III) complexes bearing redox-active ligands studied in (a) chapter 1 and 2 (b) chapter 3 in this thesis.

Scheme 2. Redox behavior of the ligand moiety in the rhodium(III) complexes.

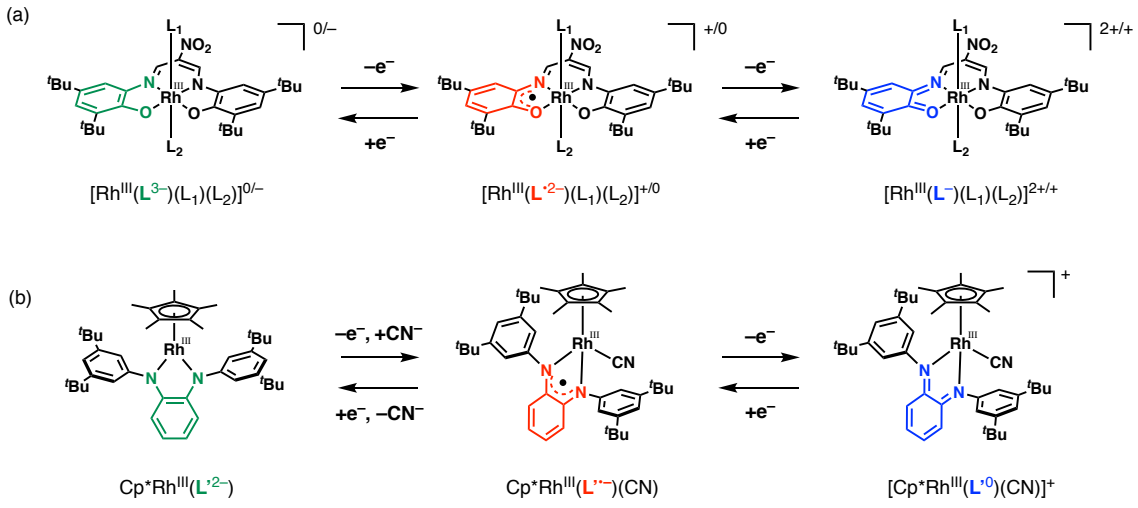

This thesis entitled “Studies on C–H Functionalization by Rhodium(III) Complexes Bearing Redox-active Ligands” consists of three chapters.

In chapter 1, the rhodium(III) complexes bearing a redox-active tetradentate ligand $\mathbf{L}^{3-}$ (Figure 2a) are synthesized and characterized. Intermolecular C(sp^3)–H amination of xanthene with tosyl azide catalyzed by the rhodium(III) complex is investigated, where mechanistic studies suggested that the reaction involves outer-sphere mechanism. The experimental and computational results show involvement of a ligand-based redox reaction in the C–H amination. This is the first example of catalytic intermolecular C–H amination via ligand-based redox.

In chapter 2, inner-sphere C(sp^2)–H activation of toluene by the rhodium(III) complex bearing the same ligand $\mathbf{L}^{3-}$ and the following iodination is investigated. Characterization of the rhodium(III) complex after the iodination show that one-electron oxidation of the ligand $\mathbf{L}^{3-}$ is involved in the iodination.

In chapter 3, the rhodium(III) complexes bearing phenylenediamido ($\mathbf{L'}^{2-}$), diiminobenzosemiquinonato ($\mathbf{L'}^{\bullet-}$), and diiminobenzoquinone ($\mathbf{L'}^{0}$) ligands are synthesized and characterized (Scheme 2b). The catalytic activity of these complexes in outer sphere intramolecular C(sp^3)–H amination of 2,4,6-triisopropyl-phenylsulfonylazide is examined. Among the three, the one-electron oxidized form showed the highest reactivity, suggesting the nitrene radical species $[Cp^*Rh^{III}\mathbf{L'}^{0}(RN^{\bullet-})]^{+}$ (R = 2,4,6-triisopropyl-phenylsulfonyl) is the key reactive intermediate. In this system, one-electron oxidized ligand enhances the coordination of external substrates to the metal center to increase the rate of amination reaction.

References

(1) Dick, A. R.; Sanford, M. S. *Tetrahedron*, **2006**, *62*, 2439–2463.

(2) Crabtree, R. H. *J. Chem. Soc. Dalton. Trans.*, **2001**, 2437–2450.

(3) Chen, X.; Engle, K. M.; Wang, D.-H.; Yu, J.-Q. *Angew. Chem. Int. Ed.*, **2009**, *48*, 5094–5115.

(4) Lyons, T. W.; Sanford, M. S. *Chem. Rev.*, **2010**, *110*, 1147–1169.

(5) Wencel-Delord, J.; Dröge, T.; Liu, F.; Glorius, F. *Chem. Soc. Rev.*, **2011**, *40*, 4740–4761.

(6) Shilov, A. E.; Shteinman, A. A. *Coord. Chem. Rev.*, **1977**, *24*, 97–143.

(7) Shilov, A. E.; Shul’pin, G. B. *Chem. Rev.*, **1997**, *97*, 2879–2932.

(8) Jia, C.; Kitamura, T.; Fujiwara, Y. *Acc. Chem. Res.*, **2001**, *34*, 633–639.

(9) Labinger, J. A.; Bercaw, J. E. *Nature*, **2002**, *417*, 507–514.

(10) Ritleng, V.; Sirlin, C.; Pfeffer, M. *Chem. Rev.*, **2002**, *102*, 1731–1769.

(11) Crebtree, R. H. *J. Organomet. Chem*., **2004**, *689*, 4083–4091.
(12) Periana, R. A.; Bhalla, G.; Tenn, W. J.; Young, K. J. H.; Liu, X. Y.; Mironov, O.; Jones, C. J.; Zaitdinnov, V. R. *J. Mol. Catal. A*., **2004**, *220*, 7–25.
(13) Jazzar, R.; Hitce, J.; Renaudat, A.; Sofack-Kreutzer, J.; Baudoin, O. *Chem. Eur. J*., **2010**, *16*, 2654–2672.
(14) Colby, D. A.; Bergman, R. G.; Ellman, J. A. *Chem. Rev*., **2010**, *110*, 624–655.
(15) Hashiguchi, B. G.; Bischof, S. M.; Konnick, M. M.; Periana, R. A. *Acc. Chem. Res.*, **2012**, *45*, 885–898.
(16) Gandeepan, P.; Müller, T.; Zell, D.; Cera, G.; Warratz, S.; Ackermann, L. *Chem. Rev*., **2019**, *119*, 2192–2452.
(17) de Montellano, P. R. O. *Chem. Rev.*, **2010**, *110*, 932–948.
(18) Lewis, J. C.; Coello, P. S.; Arnold, F. H. *Chem. Soc. Rev*., **2011**, *40*, 2003–2021.
(19) Che, C.-M.; Lo, V. K.-Y.; Zhou, C.-Y.; Huang, J.-S. *Chem. Soc. Rev.*, **2011**, *40*, 1950–1975.
(20) Lu, H.; Zhang, X. P. *Chem. Soc. Rev.*, **2011**, *40*, 1899–1909.
(21) Oloo, W. N.; Que, L. *Acc. Chem. Res.*, **2015**, *48*, 2612–2621.
(22) Singh, R.; Mukherjee, A. *ACS Catal.*, **2019**, *9*, 3604–3617.
(23) Colby, D. A.; Tsai, A. S.; Bergman, R. G.; Ellman, J. A. *Acc. Chem. Res.*, **2012**, *45*, 814–825.
(24) Song, G.; Wang, F.; Li, X. *Chem. Soc. Rev*., **2012**, *41*, 3651–3678.
(25) Qi, X.; Li, Y.; Bai, R.; Lan, Y. *Acc. Chem. Res.*, **2017**, *50*, 2799–2808.
(26) Sinha, S. B.; Shopov, D. Y.; Sharninghausen, L. S.; Vinyard, D. J.; Mercado, B. Q.; Brudwig, G. W.; Crabtree, R. H. *J. Am. Chem. Soc.*, **2015**, *137*, 15692–15695.
(27) Chirik, P. J.; Wieghardt, K. *Science*, **2010**, *327*, 794–795.
(28) Kaim. W. *Inorg. Chem*., **2011**, *50*, 9752–9765.
(29) Kaim, W.; *Eur. J. Inorg. Chem.*, **2012**, 343–348.
(30) van der Vlugt, J. I.; Reek, J. N. H. *Angew. Chem., Int. Ed.*, **2009**, 48, 8832–8846.
(31) Dzik, W. I.; van der Vlugt, J. I.; Reek, J. N. H.; de Bruin, B. *Angew. Chem., Int. Ed.*, **2011**, *50*, 3356–3358.
(32) van der Vlugt, J. I. *Eur. J. Inorg. Chem.*, **2012**, 363–375.
(33) Lyaskovskyy, V.; de Bruin, B. *ACS Catal*., **2012**, *2*, 270–279.
(34) Luca, O. R.; Crabtree, R. H. *Chem. Soc. Rev.*, **2013**, *42*, 1440–1459.
(35) van der Vlugt, J. I. *Chem. Eur. J*., **2019**, *25*, 2651–2662.
(36) Schrauzer, G. N.; Mayweg, V. *J. Am. Chem. Soc*., **1962**, *84*, 3221–3221.
(37) Davison, A.; Edelstein, N.; Holm, R. H.; Maki, A. H. *Inorg. Chem.*, **1963**, *2*, 1227–1232.

(38) Sproules, S.; Wieghardt, K. *Coord. Chem. Rev.*, **2010**, *254*, 1358–1382.
(39) Sproules, S.; Wieghardt, K. *Coord. Chem. Rev.*, **2010**, *255*, 837–860.
(40) Eisenberg, R.; Gray, H. B. *Inorg. Chem.*, **2011**, *50*, 9741–9751.
(41) Kaim, W. *Dalton. Trans*., **2019**, *48*, 8521–8529.
(42) Caulton, K. G; *Eur. J. Inorg. Chem.*, **2012**, 435–443.
(43) Camp, C.; Arnold, J. *Dalton. Trans.*, **2016**, *45*, 14462–14498.
(44) Khusniyarov, M. M.; Bill, E.; Weyhermüller, T.; Bothe, E.; Wieghardt, K. *Angew. Chem. Int. Ed*., **2011**, *50*, 1652–1655.
(45) Pierpont, C. G.; Buchanan, R. M. *Coord. Chem. Rev.*, **1981**, *38*, 45–87.
(46) Mederos, A.; Domínguez, S.; Hernández-Molina, R.; Sanchiz, J.; Brito, F. *Coord. Chem. Rev.*, **1999**, *193-195*, 913–939.
(47) Pierpont, C. G. *Coord. Chem. Rev.*, **2001**, *216-217*, 99–125.
(48) Pierpont, C. G. *Coord. Chem. Rev.*, **2001**, *219-221*, 415–433.
(49) Broere, D. L. J.; Plessius, R.; van der Vlugt, J. I. *Chem. Soc. Rev.*, **2015**, *44*, 6886–6915.
(50) Knijnenburg, Q.; Gambarotta, S.; Budzelaar, P. H. M. *Dalton Trans.*, **2006**, 5442–5448.
(51) Gibson, V. C.; Redshaw, C.; Solan, G. A. *Chem. Rev.*, **2007**, *107*, 1745–1776.
(52) Blanchard, S.; Derat, E.; Desage-El Murr, M.; Fensterbank, L.; Malacria, M.; Mouriès-Mansuy, V. *Eur. J. Inorg. Chem*. **2012**, 376–389.
(53) Shimazaki, Y.; Tani, F.; Fukui, K.; Naruta, Y.; Yamauchi, O. *J. Am. Chem. Soc.*, **2003**, *125*, 10512–10523.
(54) Storr, T.; Wasinger, E. C.; Pratt, R. C.; Stack, T. D. P. *Angew. Chem. Int. Ed*., **2007**, *46*, 5198–5201.
(55) Storr, T.; Verma, P.; Pratt, R. C.; Wasinger, E. C.; Shimazaki, Y.; Stack, T. D. P. *J. Am. Chem. Soc.*, **2008**, *130*, 15448–15459.
(56) Orio, M.; Jarjayes, O.; Kanso, H.; Philouze, C.; Neese, F.; Thomas, F. *Angew. Chem. Int. Ed.*, **2010**, *49*, 4989–4992.
(57) Kurahashi, T.; Fujii, H. *J. Am. Chem. Soc.*, **2011**, *133*, 8307–8316.
(58) Lyons, C. T.; Stack, T. D. P. *Coord. Chem. Rev.*, **2013**, *257*, 528–540.
(59) Thomas, F. *Dalton Trans*., **2016**, *45*, 10866–10877.
(60) Fajer, J.; Borg, D. C.; Forman, A.; Dolphin, D.; Felton, R. H.; *J. Am. Chem. Soc.*, **1970**, *92*, 3451–3459.
(61) Dolphin, D.; Felton, R. H. *Acc. Chem. Res*., **1974**, *7*, 26–32.
(62) Fujii, H. *Coord. Chem. Rev*., **2002**, *226*, 51–60.
(63) Rittle, J.; Green, M. T. *Science*, **2010**, *330*, 933–937.

(64) Goswami, M.; Lyaskovskyy, V.; Domingos, S. R.; Buma, W. J.; Woutersen, S.; Troeppner, O.; Ivanović-Burmazović, I.; Lu, H.; Cui, X.; Zhang, X. P.; Reijerse, E. J.; DeBeer, S.; van Schooneveld, M. M.; Pfaff, F. F.; Ray, K.; de Bruin, B. *J. Am. Chem. Soc.* **2015,** *137*, 5468–5479.
(65) Koivisto, B. D.; Hicks, R. G. *Coord. Chem. Rev.*, **2005**, *249*, 2612–2630.
(66) Tejel, C; Ciriano, M. A.; del Río, M. P.; van den Bruele, F. J.; Hetterscheid, D. G. H.; i Spithas, N. T.; de Bruin, B. *J. Am. Chem. Soc*., **2008**, *130*, 5844–5845.
(67) Lu, C. C.; George, S. D.; Weyhermüller, T.; Bill, E.; Bothe, E.; Wieghardt, K. *Angew. Chem. Int. Ed*., **2008**, *47*, 6384–6387.
(68) Ehret, F.; Bubrin, M.; Záliš, S.; Kaim, W. *Z. Anorg. Allg. Chem*., **2014**, *640*, 2781–2787.
(69) Horak, K. T.; Agapie, T. *J. Am. Chem. Soc.*, **2016**, *138*, 3443–3452.
(70) Travieso-Pnente, R; Broekman, J. O. P.; Chang, M.-C.; Demeshko, S.; Meyar, F.; Otten, E. *J. Am. Chem. Soc.* **2016**, *138*, 5503–5506.
(71) Myers, T. W.; Berben, L. A. *J. Am. Chem. Soc.*, **2011**, *133*, 11865–11867.
(72) Broere, D. L. J.; de Bruin, B.; Reek, J. N. H.; Lutz, M.; Dechert, S.; van der Vlugt, J. I. *J. Am. Chem. Soc.* **2014,** *136*, 11574–11577.
(73) Zhou, W.; Patrick, B. O.; Smith, K. M. *Chem. Commun*., **2014**, *50*, 9958–9960.
(74) Broere, D. L. J.; van Leest, N. P.; de Bruin, B.; Siegler, M. A.; van der Vlugt, J. I. *Inorg. Chem.* **2016,** *55*, 8603–8611.
(75) Bagh, B.; Broere, D. L. J.; Sinha, V.; Kuijpers, P. F.; van Leest, N. P.; de Bruin, B.; Demeshko, S.; Siegler, M. A.; van der Vlugt, J. I. *J. Am. Chem. Soc.* **2017,** *139*, 5117–5124.

Chapter 1

Catalytic Intermolecular C–H Amination Driven by Ligand-to-Nitrene One-Electron Transfer

Introduction

Nitrene-bound transition-metal complexes are involved as the key reactive intermediates in C–H bond functionalization such as C=C aziridination, and electron transfer oxidation.[1-10] A better understanding of the relationships between electronic structure and reactivity of the nitrene-complexes is prerequisite in the development of efficient and selective catalysts for such reactions. When nitrene binds to *early*-transition-metal elements, the resultant complexes feature a metal-nitrogen multiple bond, namely metal-imido (M=NR) complexes, because the *early*-transition-metal ions have suitable empty d-orbitals that can make π-bonding interaction with a filled p-orbital of the nitrene ligand (Type 1 in Scheme 1).[11-16] Thus, there are a large number of examples of metal-imido complexes of *early*-transition-metal elements that exhibit electrophilic reactivity.[11-16] On the other hand, *late*-transition-metal nitrene complexes with octahedral structure have filled d_π orbitals, so that the π-bonding interaction with filled p-orbitals of the nitrene ligand is virtually impossible (Scheme 1). Thus, the nitrene-bound *late*-transition-metal complexes tend to show single-bond character (M–NR) (Type 2), exhibiting nucleophilic reactivity.[17]

Scheme 1. Schematic classification of nitrene bound octahedral metal complexes and $\pi_{d\text{-}p}$ interaction.

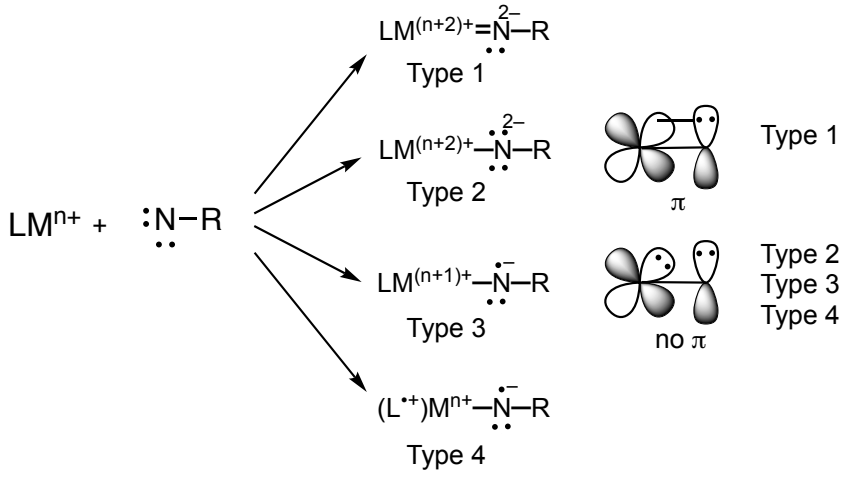

The third class of nitrene-bound metal complexes are nitrene-radical complexes having a nitrogen atom with formally seven valence electrons, which can be generated via one-electron transfer from the metal center to the nitrene moiety (Type 3 in Scheme 1).[18,19] Such nitrene radical complexes are expected to have radical character. A typical example is the well characterized nitrene-radical cobalt(III)-porphyrin complexes that can be adopted in the aziridination, C–H bond amination, and C–H bond amidation.[20-22] However, such nitrene-radical complexes are very limited.[20-27] Recently, the combination of *a redox-active ligand* and a *redox-innocent* metal ion was employed for accessing nitrene radical metal complexes (Type 4 in Scheme 1).[8-10, 28,29] In this case, one-electron transfer takes place from the supporting ligand to the nitrene nitrogen atom without changing the metal oxidation state. For instance, a palladium(II) complex with a redox active NNO pincer ligand (L^{2-}) induces an *intramolecular* cyclization of 4-phenylbutaneazide to 2-phenylpyrrolidine via a $Pd^{II}(L^{\bullet-})(RN^{\bullet-})$ intermediate (R = -$(CH_2)_4Ph$).[28, 29]

Itoh and his co-workers reported a series of *late*-transition-metal complexes $[M^{II}(\mathbf{L}^{3-})]^-$ (M = Ni, Cu, and Pd) supported by a planer tetradentate ligand ($\mathbf{L}^{3-}$) consisting of a β-diketiminate framework with two aminophenol moieties.[30,31] One-electron oxidation of the complexes (both chemically and electrochemically) gave the corresponding ligand-radical complexes $[M(\mathbf{L}^{\bullet 2-})]^{2-}$.[30,31] Therefore, the author envisioned that the redox-active ligand, $\mathbf{L}^{3-}$, can facilitate formation of a nitrene radical complex having metal–nitrene single bond character through ligand to nitrene one-electron transfer when combined with a redox innocent transition metal ion. In this work, the author employs rhodium(III) ion as the central metal, since most of the Werner type octahedral rhodium(III) complexes are hardly oxidized to the higher oxidation states. In this work, the author demonstrates the first intermolecular C(sp^3)–H amination via ligand-based redox. DFT calculations indicate that a triplet nitrene di-radical rhodium(III) complex works as a reactive intermediate in the C–H amination reaction.

In this chapter, the rhodium(III) complexes bearing the redox-active tetradentate ligand ($\mathbf{L}^{3-}$) ($[Rh^{III}(\mathbf{L}^{3-})(p\text{-X-}C_6H_4NH_2)_2]$ ($\mathbf{1^X}$, X =H, OMe, Cl) and ($^n Bu_4N[Rh^{III}(\mathbf{L}^{3-})(Y)(Sol)]^-$ ($[\mathbf{2^{Y/Sol}}]^-$, Y = Cl^-, Br^-, or I^- and Sol = acetonitrile (AN), water (H_2O), tetrahydrofuran (THF), or pyridine (PY)) have been synthesized (Figure 1). The rhodium(III) complexes ($\mathbf{1^X}$ or $[\mathbf{2^{Y/Sol}}]^-$) showed catalytic activity in the *intermolecular* C–H bond amination reaction using tosyl azide (TsN_3) as the nitrene source (Scheme 2). The reaction of $\mathbf{1^X}$ (or $[\mathbf{2^{Y/Sol}}]^-$) and TsN_3 generates a nitrene-radical rhodium(III) complex supported by the ligand radical $[Rh^{III}(\mathbf{L}^{\bullet 2-})(TsN^{\bullet-})(L_{ax})]$ (L_{ax} = *p*-X-$C_6H_4NH_2$, Cl^-, Br^-, I^-) (**DR** in Scheme 2), which induces catalytic amination reaction

of xanthene (Scheme 2). Density functional theory (DFT) studies have suggested that the diradical (**DR**) electronic configuration of $[Rh^{III}(\mathbf{L}^{\bullet 2-})(TsN^{\bullet -})(L_{ax})]$ with a single bond character between the metal center and the nitrene radical nitrogen atom is a plausible reactive intermediate in the C–H bond abstraction and nitrogen-rebound mechanism.

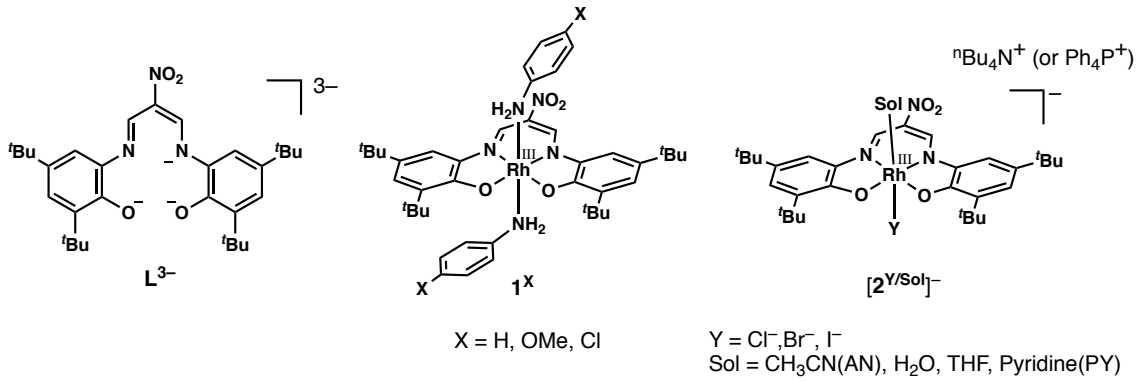

Figure 1. Chemical structures of supporting ligand $\mathbf{L}^{3-}$, rhodium(III) complexes $\mathbf{1}^{\mathbf{X}}$, and $[\mathbf{2}^{\mathbf{Y/Sol}}]^{-}$.

Scheme 2. Catalytic C–H amination of xanthene with tosyl azide (TsN_3) by $\mathbf{1}^{\mathbf{X}}$ or $^{n}Bu_4N[\mathbf{2}^{\mathbf{Y/Sol}}]$ (above) and the diradical intermediate (**DR**) for C–H amination (below).

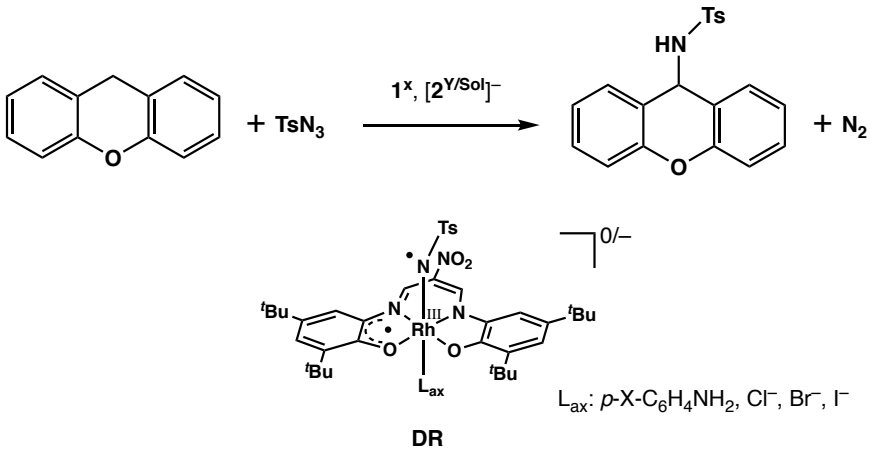

Experimental

General. The reagents used in this study, except the compounds mentioned below, were commercial products of the highest available purity and were used as received without further purification, unless otherwise noted. All solvents used in this study were

purified by the standard procedure.[32] The ligand $\mathbf{L}H_3$, $[Rh^{I}(cod)Cl]_2$, tosyl azide, 4-phenylbutaneazide, and xanthene-d_2 were synthesized according to the reported procedures.[30,33-36] ^1H and ^{13}C NMR spectra were recorded at 400 MHz and 101 MHz on a JEOL-ECP400 or a JEOL-ECS400 spectrometer. Fast atom bombardment mass spectroscopy (FAB-MS) spectra were recorded with a JEOL-JMS-700 spectrometer. Electrospray ionization mass spectroscopy (ESI-MS) spectra were recorded with a BRUKER micrOTOF II spectrometer. Electron paramagnetic resonance (EPR) spectra were taken on a BRUKER X-band spectrometer (EMX-Micro) under non-saturating microwave power conditions (1.0 mW) operating at 9.680 GHz. Elemental analysis was carried out with a Yanaco CHN-Corder MT-5. Electrochemical measurements were performed with a Hokuto Denko HZ-7000. A set of a carbon working electrode, an $Ag/AgNO_3/CH_3CN$ reference electrode, and a platinum counter electrode was employed in these experiments.

Synthesis. $[Rh^{I}(\mathbf{L}H_2^{-})(cod)]$. $\mathbf{L}H_3$ (200 mg, 0.382 mmol) and $[Rh^{I}(cod)Cl]_2$ (94.2 mg, 0.191 mmol) were dissolved in THF (4 mL). 1 equiv of triethylamine (53.2 μL, 0.382 mmol) was added to the mixture and the mixture was stirred for 2 h at room temperature. Slow diffusion of methanol to the reaction mixture produced yellow crystal of $[Rh^{I}(\mathbf{L}H_2^{-})(cod)]$. Yield: 267 mg, (95%). Single crystals suitable for X–ray crystallographic analysis were obtained by recrystallization from acetone and methanol. ^1H NMR ($CDCl_3$, 400 MHz): (isomer A) δ 8.86 (s, 2H), 7.17 (d, 2H, J = 1.6 Hz), 6.77 (d, 2H, J = 2.0 Hz), 5.76 (s, 2H), 4.04 (t, 2H, J = 6.80 Hz), 3.58 (s, 2H), 3.18 (q, 2H, J = 6.8 Hz), 2.61−2.48 (m, 2H), 2.10−2.00 (m, 2H), 1.98−1.82 (m, 2H), 1.44 (s, 18H), 1.32 (s, 18H); (isomer B) δ 8.79 (s, 2H), 7.17 (d, 2H, J = 1.6 Hz), 6.87 (d, 2H, J = 2.0 Hz), 5.98 (s, 2H), 3.49 (s, 4H), 2.27 (s, 4H), 1.81−1.71 (m, 4H), 1.44 (s, 18H), 1.32 (s, 18H). ^{13}C NMR ($CDCl_3$, 101 MHz, ppm): 158.35, 158.23, 144.25, 144.17, 142.85, 142.56, 139.56, 139.45, 136.12, 136.08, 122.11, 122.09, 121.95, 118.82, 87.62, 87.50, 84.93, 84.80, 80.87, 80.74, 58.67, 53.58, 35.28, 35.25, 34.61, 33.17, 31.70, 30.15, 29.50, 27.45, 18.60. Anal. Calcd for $[Rh^{I}(\mathbf{L}H_2^{-})(cod)]\cdot THF\cdot CH_3OH$ ($C_{44}H_{68}RhN_3O_6$): C, 63.07; H, 8.18; N, 5.01; Found: C, 63.21; H, 8.50; N, 5.04. FAB-MS (pos): m/z = 734 ($[M]^+$) .

$[Rh^{III}(\mathbf{L}^{3-})(PhNH_2)_2]$ (**1^H**). $[Rh^{I}(\mathbf{L}H_2^{-})(cod)]$ (36.7 mg, 50.0 μmol) was dissolved in THF (3 mL) and stirred at room temperature for 10 min. Triethylamine (14μL, 100 μmol) and then aniline (9.2 μL, 100 μmol) were added to the solution. The reaction mixture was stirred at room temperature for 3 h under air. Precipitated material was removed by filtration and the filtrate was evaporated in vacuo. The residue was dissolved in dichloromethane (CH_2Cl_2). Slow diffusion of ethanol into the CH_2Cl_2 solution gave orange needle crystals. Yield: 28.3 mg (70 %). Single crystals suitable

for X–ray crystallographic analysis were obtained by recrystallization from acetone and *n*-hexane. ^{1}H NMR ($CDCl_3$, 400 MHz): δ 8.84 (d, 2H, J = 2.0 Hz), 7.33 (d, 2H, J = 1.6 Hz), 7.23 (d, 2H, J = 2.0Hz), 6.94, 6.92 (dd, 2H, J = 7.2 Hz, 7.6 Hz), 6.81, 6.79 (dd, 2H, J = 8.0 Hz, 7.6 Hz), 6.09 (d, 2H, J = 7.6 Hz), 4.07 (br s, 4H) 1.67 (s, 18H),1.38 (s, 18H). ^{13}C NMR ($CDCl_3$, 101 MHz, ppm): 162.82, 140.11, 137.34, 137.29, 131.78, 128.57, 126.24, 122.43, 120.36, 109.28, 35.81, 34.61, 32.07, 29.96. Anal. Calcd for $\mathbf{1^H}\cdot 0.5H_2O$ ($C_{43}H_{57}RhN_5O_{4.5}$): C, 63.07; H, 7.02; N, 8.55; Found: C, 63.10; H, 7.19; N, 8.53. FAB-MS (pos): m/z = 809 ([M]$^+$).

[Rh^{III}(L^{3-})(*p*-methoxyaniline)$_2$] ($\mathbf{1^{OMe}}$). $\mathbf{1^{OMe}}$ was prepared by the method described for the synthesis of [Rh^{III}L^{3-}(PhNH$_2$)$_2$]($\mathbf{1^H}$) except the use of *p*-methoxyaniline instead of aniline. The crude product was purified by silica gel column chromatography (eluent; $AcOCH_3$: *n*-hexane = 1 : 5). Yield: 20.4 mg (47%). ^{1}H NMR ($CDCl_3$, 400 MHz): δ 8.89 (d, 2H, J = 2.0 Hz), 7.33 (d, 2H, J = 1.6 Hz), 7.20 (d, 2H, J = 2.0 Hz), 6.30 (d, 4H, J = 8.4 Hz), 6.01 (d, 4H, J = 8.8 Hz), 3.99 (br s, 4H), 3.60 (s, 6H), 1.65(s, 18H), 1.30 (s, 18H).^{13}C NMR ($CDCl_3$, 101 MHz, ppm): 162.80, 157.67, 140.06, 138. 08, 137.26, 137.09, 130.03, 127.38, 122.41, 121.44, 113.75, 109.23, 55.49, 35.79, 34.60, 32.07, 29.96. Anal. Calcd for $\mathbf{1^{OMe}}\cdot 1.5H_2O$ ($C_{45}H_{63}RhN_5O_{7.5}$): C, 60.26; H, 7.08; N, 7.81; Found: C, 60.28; H, 7.18; N, 7.75. FAB-MS (pos): m/z = 869 ([M]$^+$).

[Rh^{III}(L^{3-})(*p*-chloroaniine)$_2$] ($\mathbf{1^{Cl}}$). $\mathbf{1^{Cl}}$ was prepared by the method described for the synthesis of [Rh^{III}L^{3-}(PhNH$_2$)$_2$]($\mathbf{1^H}$) except the use of *p*-chloroaniline instead of aniline. The crude product was purified by silica gel column chromatography (eluent; $AcOCH_3$: *n*-hexane = 1 : 6). Yield: 11.4 mg (26%). ^{1}H NMR ($CDCl_3$, 400MHz): δ 8.98 (d, 2H, J = 1.6 Hz), 7.32 (d, 2H, J = 2.4 Hz), 7.21 (d, 2H, J = 2.0Hz), 6.78 (d, 4H, J = 8.4 Hz), 6.10 (d, 4H, J = 8.8 Hz), 4.09 (br s, 4H), 1.64 (s, 18H), 1.37 (s, 18H). ^{13}C NMR ($CDCl_3$, 101 MHz, ppm): 162.86, 140.30, 138.39, 137.26, 136.76, 136.16, 131.78, 128.72, 127.24, 122.81, 121.94, 109.05, 35.79, 34.60, 32.08, 29.91. Anal. Calcd for $\mathbf{1^{Cl}}\cdot 0.5H_2O$ ($C_{43}H_{55}RhN_5O_{4.5}Cl_2$): C, 58.18; H, 6.25; N, 7.89; Found: C, 58.36; H, 6.62; N, 7.79. FAB-MS (pos): m/z = 877 ([M]$^+$).

[Rh^{III}(L$^{\cdot 2-}$)(PhNH$_2$)$_2$]SbF$_6$ ([$\mathbf{1^H}$]SbF$_6$). A CH_2Cl_2 (2 mL) solution of $AgSbF_6$ (21.5 mg, 62.6 μmol) was added to complex $\mathbf{1^H}$ (35.0 mg, 43.2 μmol) in CH_2Cl_2 (2 mL) with stirring at room temperature. The reaction mixture was added dropwise to *n*-hexane (50 mL) with vigorous stirring. After reducing volume of the solvent to 5 mL, generated dark red precipitates were collected by filtration. Dark red crystals were obtained by slow diffusion of cyclohexane into a CH_2Cl_2 solution containing the complex. The crystals were suitable for X-ray crystallographic analysis. Yield: 38.0 mg (83%).

Anal. Calcd for [$\mathbf{1^H}$][SbF_6]·H_2O ($C_{43}H_{58}RhN_5O_5SbF_6$): C, 48.56; H, 5.50; N, 6.58; Found: C, 48.54; H, 5.53; N, 6.63.

^{n}Bu$_4$N[Rh^{III}($\mathbf{L}^{3-}$)(Cl)(CH$_3$CN)] (^{n}Bu$_4$N[$\mathbf{2^{Cl/AN}}$]). Toluene (2 mL) was added to a mixture of [Rh^I($\mathbf{L}H_2^-$)(cod)] (50.0 mg, 0.68 μmol) and tetra-*n*-butylammonium chloride (^{n}Bu$_4$NCl, 16.7 mg, 0.60 μmol), and the resultant solution was stirred at room temperature under air. After 5 h, *n*-hexane (40 mL) was added to the solution with vigorous stirring. An orange powder was precipitated from the solution, which was collected by filtration (48.5 mg). Then, the orange powder (48.5 mg) was dissolved in CH_3CN. Single-crystals of ^{n}Bu$_4$N[$\mathbf{2^{Cl/AN}}$] were obtained by vapor diffusion of diethyl ether into the CH_3CN solution, which were collected by filtration and dried under air. The crystals were suitable for X–ray crystallographic analysis. Yield: 21.9 mg (34 %). ^{1}H NMR (CD_3CN, 400 MHz): δ 9.20 (d, 2H, J = 1.6 Hz), 7.58 (d, 2H, J = 2.8 Hz), 7.09 (d, 2H, J = 2.0 Hz), 3.12−3.02 (m, 8H), 1.97 (s, 3H), 1.65−1.51 (m, 26H), 1.42−1.28 (m, 26H), 0.936 (t, 12H, J = 7.2 Hz). ^{13}C NMR (CD_3CN, 101 MHz, ppm): 166.45, 139.52, 139.27, 137.69, 135.43, 122.12, 109.42, 59.27, 36.10, 34.87, 32.17, 30.08, 24.27, 20.30, 13.78. Decomposition temperature: 180−190 °C. Anal. Calcd for ^{n}Bu$_4$N[$\mathbf{2^{Cl/AN}}$] ($C_{49}H_{81}ClN_5O_4Rh$): C, 62.44; H, 8.66; N,7.43; Found: C,62.42; H,8.99; N,7.79. ESI-MS (neg): m/z = 658.2 ([M − CH_3CN]$^-$).

Ph$_4$P[Rh^{III}($\mathbf{L}^{3-}$)(Cl)(CH$_3$CN)] (Ph$_4$P[$\mathbf{2^{Cl/AN}}$]). This complex was prepared by the same method described for ^{n}Bu$_4$N[$\mathbf{2^{Cl/AN}}$] except for using Ph$_4$PCl instead of ^{n}Bu$_4$NCl. Yield: 33.8 mg (48%). ^{1}H NMR (CD_3CN, 400 MHz): δ 9.20 (d, 2H, J = 1.6 Hz), 7.98−7.86 (m, 4H), 7.81–7.63 (m, 16H), 7.58 (d, 2H, J = 2.4 Hz), 7.09 (d, 2H, J = 2.0 Hz), 1.58 (s, 18H), 1.37 (s, 18H). ^{13}C NMR (CD_3CN, 101 MHz, ppm): 166.37, 139.51, 139.29, 137.73, 136.39, 135.74, 135.64, 135.47, 131.37, 131.25, 122.12, 109.45, 36.09, 34.87, 32.16, 30.08. Decomposition temperature: 168−185 °C. Anal. Calcd for $C_{57}H_{65}ClN_4O_4RhP·Et_2O$: C,65.79; H,6.79; N,5.03; Found: C,65.61; H,6.74; N,5.10. ESI-MS (neg): m/z = 658.2 ([M − CH_3CN]$^-$).

^{n}Bu$_4$N[Rh^{III}($\mathbf{L}^{3-}$)(Br)(CH$_3$CN)] (^{n}Bu$_4$N[$\mathbf{2^{Br/AN}}$]). This complex was prepared by the same method described for ^{n}Bu$_4$N[$\mathbf{2^{Cl/AN}}$] except for using ^{n}Bu$_4$NBr instead of ^{n}Bu$_4$NCl. Yield: 20.6 mg (31 %). ^{1}H NMR (CD_3CN, 400 MHz): δ 9.18 (d, 2H, J = 1.6 Hz), 7.58 (d, 2H, J = 2.4 Hz), 7.09 (d, 2H, J = 2.4 Hz), 3.11–3.02 (m, 8H), 1.97 (s, 3H), 1.66–1.51 (m, 26H), 1,44–1.28 (m, 26H), 0.963 (t, 12H, J = 7.2 Hz). ^{13}C NMR (CD_3CN, 101 MHz, ppm): 166.53, 139.60, 139.50, 137.84, 135.40, 122.08, 109.34, 59.28, 36.10, 34.87, 32.17, 30.07, 24.27, 20.31, 13.78. Decomposition temperature: 165–171 °C. Anal. Calcd for $C_{49}H_{81}BrN_5O_4Rh·Et_2O·CH_3CN$: C,59.93; H,8.60; N,7.62; Found: C,59.93; H,8.75; N,7.47. ESI-MS (neg): m/z = 702.1 ([M − CH_3CN]$^-$).

^{n}Bu$_4$N[Rh^{III}(L^{3-})(I)(CH$_3$CN)] (^{n}Bu$_4$N[2$^{I/AN}$]). This complex was prepared by the same method described for ^{n}Bu$_4$N[2$^{Cl/AN}$] except for using ^{n}Bu$_4$NI instead of ^{n}Bu$_4$NCl. Yield: 35.3 mg (50 %). ^{1}H NMR (CD$_3$CN, 400 MHz): δ 9.14 (d, 2H, J = 1.6 Hz), 7.58 (d, 2H, J = 2.0 Hz), 7.07 (d, 2H, J = 2.4 Hz), 3.11–3.02 (m, 8H), 1.97 (s, 3H), 1.65–1.51 (m, 26H), 1.41–1.28 (m, 26H), 0.963 (t, 12H, J = 7.2 Hz). ^{13}C NMR (CD$_3$CN, 101 MHz, ppm): 166.59, 139.92, 139.68, 138.0, 135.27, 121.97, 109.21, 59.27, 36.06, 34.86, 32.17, 30.03, 24.26, 20.30, 13.77. Decomposition temperature: 150−159 °C. Anal. Calcd for C$_{49}$H$_{81}$IN$_5$O$_4$Rh·Et$_2$O·0.7CH$_3$CN: C,57.47; H,8.25; N,7.02; Found: C,57.83; H,8.41; N,7.01. ESI-MS (neg): m/z = 750.1 ([M − CH$_3$CN]$^-$).

^{n}Bu$_4$N[Rh^{III}(L^{3-})(Cl)(H$_2$O)] (^{n}Bu$_4$N[2$^{Cl/H2O}$]). This complex was obtained by the same method described for ^{n}Bu$_4$N[2$^{Cl/AN}$] except for using water and acetone for crystallization instead of CH$_3$CN. The obtained single crystals were suitable for X–ray crystallographic analysis. Yield: 43.0 mg (69 %). ^{1}H NMR (acetone-d_6, 400 MHz): δ 9.37 (d, 2H, J = 1.2 Hz), 7.65 (d, 2H, J = 2.0 Hz), 7.05 (d, 2H, J = 2.8 Hz), 3.42–3.33 (m, 8H), 1.83–1.71 (m, 8H), 1.59 (s, 18H), 1.45–1.33 (m, 26H), 0.953 (t, 12H, J = 7.6 Hz). ^{13}C NMR (acetone-d_6, 101 MHz, ppm): 166.67, 139.63, 139.23, 137.28, 134.35, 121.25, 108.82, 59.28, 35.99, 34.74, 32.39, 24.36, 20.31, 13.86. Decomposition temperature: 192−197 °C. Anal. Calcd for C$_{47}$H$_{80}$ClN$_4$O$_5$Rh: C, 61.39; H, 8.77; N, 6.09; Found: C, 61.00; H, 8.87; N, 6.07. ESI-MS (neg): m/z = 658.2 ([M − H$_2$O]$^-$).

^{n}Bu$_4$N[Rh^{III}(L^{3-})(Cl)(THF)] (^{n}Bu$_4$N[2$^{Cl/THF}$]). This complex was obtained by the same method described for ^{n}Bu$_4$N[2$^{Cl/AN}$] except for using diethyl ether and THF for crystallization instead of CH$_3$CN. Yield: 39.4 mg (60 %). ^{1}H NMR (acetone-d_6, 400 MHz): δ 9.37 (d, 2H, J = 1.6 Hz), 7.65 (d, 2H, J = 2.0 Hz), 7.04 (d, 2H, J = 2.4 Hz), 3.66–3.58 (m, 4H), 3.47–3.38 (m, 8H), 1.86–1.75 (m, 12H), 1.59 (s, 18H), 1.48–1.33 (m, 26H), 0.969 (t, 12H, J = 7.2 Hz). ^{13}C NMR (acetone-d_6, 101 MHz, ppm): 166.70, 139.63, 139.22, 137.24, 134.31, 121.25, 108.82, 68.05, 59.29, 36.00, 34.75, 32.40, 26.16, 24.34, 20.32, 13.85. Decomposition temperature: 175−183 °C. Anal. Calcd for C$_{51}$H$_{86}$ClN$_4$O$_5$Rh: C, 62.92; H, 8.90; N,5.75; Found: C,62.78; H, 9.34; N, 5.62. ESI-MS (neg): m/z = 658.2 ([M – THF]$^-$).

^{n}Bu$_4$N[Rh^{III}(L^{3-})(Cl)(py)] (^{n}Bu$_4$N[2$^{Cl/PY}$]). This complex was prepared by the same method described for ^{n}Bu$_4$N[2$^{Cl/AN}$] except for using diethyl ether and pyridine for crystallization instead of CH$_3$CN. Yield: 30.6 mg (46 %). ^{1}H NMR (acetone-d_6, 400 MHz): δ 9.42 (d, 2H, J = 1.6 Hz), 8.16 (d, 2H, J = 6.4 Hz), 7.65 (tt, 1H, J = 1.2, 7.6 Hz), 7.56 (d, 2H, J = 2.4 Hz), 7.21 (t, 2H, J = 7.2 Hz), 6.96 (d, 2H, J = 2.0 Hz), 3.41–3.31 (m, 8H), 1.76 (qu, 8H, J = 8.0 Hz), 1.57 (s, 18H), 1.38 (se, 8H, J = 8.0 Hz), 1.29 (s, 18H), 0.951 (t, 12H, J = 7.2 Hz). ^{13}C NMR (acetone-d_6, 101 MHz, ppm): 166.29, 152.69,

150.67, 139.03, 138.98, 138.78, 136.15, 134.28, 127.98, 125.02, 121.39, 108.63, 59.25, 36.08, 34.67, 32.31, 24.36, 20.31, 13.87. Decomposition temperature: 250−265 °C. Anal. Calcd for $C_{52}H_{83}ClN_5O_4Rh$: C, 63.69; H, 8.53; N, 7.14; Found: C, 63.61; H, 8.68; N, 7.20. ESI-MS (neg): *m*/*z* = 737.3([M]$^-$), 658.2 ([M – pyridine]$^-$).

Iminosemiquinone Complex (Ph_4P[**3**]). Tosyl azide (190 mg, 0.991 mmol) was added to a CH_2Cl_2 solution (3 mL) of $Ph_4P[Rh^{III}(\mathbf{L}^{3-})(Cl)(CH_3CN)]$ (50.0 mg, 48.1 μmol), and the resultant solution was stirred for 30 min. The reaction solution was added to *n*-hexane (40 mL) with vigorous stirring to give a brown solid (40.0 mg, 71%), which was collected by centrifugation. Single crystals of Ph_4P[**3**] was obtained by slow diffusion of *n*-hexane to the acetone solution of Ph_4P[**3**]. The single crystals were suitable for X–ray crystallographic analysis. Yield: 29.7mg (53%). Decomposition temperature: 169−174 °C. Anal. Calcd. for $C_{65}H_{76}ClN_4O_7PRhS$: C, 63.64; H, 6.24; N, 4.57; Found: C, 63.57; H, 6.40; N, 4.57. ESI-MS (neg): *m*/*z* = 828.2 ([M]$^-$).

^{n}Bu$_4$N[$Rh^{III}(\mathbf{L}^{3-})(Cl)(NH{=}CH(CH_2)_3Ph)$] (^{n}Bu$_4$N[**4**^{Cl}]). 4-Phenylbutaneazide (186 mg, 1.06 mmol) was added to a CH_2Cl_2 solution (3 mL) of ^{n}Bu$_4$N[**2**$^{Cl/AN}$] (50.0 mg, 53.0 μmol) and the solution was stirred for 1 h at room temperature. The mixture was poured into *n*-hexane (40 mL) with vigorous stirring to yield a red powder, which was collected by centrifugation. Yield: 33.5 mg (60%). ^{1}H NMR (CD_3CN, 400 MHz): δ 9.23 (d, 2H, *J* = 2.4 Hz), 8.54 (d, 1H, *J* = 21 Hz,), 7.56 (d, 2H, *J* = 2.0 Hz), 7.47 (dtd, 1H, *J* = 21.0, 6.0, 2.0 Hz), 7.16–7.03 (m, 5H), 6.76 (d, 2H, *J* = 6.8 Hz), 3.08–2.99 (m, 8H), 2.07–1.97 (m, 4H), 1.62–1.40 (m, 28 H), 1.40–1.20 (m, 30 H), 0.935 (t, 12H, *J* = 8.0 Hz), 0.859 (t, 2H, *J* = 7.2 Hz). ^{13}C NMR (CD_3CN, 101 MHz, ppm): 182.66, 165.95, 141.92, 139.28, 139.17, 137.18, 135.45, 129.28, 129.17, 126.76, 122.16, 109.32, 59.26, 37.01, 36.11, 34.85, 34.51, 32.17, 30.16, 27.34, 24.26, 20.30, 13.78. Decomposition temperature: 173−185 °C. Anal. Calcd. for $C_{57}H_{91}Cl_1N_5O_4Rh$: C, 65.28; H, 8.75; N, 6.68; Found: C, 65.27; H, 9.18; N, 6.47. ESI-MS (neg): *m*/*z* = 805.3 ([M]$^-$), 658.2 ([M – (NH=CH(CH$_2$)$_3$Ph)]$^-$.

$[Rh^{III}(\mathbf{L}^{3-})(NH{=}CH(CH_2)_3Ph)$(*p*-methoxyaniline)] (**4**$^{aniline\text{-}OMe}$). 4-Phenylbutaneazide (35.4 mg, 0.202 mmol) was added to a toluene solution (8 mL) of $[Rh^{III}(\mathbf{L}^{3-})$(*p*-methoxyaniline)$_2$] (160.0 mg, 0.184 mmol) and the resultant solution was refluxed for 18 h. The solvent was removed under reduced pressure, and the crude product was purified by silica gel chromatography (ethyl acetate/$CHCl_3$ = 1:25). Yield: 44.8 mg, 27%). Single crystals suitable for X–ray crystallographic analysis were obtained by slow evaporation of acetone/H_2O solution of **4**$^{aniline\text{-}OMe}$. ^{1}H NMR ($CDCl_3$, 400 MHz): δ 9.15 (d, 2H, *J* = 1.6 Hz), 7.77 (d, 1H *J* = 21.2 Hz,), 7.46 (d, 2H, *J* = 2.0 Hz), 7.38 (dt, 1H, *J* = 21.2, 4.0 Hz), 7.20 (d, 2H, *J* = 2.0 Hz), 7.18–7.08 (m, 3H), 6.79 (d, 2H,

J = 6.4 Hz), 6.34 (d, 2H, J = 9.2 Hz), 6.04 (d, 2H, J = 8.8 Hz), 3.63 (s, 3H), 2.22 (t, 2H, J = 7.2 Hz), 2.05 (q, 2H, J = 6.8 Hz), 1.63–1.49 (m, 20H), 1.24 (s, 18H). ^{13}C NMR ($CDCl_3$, 101 MHz): 183.27, 169.39, 157.51, 139.87, 139.82, 137.41, 137.13, 136.96, 130.27, 128.63, 128.37, 127.48, 126.39, 122.40, 121.25, 113.71, 109.11, 55.48, 37.67, 35.81, 34.57, 33.99, 32.08, 29.89, 25.91. mp: 196−198 °C. Anal. Calcd for $C_{48}H_{64}N_5O_5Rh\cdot 2H_2O\cdot (CH_3)_2CO$: C, 61.99; H, 7.55; N, 7.09; Found: C, 62.38; H, 7.55; N, 7.48.

Catalytic Amination of Xanthene by TsN_3 by $\mathbf{1^H}$. A solution of tosyl azide (6.91 mg, 35.0 μmol) and $(Boc)_2O$ (7.64 mg, 35.0 μmol) in toluene (1 mL) was added to $\mathbf{1^x}$ (2.83 mg, 3.50 μmol) and xanthene (6.38 mg, 35.0 μmol) in a 50 mL Schlenk tube covered with aluminum foil. After purge of dioxygen in the solvent by freeze−pump−thaw cycle (three times), the mixture was stirred at 100 ℃ for 24 h under dinitrogen atmosphere. All volatiles were evaporated in vacuo and the crude products was analyzed by ^{1}H NMR spectroscopy ($CDCl_3$, 400 MHz, Internal Standard; 1,1,2,2−tetracroloethane (14.5 mg, 86.4 μmol).

Catalytic Amination of Xanthene by TsN_3 by ^{n}Bu$_4$N[$2^{Y/Sol}$]. The same method described for $\mathbf{1^H}$ was performed except for using 4 mL vial as reaction vessel and 1,4-dimethoxybenzene as an internal standard (4.84 mg, 35.0 μmol).

Kinetic Isotope Effect Measurement. The solution of tosyl azide (6.91 mg, 35.0 μmol) and $(Boc)_2O$ (7.64 mg, 35.0 μmol) in toluene (1 mL) was added into mixture of $\mathbf{1^H}$ (2.83 mg, 3.50 μmol) and xanthene (3.19 mg, 17.5 μmol) and xanthene−d_2 (3.22 mg, 17.5 μmol) in a 50 mL Schlenk tube. After purge of dioxygen in the solvent by freeze−pump−thaw cycle (three times), the mixture was stirred at 100 ℃ for 24 h under dinitrogen atmosphere. All volatiles were evaporated in vacuo and the crude products was analyzed by NMR spectroscopy (DMSO−d_6, 400 MHz, Internal Standard; 1,1,2,2−tetracroloethane (14.5 mg, 86.4 μmol)).

Theoretical Calculation for $\mathbf{1^H}$. Energy calculations in the triplet and singlet states were performed using unrestricted density functional theory implemented with the Gaussian09 program package.[37] The open-shell singlet state was computed using the broken-symmetry approach. Geometry optimizations were performed with the B3LYP functional.[38,39] For the Rh atom, the SDD basis set[40] and for the other atoms, D95** basis set[41] were used. The computed kinetic isotope effect (k_H/k_D) was obtained by transition state theory[42] with the Wigner tunneling correction.

KIE calculations. The values of KIE in the C–H amination of xanthene by **$\mathbf{1^H}$-DR-T** were obtained by transition state theory with the following expression.

$$\frac{k_H}{k_D} = \left(\frac{m_D^R m_H^\#}{m_H^R m_D^\#}\right)^{3/2} \left(\frac{I_{xD}^R I_{yD}^R I_{zD}^R}{I_{xH}^R I_{yH}^R I_{zH}^R}\right)^{1/2} \left(\frac{I_{xH}^\# I_{yH}^\# I_{zH}^\#}{I_{xD}^\# I_{yD}^\# I_{zD}^\#}\right)^{1/2} \frac{q_{vD}^R q_{vH}^\#}{q_{vH}^R q_{vD}^\#} \exp\left(-\frac{E_H^\# - E_D^\#}{RT}\right)$$

Here *m, I, q*, and *E* indicate the molecular mass, the moment of inertia, the vibrational partition function, and the activation energy, respectively. The superscript *R* specifies the reactant complex **1^{H}-DR-T**, and the superscript # indicates the transition state. The subscript *H* means the species including xanthene and the subscript *D* means the species including dideuterated-xanthene. Table 1 summarizes computed values of k_H/k_D.

Table 1. Kinetic isotope effects for the C–H amination of xanthene by **1^{H}-DR-T**.

Temperature (K)	k_H/k_D	k_H/k_D[a]
300	5.616	8.345
325	4.980	7.234
350	4.490	6.383
375	4.102	5.713
400	3.788	5.173

[a] Wigner tunneling correction.

Theoretical Calculations for [3]$^{-}$. Density functional theory (DFT) calculations were performed with "ultrafine" grid by using Gaussian 09 (Revision D.01, Gaussian, Inc.).[37] Geometry optimizations were carried out at the UB3LYP/def2-TZVP level of theory[43]. Graphical outputs of the computational results were generated with the GaussView software program.[44]

X-ray Crystallography. The single crystal was mounted on a loop with a mineral oil, and all X-ray date were collected on a Rigaku R-AXIS RAPID diffractometer using filtered Mo-Kα radiation. The structures were solved by direct method (*SIR-2011*)[45] and expanded using Fourier techniques. The non-hydrogen atoms were refined anisotropically by full-matrix least squares on F^2. The hydrogen atoms were attached at idealized positions on carbon atoms and were not refined. All structures in the final stage of refinement showed no movement in the atom position. The calculations were performed using Single-Crystal Structure Analysis Software version 4.2.2.[46] Crystallographic parameters are summarized in Table 2.

Table 2. Crystallographic data for [Rh^{I}(**L**H$_2$)(cod)], [Rh^{III}(**L**$^{3-}$)(aniline)$_2$] (**1^{H}**), [Rh^{III}(**L**$^{\bullet 2-}$)(aniline)$_2$]SbF$_6$ ([**1^{H}**]SbF$_6$), ^{n}Bu$_4$N[Rh^{III}(**L**$^{3-}$)(Cl)(CH$_3$CN)] (^{n}Bu$_4$N[**2$^{Cl/AN}$**]·CH$_3$CN), ^{n}Bu$_4$N[Rh^{III}(**L**$^{3-}$)(Cl)(H$_2$O)] (^{n}Bu$_4$N[**2$^{Cl/H2O}$**]), Ph$_4$P[**3**]·acetone, and [Rh^{III}(**L**$^{3-}$)(NH=CH(CH$_2$)$_3$Ph)(*p*-methoxyaniline)] (**4$^{aniline\text{-}OMe}$**·acetone·H$_2$O).

	[Rh^{I}(**L**H$_2^-$)(cod)]	**1^{H}**·acetone	[**1^{H}**]SbF$_6$
formula	C$_{40}$H$_{60}$N$_3$O$_5$Rh	C$_{46}$H$_{62}$N$_5$O$_5$Rh	C$_{43}$H$_{56}$F$_6$N$_5$O$_4$RhSb
fw	765.84	867.93	1045.59
crystal system	monoclinic	monoclinic	orthorhombic
space group	$P2_1/c$ (#14)	$P2_1/c$ (#14)	$Pca2_1$ (#29)
a, Å	12.6767(6)	12.1457(6)	18.6586(7)
b, Å	17.8148(9)	18.9914(10)	11.3078(5)
c, Å	18.2085(7)	19.1816(10)	21.2760(7)
α, deg	90	90	90
β, deg	101.8413(13)	94.0290(12)	90
γ, deg	90	90	90
V, Å^3	4024.6(3)	4413.6(4)	4489.0(3)
Z	4	4	4
D_{calced}, g cm^{-3}	1.264	1.306	1.547
F(000)	1624.00	1832.00	2124.00
μ, cm^{-1}	4.670	4.358	10.387
cryst size, mm	0.20 × 0.10 × 0.05	0.60 × 0.30 × 0.30	0.40 × 0.40 × 0.10
T, K	123	103	103
$2\theta_{max}$, deg	54.9	54.9	55.0
reflns. obsd	9170	10069	10095
no. of params	502	576	598
$R1$[a]	0.0465	0.0307	0.0234
$wR2$[b]	0.1206	0.0951	0.0639
GOF	1.216	1.169	0.787
max./min. $\Delta\rho$, e Å^{-3}	1.28/–0.87	1.03/–0.58	1.91/–0.70

[a] $R1 = \Sigma(|F_o| - |F_c|)/\Sigma|F_o|$. [b] $wR2 = (\Sigma(w(F_o^2 - F_c^2)^2)/\Sigma w(F_o^2)^2)^{1/2}$.

Table 2. Crystallographic data for [Rh^{I}(**L**H_2)(cod)], [Rh^{III}(**L**$^{3-}$)(aniline)$_2$] (**1^{H}**), [Rh^{III}(**L**$^{\bullet 2-}$)(aniline)$_2$]SbF_6 ([**1^{H}**]SbF_6), $^{n}Bu_4N$[Rh^{III}(**L**$^{3-}$)(Cl)(CH_3CN)] ($^{n}Bu_4N$[**2$^{Cl/AN}$**] ·CH_3CN), $^{n}Bu_4N$[Rh^{III}(**L**$^{3-}$)(Cl)(H_2O)] ($^{n}Bu_4N$[**2$^{Cl/H2O}$**]), Ph_4P[**3**]·acetone, and [Rh^{III}(**L**$^{3-}$)(NH=CH(CH_2)$_3$Ph)(*p*-methoxyaniline)] (**4$^{aniline\text{-}OMe}$**·acetone·H_2O). (continued).

	$^{n}Bu_4N$[**2$^{Cl/AN}$**]·CH_3CN	$^{n}Bu_4N$[**2$^{Cl/H2O}$**]
formula	$C_{51}H_{84}ClN_6O_4Rh$	$C_{47}H_{80}ClN_4O_5Rh$
fw	983.62	919.53
crystal system	triclinic	triclinic
space group	*P*-1 (#2)	*P*-1 (#2)
a, Å	11.4013(5)	13.909(2)
b, Å	15.5803(8)	14.837(2)
c, Å	17.5584(8)	14.992(3)
α, deg	107.535(8)	114.508(3)
β, deg	106.156(8)	97.402(4)
γ, deg	104.252(7)	109.859(4)
V, Å^3	2664.7(4)	2512.7(7)
Z	2	2
D_{calced}, g cm^{-3}	1.226	1.215
F(000)	1052.00	984.00
μ, cm^{-1}	4.161	4.369
cryst size, mm	0.60 × 0.50 × 0.10	0.20 × 0.20 × 0.10
T, K	123	103
$2\theta_{max}$, deg	55.0	55.0
reflns. obsd	12094	11330
no. of params	667	602
*R*1[a]	0.0457	0.0885
*wR*2[b]	0.1301	0.2420
GOF	1.593	1.605
max./min. $\Delta\rho$, e Å^{-3}	2.87/–0.78	4.14/–2.10

[a] $R1 = \Sigma(|F_o| - |F_c|)/\Sigma|F_o|$. [b] $wR2 = (\Sigma(w(F_o^2 - F_c^2)^2)/\Sigma w(F_o^2)^2)^{1/2}$.

Table 2. Crystallographic data for [Rh^{I}(**L**H$_2$)(cod)], [Rh^{III}(**L**$^{3-}$)(aniline)$_2$] (**1^{H}**), [Rh^{III}(**L**$^{\bullet 2-}$)(aniline)$_2$]SbF$_6$ ([**1^{H}**]SbF$_6$), ^{n}Bu$_4$N[Rh^{III}(**L**$^{3-}$)(Cl)(CH$_3$CN)] (^{n}Bu$_4$N[**2$^{Cl/AN}$**]·CH$_3$CN), ^{n}Bu$_4$N[Rh^{III}(**L**$^{3-}$)(Cl)(H$_2$O)] (^{n}Bu$_4$N[**2$^{Cl/H2O}$**]), Ph$_4$P[**3**]·acetone, and [Rh^{III}(**L**$^{3-}$)(NH=CH(CH$_2$)$_3$Ph)(*p*-methoxyaniline)] (**4$^{aniline\text{-}OMe}$**·acetone·H$_2$O). (continued).

	Ph$_4$P[**3**]·acetone	**4$^{aniline\text{-}OMe}$**·acetone·H$_2$O
formula	C$_{65}$H$_{76}$ClN$_4$O$_7$PRhS	C$_{51}$H$_{72}$N$_5$O$_7$Rh
fw	1226.73	950.03
crystal system	triclinic	monoclinic
space group	*P*-1 (#2)	*P*2$_1$ (#4)
a, Å	11.1686(9)	8.5178(4)
b, Å	11.8470(10)	20.9407(7)
c, Å	24.898(2)	13.8465(5)
α, deg	77.387(6)	90
β, deg	79.345(6)	97.830(1)
γ, deg	78.883(6)	90
V, Å^3	3119.2(5)	2446.77(16)
Z	2	2
D_{calced}, g cm^{-3}	1.306	1.289
F(000)	1286.00	1006.00
μ, cm^{-1}	4.296	4.020
cryst size, mm	0.60 × 0.50 × 0.20	0.20 × 0.10 × 0.10
T, K	123	103
2θ_{max}, deg	55.0	55.0
reflns. obsd	14219	11151
no. of params	721	645
Flack parameter	–	0.46(2)
*R*1[a]	0.0630	0.0431
*wR*2[b]	0.1746	0.1101
GOF	1.067	1.272
max./min. $\Delta\rho$, e Å^{-3}	2.22/–1.00	2.54/–0.90

[a] $R1 = \Sigma(|F_o| - |F_c|)/\Sigma|F_o|$. [b] $wR2 = (\Sigma(w(F_o^2 - F_c^2)^2)/\Sigma w(F_o^2)^2)^{1/2}$.

Results and Discussion

Synthesis, Characterization, and Crystal Structures of Rhodium(III) Complexes. The synthetic procedures for $\mathbf{1}^{\mathbf{X}}$ and $[\mathbf{2}^{\mathbf{Y/Sol}}]^-$ are outlined in Scheme 3. First, $[Rh^I(\mathbf{L}H_2^-)(cod)]$ (cod = 1,5-cyclooctadiene) was prepared by treating $[Rh^I(cod)Cl]_2$ with $\mathbf{L}H_3$ in the presence of an equimolar amount of Et_3N in THF. The crystal structure analysis of $[Rh^I(\mathbf{L}H_2^-)(cod)]$ showed that the Rh ion is coordinated with the two nitrogen atoms of mono-deprotonated ligand $\mathbf{L}H_2^-$ at the β-diketiminate moiety and 1,5-cyclooctadiene in a η^2-π-coordination mode to adopt a square planer geometry, where the two phenol groups remain uncoordinated (Scheme 3 and Figure 2).

Scheme 3. Synthetic Scheme of $\mathbf{1}^{\mathbf{X}}$ and $[\mathbf{2}^{\mathbf{Y/Sol}}]^-$.

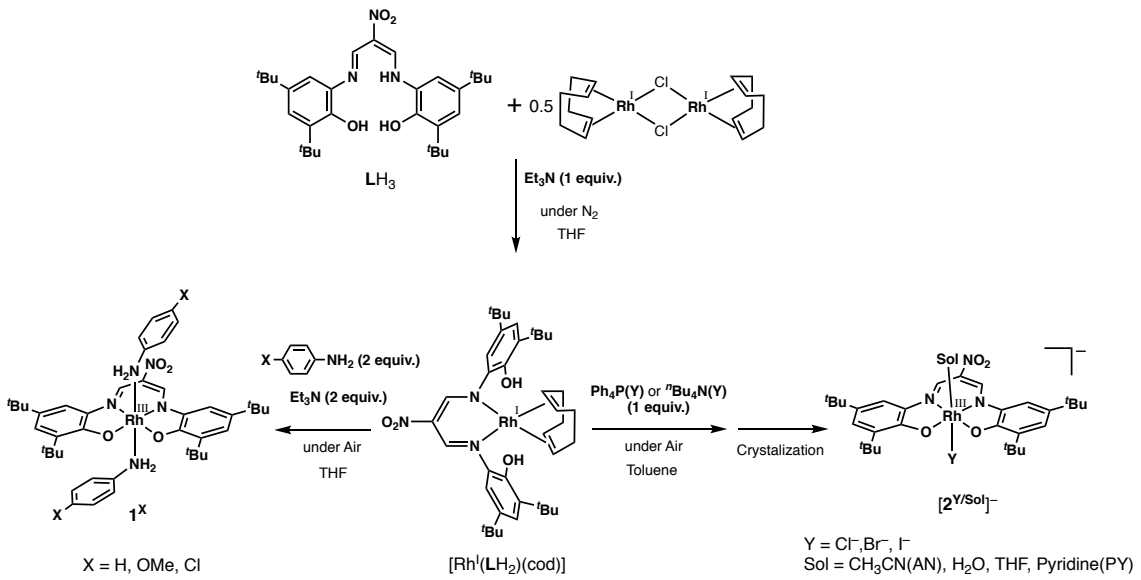

The overall geometry around the rhodium center is close to those of $[Rh^I\{\kappa^2(N,N)$-(Ar)*N*C(Me)CHC(Me)*N*(Ar)}(cod)] (Ar = 2,6-dimethylphenyl) and $[Rh^I\{\kappa^2(N,N)$-(C_6F_5)*N*C(Me)CHC(Me)*N*(C_6F_5)}(cod)].[47,48] $[Rh^I(\mathbf{L}H_2^-)(cod)]$ was employed as a starting material for the synthesis of the series of rhodium(III) complexes $\mathbf{1}^{\mathbf{X}}$ and $[\mathbf{2}^{\mathbf{Y/Sol}}]^-$ (Scheme 3). The treatment of $[Rh^I(\mathbf{L}H_2^-)(cod)]$ with aniline derivatives and 2 equivalents of Et_3N (for $\mathbf{1}^{\mathbf{X}}$) or halide anions (for $[\mathbf{2}^{\mathbf{Y/Sol}}]^-$) in air gave rhodium(III) complexes as orange solids. As for complex $[\mathbf{2}^{\mathbf{Y/Sol}}]^-$, crystallization using coordinating solvents (acetonitrile(AN), H_2O, THF, and pyridine(PY)) gave the corresponding solvent-coordinated rhodium(III) complexes, $[\mathbf{2}^{\mathbf{Y/Sol}}]^-$ (Y = Cl^-, Br^-, I^-; Sol = AN, H_2O, THF, and PY) as ^{n}Bu$_4$N salts. ^{1}H NMR spectra of the complexes displayed sharp signals in a diamagnetic region δ = 0.0–10.0 (see Experimental section). The numbers of the

observed ^{1}H signals indicate that the complexes have C_s symmetry, having a mirror plane passing through the two axial ligands, rhodium(III) center, and the carbon atom connected to the nitro group.

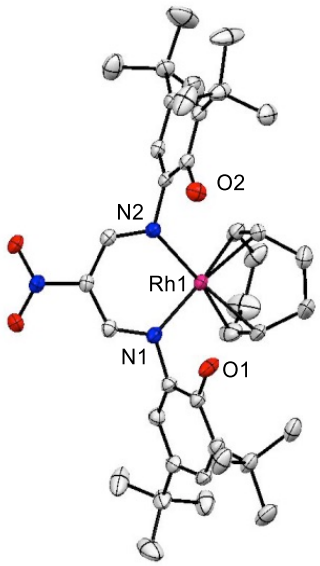

Figure 2. ORTEP diagram of $Rh^{I}(\mathbf{L}H_2^{-})$(cod) (cod = 1,5-cyclooctadiene) showing 50% ellipsoids. The solvent molecule (methanol) and hydrogen atoms are omitted for clarity.

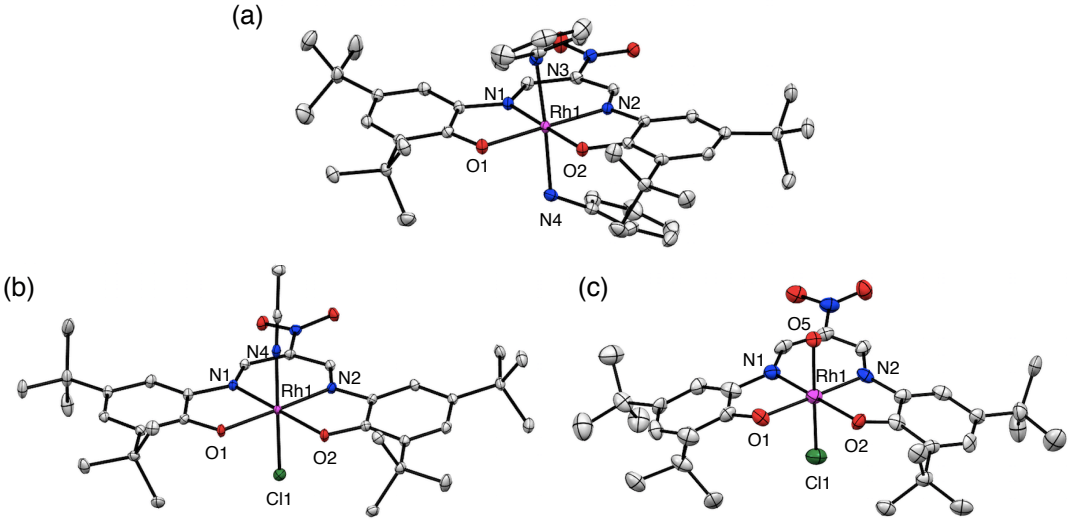

Figure 3. ORTEP diagrams of (a) $\mathbf{1}^{\mathbf{H}}$, (b) ^{n}Bu$_4$N[$\mathbf{2}^{\mathbf{ClAN}}$], and (c) ^{n}Bu$_4$N[$\mathbf{2}^{\mathbf{ClH2O}}$] showing 50% ellipsoids. Hydrogen atoms, counter cations, and solvent molecules are omitted for clarity.

Figure 3 shows ORTEP drawings of the crystal structures of the anionic parts of $\mathbf{1^H}$, ^{n}Bu$_4$N[$\mathbf{2^{Cl/AN}}$], and ^{n}Bu$_4$N[$\mathbf{2^{Cl/H2O}}$], respectively. Table 3 lists the selected bond lengths and angles of the complexes. The Rh1 atom of ^{n}Bu$_4$N[$\mathbf{2^{Cl/AN}}$] is coordinated by two oxygen atoms, O1 and O2, and two nitrogen atoms, N1 and N2, from the tetradentate ligand $\mathbf{L}^{3-}$, acetonitrile nitrogen atom, N4, and chloride anion Cl1. The N4–Rh1–Cl1 bond angle is 176.77(6)°, indicating that the rhodium center adopt an octahedral geometry. The structure of tetradentate ligand moiety $\mathbf{L}^{3-}$ is quite close to those of the reported ^{n}Bu$_4$N[M^{II}($\mathbf{L}^{3-}$)] (M = Ni, Cu, and Pd) complexes.[30,31] Brown proposed the metrical oxidation states that represent the oxidation states of 2-amidophenolato rings calculated from the crystal structures, where dianionic amidophenolato, namely fully reduced state, exhibits the metrical oxidation state of –1.6 to –2.3.[49] The present complex $\mathbf{1^H}$ showed metrical oxidation states (MOS) of –1.68(20)/–1.74(18) for the two amidophenolato rings. The overall structures and dimensions of ^{n}Bu$_4$N[$\mathbf{2^{Cl/AN}}$] and ^{n}Bu$_4$N[$\mathbf{2^{Cl/H2O}}$] are close to those of $\mathbf{1^H}$, and the metrical oxidation states of the ligands in ^{n}Bu$_4$N[$\mathbf{2^{Cl/AN}}$] and ^{n}Bu$_4$N[$\mathbf{2^{Cl/H2O}}$] are –1.76(16)/–1.58(17) and −1.55(26)/−1.91(18), respectively (Table 3). These results clearly indicate that the tetradentate ligands in the three complexes take a fully reduced trianionic form, $\mathbf{L}^{3-}$.

Table 3. Selected bond lengths (Å) and angles (°) and metrical oxidation states of the amidophenolato moieties of $\mathbf{1^H}$, ^{n}Bu$_4$N[$\mathbf{2}^{Cl/AN}$], and ^{n}Bu$_4$N[$\mathbf{2}^{Cl/H2O}$].

	$\mathbf{1^H}$	^{n}Bu$_4$N[$\mathbf{2^{Cl/AN}}$]	^{n}Bu$_4$N[$\mathbf{2^{Cl/H2O}}$]
Rh1－N3/Cl1	2.0867(14)	2.3103(6)	2.279(2)
Rh1－N4/O5	2.0866(14)	2.0218(17)	2.118(4)
Rh1－O1	2.0072(12)	2.0294(15)	2.044(5)
Rh1－O2	2.0190(11)	2.0468(18)	2.044(3)
Rh1－N1	1.9763(13)	1.985(2)	1.961(4)
Rh1－N2	1.9817(13)	1.9755(18)	1.981(6)
N3/Cl1－Rh1－N4/O5	176.91(5)	176.77(6)	178.02(15)
O1－Rh1－O2	96.57(5)	98.87(7)	98.93(17)
O1－Rh1－N1	83.22(5)	82.32(7)	82.0(2)
O2–Rh1–N2	82.79(5)	82.02(8)	81.64(18)
N1－Rh1－N2	97.44(5)	96.80(8)	97.5(2)
MOS*	–1.68(20)/–1.74(18)	–1.76(16)/–1.58(17)	−1.55(26)/−1.91(18)

*Metrical oxidation states.[49]

Substitution of Axial Ligands of ^{n}Bu$_4$N[2$^{Cl/Sol}$]. The ESI-mass spectra of acetone solutions dissolving ^{n}Bu$_4$N[**2**$^{Y/Sol}$] (Y = Cl, Br, or I; Sol = CH_3CN, H_2O, or THF), beside ^{n}Bu$_4$N[**2**$^{Cl/PY}$], exhibited peak clusters corresponding to the chemical formula of [Rh^{III}(**L**$^{3-}$)(Y)]$^{-}$, lacking the coordinating solvent molecules (Sol) (see Experimental section). The results suggest that the coordinating solvents easily dissociated from the rhodium(III) center under the ESI-MS measurement conditions. In order to examine the reactivity toward the ligand substitution of ^{n}Bu$_4$N[**2**$^{Cl/Sol}$] (Sol = CH_3CN, H_2O, or THF), the substitution reaction with pyridine (PY) was carried out. Figure 4 shows a ^{1}H NMR spectral change of ^{n}Bu$_4$N[**2**$^{Cl/AN}$] upon an addition of pyridine (PY) in acetone-d_6. Although six-coordinate Werner type rhodium(III) complexes are known to be inactive in ligand substitution reactions,[50] ligand substitution of the axial solvent with PY readily occurred. The resulting spectrum was identical with that of ^{n}Bu$_4$N[**2**$^{Cl/PY}$], clearly demonstrating that the axial acetonitrile (AN) was replaced with pyridine (PY). Similar ^{1}H NMR spectral changes were observed for reactions of ^{n}Bu$_4$N[**2**$^{Cl/THF}$] and ^{n}Bu$_4$N[**2**$^{Cl/H2O}$] with pyridine (PY) in acetone-d_6 (Figure S1). The ligand exchange with pyridine completed within 30 minutes, when one equivalent of pyridine was added to acetone solutions of ^{n}Bu$_4$N[**2**$^{Cl/Y}$] (Y = AN, H_2O, THF). Thus, the binding constant between rhodium(III) and pyridine is significantly larger than those between rhodium(III) with other solvent molecules (Sol). In fact, PY of ^{n}Bu$_4$N[**2**$^{Cl/PY}$] was hardly dissociated from the rhodium center when it was dissolved in CD_3CN. Attempts to monitor the solvent-exchange reactions between ^{n}Bu$_4$N[**2**$^{Cl/Y}$] complexes (Y = AN, H_2O, or THF) to obtain the relative binding constants of Y were unsuccessful, because the ^{1}H NMR and UV-vis spectra in acetone of these complexes were nearly identical (indistinguishable).

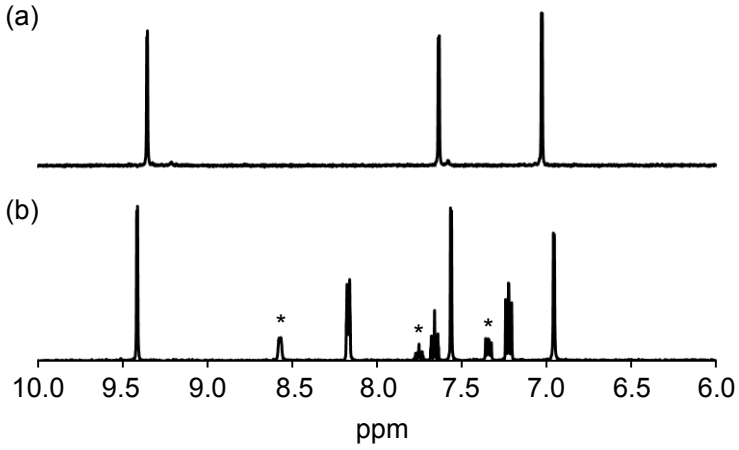

Figure 4. (a) ^{1}H NMR spectrum of ^{n}Bu$_4$N[**2**^{ClAN}] in acetone-d_6, and (b) that obtained upon addition of a slightly excess amount of pyridine. * indicates H signals of free pyridine.

Electrochemical Property of the Rhodium(III) Complexes. In order to investigate the redox properties of the rhodium(III) complexes, cyclic voltammograms of $\mathbf{1}^{\mathbf{X}}$ and $^{n}Bu_4N[\mathbf{2}^{\mathbf{Y/Sol}}]$ were measured. $\mathbf{1}^{\mathbf{H}}$ exhibited two reversible redox couples at $E_{1/2}$ = 0.22 and 0.62 V *vs*. Fc/Fc^{+}(ferrocene/ferrocenium ion) and one irreversible oxidation process at E^{pa} = 1.34 V in a range from –1.5 to +1.5 V in CH_2Cl_2 (Figure 5). Furthermore, $\mathbf{1}^{\mathbf{OMe}}$ and $\mathbf{1}^{\mathbf{Cl}}$ had also two redox couples at 0.22 and 0.61 V for $\mathbf{1}^{\mathbf{OMe}}$ and 0.26 and 0.67 V for $\mathbf{1}^{\mathbf{Cl}}$ (Table 4). The redox potentials for the two couples for the three complexes are very close to each other. $^{n}Bu_4N[\mathbf{2}^{\mathbf{Cl/AN}}]$ also showed two reversible redox waves at $E_{1/2}$ = 0.03 and 0.45 V vs Fc/Fc^{+} (ferrocene/ferrocenium ion) and an irreversible oxidation peak at E^{pa} = + 1.20 V in a range from –1.0 to +1.5 V in CH_3CN (Figure 6). The redox potentials of $^{n}Bu_4N[\mathbf{2}^{\mathbf{Y/Sol}}]$ are more negative as compared to those of $\mathbf{1}^{\mathbf{X}}$ (Table 4). This is probably due to the difference of the net charge of the complexes. The redox potentials of the first two reversible waves are quite close to those of the ligand-based consecutive oxidation of the monoanionic nickel(II), copper(II), and palladium(II) complexes $[M^{II}(\mathbf{L}^{3-})]^{-}$ reported previously; $[M^{II}(\mathbf{L}^{3-})]^{-}$ to $[M^{II}(\mathbf{L}^{\bullet 2-})]$ to $[M^{II}(\mathbf{L}^{-})]^{+}$ (Table 4).[30,31] Furthermore, other rhodium(III) complexes $^{n}Bu_4N[\mathbf{2}^{\mathbf{Br/AN}}]$, $^{n}Bu_4N[\mathbf{2}^{\mathbf{I/AN}}]$, $^{n}Bu_4N[\mathbf{2}^{\mathbf{Cl/H2O}}]$, $^{n}Bu_4N[\mathbf{2}^{\mathbf{Cl/THF}}]$, and $^{n}Bu_4N[\mathbf{2}^{\mathbf{Cl/PY}}]$ showed very close $E_{1/2}$ values regardless of whether they had different axial ligands, Br^{-}, I^{-}, H_2O, THF, and PY (Table 4). All of these results strongly indicate that the two redox couples of $^{n}Bu_4N[\mathbf{2}^{\mathbf{Y/Sol}}]$ are due to the consecutive ligand-based oxidation from $\mathbf{L}^{3-}$ to $\mathbf{L}^{\bullet 2-}$, and to $\mathbf{L}^{-}$ as in the case of consecutive ligand-based oxidation of $[M^{II}(\mathbf{L}^{3-})]^{-}$ to $[M^{II}(\mathbf{L}^{\bullet 2-})]$ to $[M^{II}(\mathbf{L}^{-})]^{+}$ (M = Ni, Cu, and Pd).[30,31]

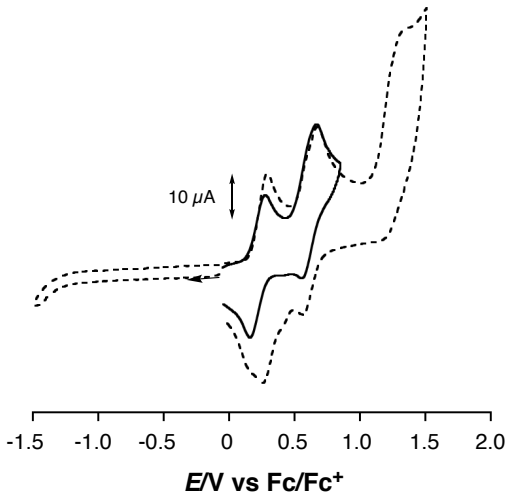

Figure 5. Cyclic voltammograms of complexes $\mathbf{1}^{\mathbf{H}}$ (1.0 mM) at room temperature in CH_2Cl_2 solution containing $^{n}Bu_4NPF_6$ (0.10 M). Working electrode: GC, counter electrode: Pt, scan rate: 100 mV/s.

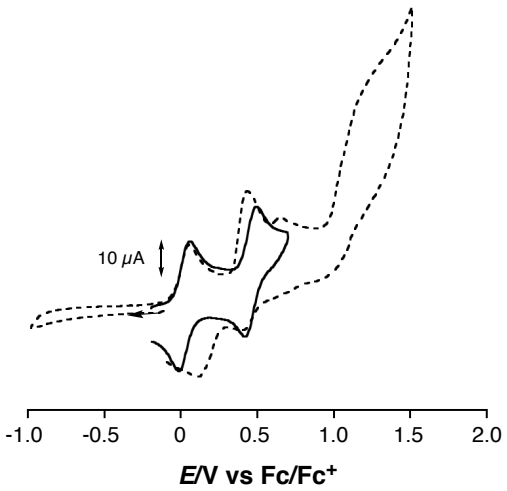

Figure 6. Cyclic voltammograms of complexes ^{n}Bu$_4$N[**2**$^{\mathbf{Cl/AN}}$] (1.0 mM) at room temperature in CH_3CN solution containing ^{n}Bu$_4$NPF$_6$ (0.10 M). Working electrode: GC, counter electrode: Pt, scan rate: 100 mV/s.

Table 4. Redox potentials ($E_{1/2}$) of **1**$^{\mathbf{X}}$, ^{n}Bu$_4$N[**2**$^{\mathbf{Y/Sol}}$], and [**M**$^{\mathbf{II}}$(**L**$^{3-}$)]$^{-}$.

Complexes	$E^1_{1/2}$ (V) [a]	$E^2_{1/2}$ (V) [a]
1$^{\mathbf{H}}$ [b]	0.22	0.62
1$^{\mathbf{OMe}}$ [b]	0.22	0.61
1$^{\mathbf{Cl}}$ [b]	0.26	0.67
^{n}Bu$_4$N[**2**$^{\mathbf{Cl/AN}}$] [c]	0.03	0.45
^{n}Bu$_4$N[**2**$^{\mathbf{Br/AN}}$] [c]	0.03	0.45
^{n}Bu$_4$N[**2**$^{\mathbf{I/AN}}$] [c]	0.01	0.44
^{n}Bu$_4$N[**2**$^{\mathbf{Cl/H2O}}$] [d]	–0.02	0.45
^{n}Bu$_4$N[**2**$^{\mathbf{Cl/THF}}$] [d]	–0.03	0.42
^{n}Bu$_4$N[**2**$^{\mathbf{Cl/PY}}$] [c]	–0.03	0.45
[Cu^{II}(**L**$^{3-}$)]$^{-}$ [b, e]	–0.06	0.46
[Ni^{II}(**L**$^{3-}$)]$^{-}$ [b, f]	0.04	0.54
[Pd^{II}(**L**$^{3-}$)]$^{-}$ [b, f]	0.07	0.54

[a] vs. Fc/Fc^+, [b] in CH_2Cl_2, [c] in CH_3CN, [d] in acetone, [e] ref. 30, [f] ref. 31

Chemical Oxidation of Complexes 1^{X} and ^{n}Bu$_4$N[2$^{Y/Sol}$]$^{-}$. To get further insight into the ligand-based oxidation of the rhodium(III) complex, the one electron-oxidized product of **1**$^{\mathbf{H}}$ was obtained by the treatment with $AgSbF_6$, and isolated as a SbF_6^- salt ([**1**$^{\mathbf{H}}$]SbF_6). Crystal structure of [**1**$^{\mathbf{H}}$]SbF_6 is shown in Figure 7, which reveals

distinct dimensional changes with respect to one of the amidophenolato moieties (ring **a**). Namely, dimensions of the two amidophenolato moieties (rings **a** and **b**) in $\mathbf{1^H}$ are very close each other, whereas ring **a** and ring **b** become inequivalent in $[\mathbf{1^H}]SbF_6$; C2–C3, C4–C5, N1–C1 and C6–O1 bonds become shorter, whereas the C1–C2, C3–C4, C5－C6 and C6–C1 are elongated (Figure 7(a) and Table S1). The results suggest that ring **a** gets contribution of a quinonoid canonical form upon the oxidation. The EPR spectrum of $[\mathbf{1^H}]SbF_6$ in CH_2Cl_2 at 100 K exhibited a typical signal for an organic radical (Figure 8). Furthermore, DFT calculated structure (B3LYP/SDD(for Rh atom), D95**(for the other atoms)) of $[\mathbf{1^H}]SbF_6$ had a dianionic radical structure of the tetradentate ligand (Figure 9). Collectively, the oxidation product can be best described as Rh^{III}-phenoxyl radial complex $[Rh^{III}(\mathbf{L}^{\bullet 2-})(PhNH_2)_2]$, in which one-electron oxidation takes place at the tetradentate ligand to give $\mathbf{L}^{\bullet 2-}$ rather than at the metal center.

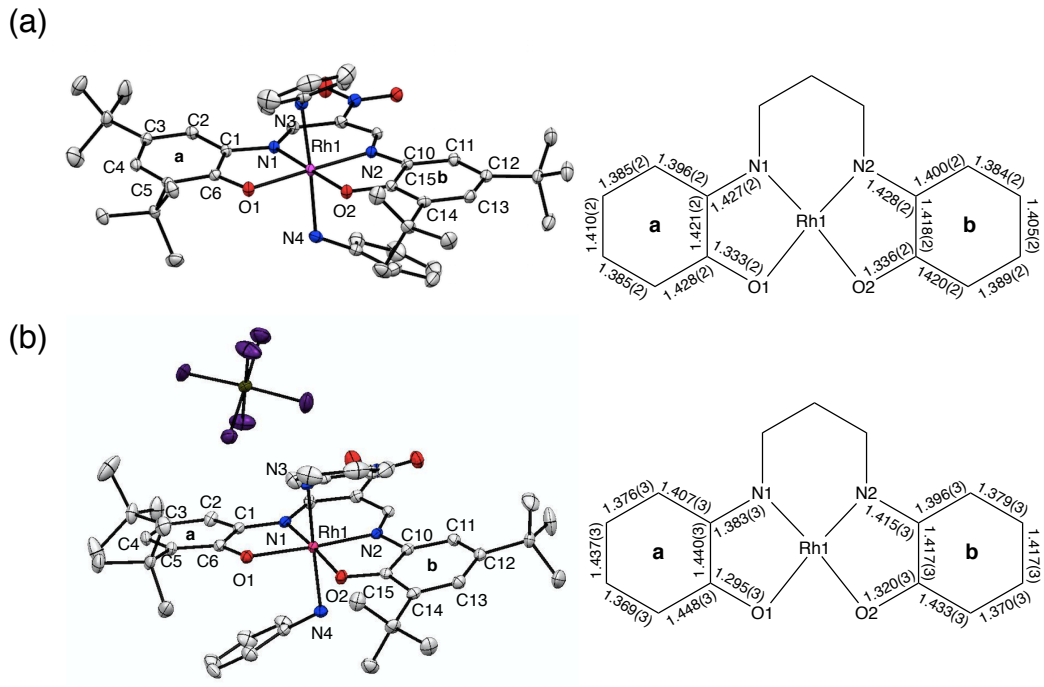

Figure 7. ORTEP diagrams of (a) $\mathbf{1^H}$ and (b) $[\mathbf{1^H}]SbF_6$ showing 50% ellipsoids (left). Selected bond lengths in ligand moiety (right). Hydrogen atoms and solvent molecules are omitted for clarity.

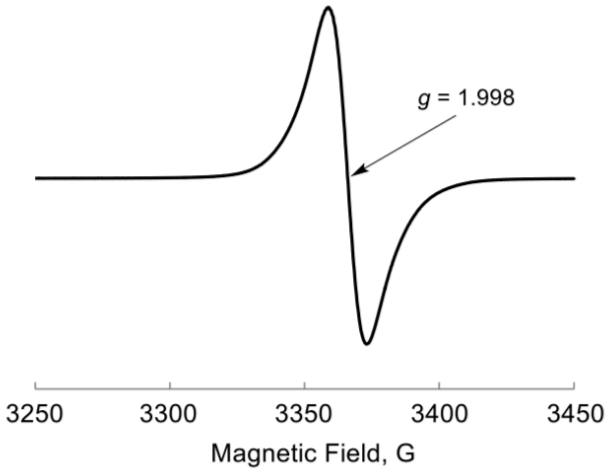

Figure 8. EPR spectrum of [$\mathbf{1}^{\mathbf{H}}$]SbF_6 (2.0 mM) in CH_2Cl_2 at 100 K.

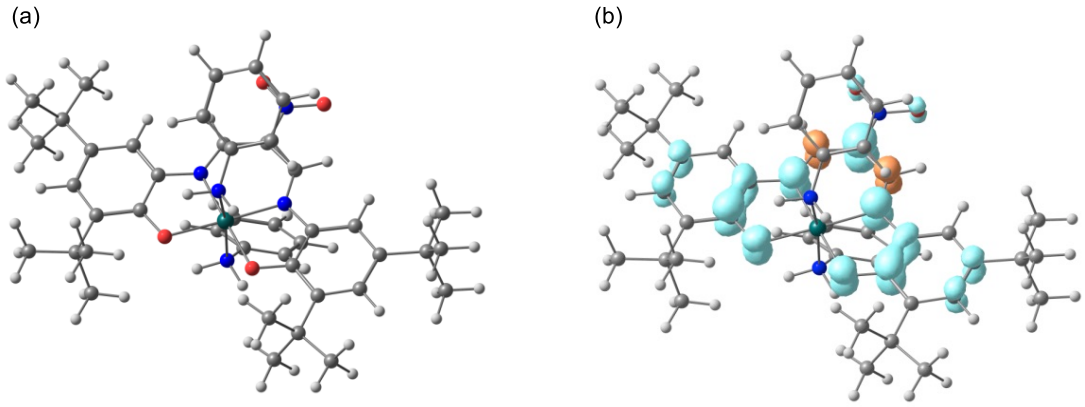

Figure 9. (a) DFT optimized structure and (b) spin density plot of [$\mathbf{1}^{\mathbf{H}}$]$^+$.

In addition, chemical oxidation of ^{n}Bu$_4$N[$\mathbf{2}^{\mathbf{Cl/AN}}$] with [(4-bromophenyl)$_3N^{\bullet+}$]$SbCl_6$ (Magic Blue, MB) was monitored by UV-vis spectroscopy at –60 °C (Figure 10). A gradual addition of MB to an acetone solution of ^{n}Bu$_4$N[$\mathbf{2}^{\mathbf{Cl/AN}}$] caused a spectral change, as shown in Figure 10a, where the intense absorption band at 470 nm due to ^{n}Bu$_4$N[$\mathbf{2}^{\mathbf{Cl/AN}}$] disappeared with concomitant appearance of new absorption bands at 540 nm (ε = 17000 M^{-1} cm^{-1}) and 660 nm (3500 M^{-1} cm^{-1}), together with a broad absorption band above 800 nm. Such a spectral change was completed when an equimolar amount of MB was added (Figure 10c), suggesting that the generated spectrum was due to the one-electron oxidized product, [Rh^{III}($\mathbf{L}^{\bullet 2-}$)(Cl)]. The appearance of the absorption band at 660 nm and the broad absorption band in the near IR (NIR) region can be ascribed to the formation

of the ligand radical species $\mathbf{L}^{\bullet 2-}$.[30,31] The addition of MB to the resulting solution of [Rh^{III}($\mathbf{L}^{\bullet 2-}$)(Cl)] resulted in a further spectral change (Figure 10b), where a new absorption band at 580 nm (ε = 11000 M^{-1} cm^{-1}) appeared with a concomitant decrease of the absorption band at 540 nm due to [Rh^{III}($\mathbf{L}^{\bullet 2-}$)(Cl)]. In this process, the NIR band over 800 nm further increased. The spectral change was completed when another one equivalent of MB was added (in total two equivalents of MB against $^{n}Bu_4N$[$\mathbf{2}^{\mathbf{Cl/AN}}$]) (Figure 10c). Thus, the generated spectrum may be due to the two-electron-oxidized complex, [Rh^{III}($\mathbf{L}^{-}$)(Cl)]$^{+}$. The broad absorption band in the NIR region is indicative of the presence of a quinonoid structure, in which the anion charge is delocalized onto the whole molecule of ligand $\mathbf{L}^{-}$.

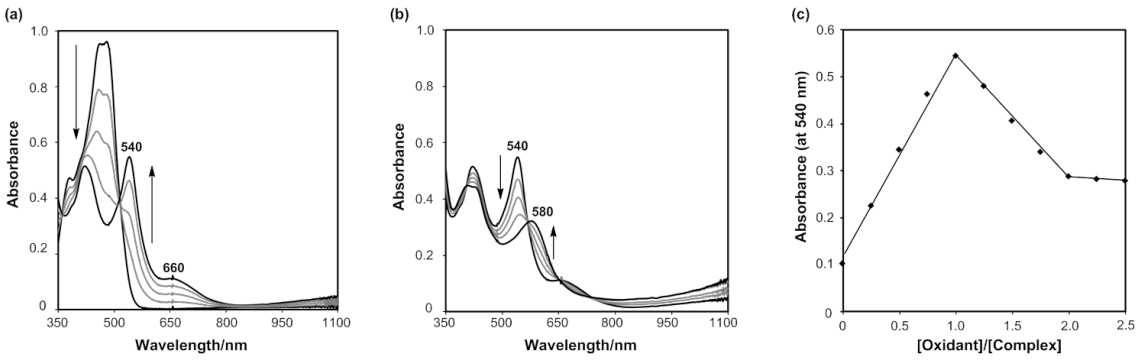

Figure 10. (a) Spectral change observed upon addition of [(4-bromophenyl)$_3N^{\bullet+}$]$SbCl_6$ (MB, 1 equiv) to $^{n}Bu_4N$[$\mathbf{2}^{\mathbf{Cl/AN}}$] (0.033 mM) in acetone at −60 °C. (b) Spectral change observed upon addition of another equivalent of MB to the resulting solution in (a). (c) Absorbance change at 540 nm in the titration experiment.

C–H Bond Amination Reaction Catalyzed by Rhodium(III) Complexes. To examine the catalytic activity of $\mathbf{1}^{\mathbf{X}}$ and $^{n}Bu_4N$[$\mathbf{2}^{\mathbf{Y/Sol}}$] in C–H amination reaction, the author employed xanthene as a substrate and tosyl azide (TsN_3) as a nitrene source. Thus, TsN_3 (35.0 μmol) was treated with the substrate (35.0 μmol) in toluene (1 mL) and $\mathbf{1}^{\mathbf{X}}$ (or $^{n}Bu_4N$[$\mathbf{2}^{\mathbf{Y/Sol}}$]) (3.50 μmol, 10 mol%) for 24 h at 100 ºC. Without the addition of the rhodium(III) complex, no amination reaction took place (Table 5, entry 1). In the cases of $\mathbf{1}^{\mathbf{X}}$, di-*tert*-butyl dicarbonate $(Boc)_2O$ was required to induce ligand-exchange reaction between the axial aniline ligand and TsN_3 (entries 3, 4, and 5). With $^{n}Bu_4N$[$\mathbf{2}^{\mathbf{Cl/AN}}$] as the catalyst, on the other hand, the C–H bond amination proceeded efficiently without adding $(Boc)_2O$ to give the aminated product *N*-xanthyl-*p*-toluenesulfonamide (**A**) in a 71 % conversion yield together with xanthone as a minor product (entry 6). The amine product (**A**) was obtained in nearly identical yields by

using ^{n}Bu$_4$N[**2**$^{\mathbf{Cl/H2O}}$] and ^{n}Bu$_4$N[**2**$^{\mathbf{Cl/THF}}$] (67 and 65 % conversion yields, respectively, entries 7 and 8). These results indicate that one of the axial solvent ligands (Sol) can be replaced with TsN_3 easier as compared to the case of the aniline ligand in **1**$^{\mathbf{H}}$ to start the catalytic cycle for the amination reaction. Because the product yields in entries 4–6 are nearly the same despite that the complex catalysts have the different axial ligands (Sol), it can be said that the axial solvent ligand (Sol = AN, H_2O, or THF) is readily replaced by TsN_3, giving the same reactive intermediate. On the other hand, the catalytic activity of ^{n}Bu$_4$N[**2**$^{\mathbf{Cl/PY}}$] was much lower than those of the former complexes because of the stronger binding of PY to the metal center (entry 7).

Table 5. Catalytic C–H bond amination of xanthene with tosyl azide.

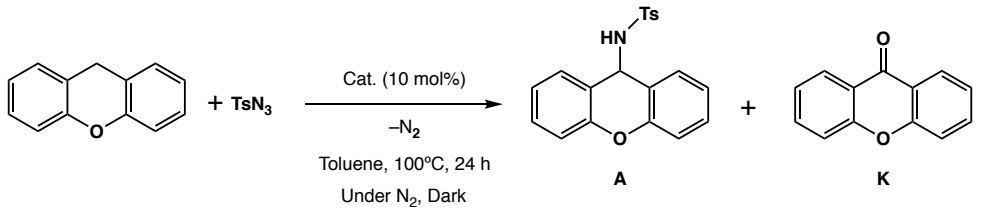

Entry	Catalyst	Additive	Conversion Yield (%)	
			A	K
1	None	None	0	0
2	**1**$^{\mathbf{H}}$	None	0	0
3	**1**$^{\mathbf{H}}$	$(Boc)_2O$[a)]	78	7
4	**1**$^{\mathbf{OMe}}$	$(Boc)_2O$[a)]	86	14
5	**1**$^{\mathbf{Cl}}$	$(Boc)_2O$[a)]	76	22
6	^{n}Bu$_4$N[**2**$^{\mathbf{Cl/AN}}$]	None	71	6
7	^{n}Bu$_4$N[**2**$^{\mathbf{Cl/H2O}}$]	None	67	5
8	^{n}Bu$_4$N[**2**$^{\mathbf{Cl/THF}}$]	None	65	5
9	^{n}Bu$_4$N[**2**$^{\mathbf{Cl/PY}}$]	None	9	14

a) 35.0 mM.

DFT Calculation. In the first step of the C–H amination, the tosyl azide complex [Rh^{III}(**L**$^{3-}$)(TsN_3)($PhNH_2$)](**1**$^{\mathbf{H}}$**-TsN$_3$**) forms *in situ,* and following dissociation of dinitrogen (N_2) from **1**$^{\mathbf{H}}$**-TsN$_3$** generates a nitrene bound rhodium complex [Rh(**L**)(NTs)($PhNH_2$)] (**1**$^{\mathbf{H}}$**-TsN**) as a key reactive intermediate. Feasibility of the

mechanism for the formation of **1^{H}-TsN** from **1^{H}-TsN$_3$** is supported by DFT calculation shown in Figure 11, where the N_2 elimination proceeds with $\Delta G^{\neq}$ = 24.3 kcal/mol. The active species **1^{H}-TsN** can be a closed-shell singlet (**1^{H}-TsN-CSS**) like [Rh^{III}(**L**$^{3-}$)(NTs)(PhNH$_2$)] or an open-shell singlet di-radical (**1^{H}-DR-OSS**) or a triplet di-radical (**1^{H}-DR-T**) of [Rh^{III}(**L**$^{\bullet 2-}$)(N$^{\bullet -}$Ts)(PhNH$_2$)]. The DFT calculation study (B3LYP/SDD (for Rh atom), D95** (for the other atoms)) indicated that **1^{H}-DR-OSS** and **1^{H}-DR-T** were close to each other in energy but energetically more stable than **1^{H}-TsN-CSS** by 13.6 and 13.7 kcal/mol, respectively. The spin density plots of **1^{H}-DR-OSS** and **1^{H}-DR-T** are shown in Figures 12(a) and 12(b), respectively, where one radical delocalizes over the redox-active tetradentate ligand to make it dianion radical structure as **L**$^{\bullet 2-}$ and another radical localizes at the nitrene nitrogen atom in both structures. The extent of the radical delocalization on the tetradentate ligand is quite close to that of [**1^{H}**]$^{+}$ (one-electron oxidized complex of **1^{H}**, Figure 9b). Therefore, the formation of the diradical species (**1^{H}-DR-OSS** or **1^{H}-DR-T**) involves an intramolecular one-electron transfer from the trianionic tetradentate ligand **L**$^{3-}$ to the nitrene nitrogen atom without change of the oxidation state of rhodium(III) center.[8-10,28,29] The calculated TsN–Rh^{III} bond length are 1.90 Å for **1^{H}-DR-OSS** and 1.99 Å for **1^{H}-DR-T**, respectively, which are significantly longer than the Rh^{III}=N double bond length in a tetrahedral complex of [Rh^{III}(NAd)(PhB(CH$_2$PPh$_2$)$_3$)] (1.780(2) Å, Ad = adamantly).[51] Thus, the calculation study suggests that TsN–Rh^{III} bond has a single bond character.

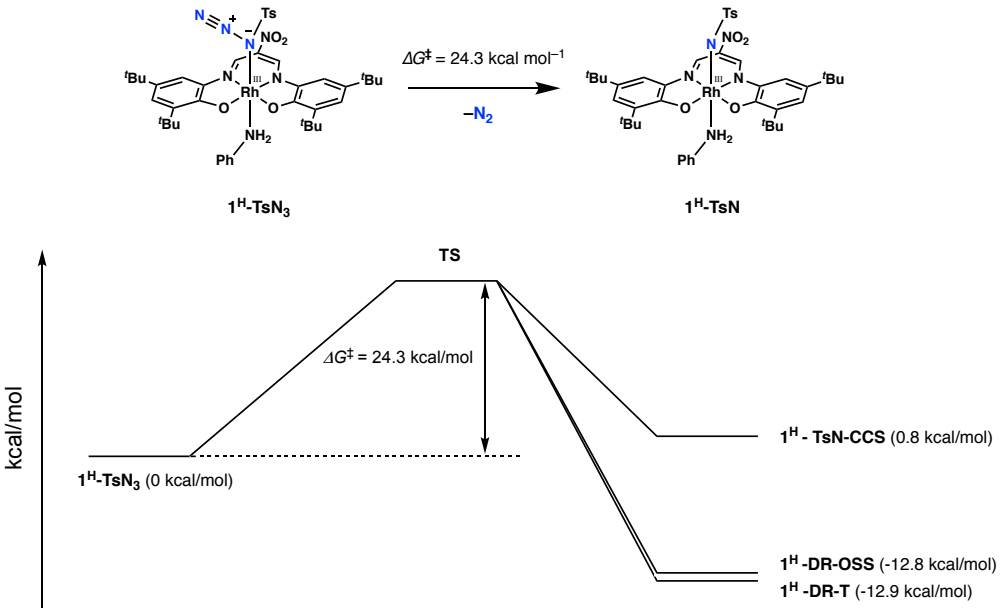

Figure 11. Free energy profile for the formation of **1^{H}-TsN**.

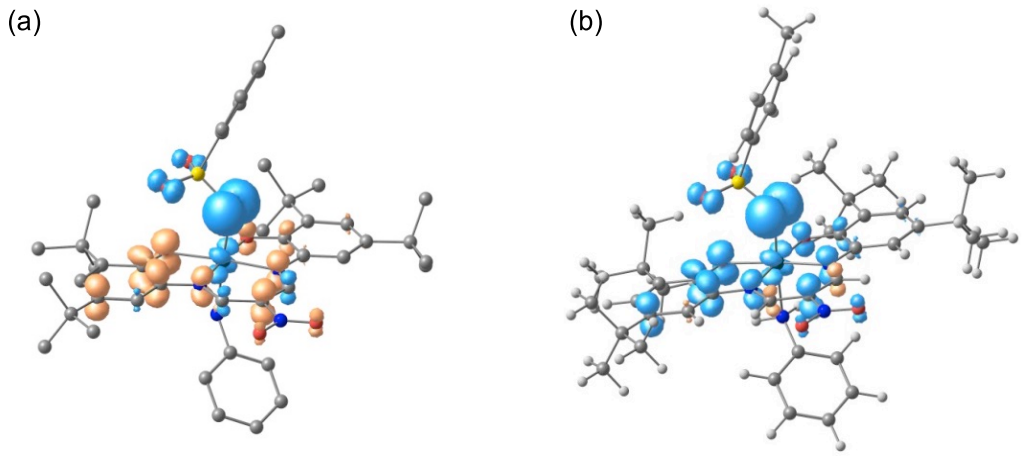

Figure 12. Spin density plots of (a) open-shell singlet (**1^{H}-DR-OSS**) and (b) triplet (**1^{H}-DR-T**) of active oxidant. The color in blue represents positive regions and the color in orange represents negative regions.

The calculated free energy profile for the C–H amination of xanthene with **1^{H}-DR-T** is displayed in Figure 13.[52] The optimized structures of the intermediates and transition states involved in the pathways are provided in Figure S3. The first step of the amination involves intermolecular H-atom abstraction from xanthene by the nitrene radical complex of **1^{H}-DR-T** to yield an intermediate **1^{H}-TsNH** and the xanthene radical (–20.1 kcal/mol). This step requires a transition state **TS2** with a barrier of 10.8 kcal/mol. Then, a subsequent radical rebound process takes place *via* a transition state **TS3** with a low barrier of 1.1 kcal/mol to yield **5^{H}**, where **TS3** and **1^{H}-TsNH(Xan)** are singlet species. When a 1 : 1 mixture of xanthene (17.5 μmol) and dideuterated-xanthene (xanthene-d_2, 17.5 μmol) were employed under the same conditions as entry 3 of Table 5, a kinetic isotope effect (KIE) of 5.0 was obtained, which was nearly the same to the calculated KIE value of 5.7 at 375 K (Figure S5, see experimental section). These results strongly support that the amination reaction involves a hydrogen atom abstraction process from the sp^3 carbon of the substrate.

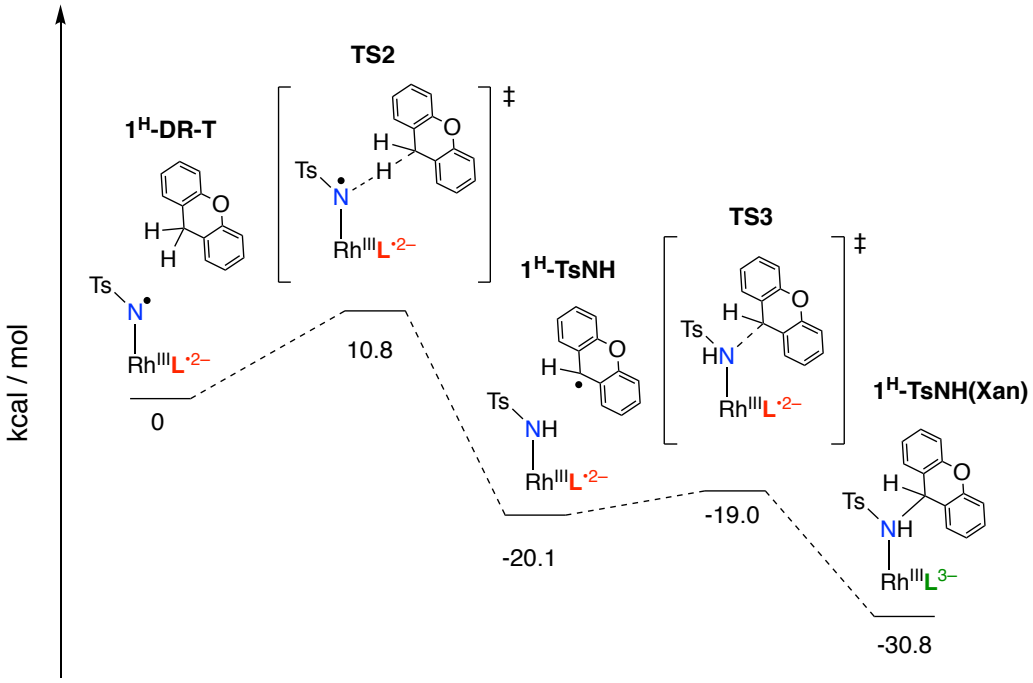

Figure 13. A computed reaction pathway for the C–H amination of xanthene. Relative SCF energies with respect to **1^{H}-DR-T** are reported in units of kcal/mol.

Direct Reaction of Rhodium(III) Complex with Organic Azides. To get further insight into the C–H amination mechanism, a fast atom bombardment-mass spectrum ((FAB-MS, positive mode) of a mixture of **1^{H}** and TsN_3 and $(Boc)_2O$, but without the substrate, in toluene was measured after the reaction at 100 °C for 24 h (Figure 14). The measured spectrum gave a peak cluster at m/z = 886.3 with an isotope distribution pattern consisting of a sum of $[Rh + \mathbf{L} + NTs + PhNH_2 + 2H]^+$ and $[Rh + \mathbf{L} + NTs + PhNH_2 + H]^+$ in a 3:2 ratio. Thus, the catalytic reaction begins from replacement of one of the two aniline ligands of **1^{H}** with TsN_3 to give $[Rh^{III}(\mathbf{L}^{3-})(N_3Ts)(PhNH_2)]$ (**1^{H}-TsN_3**), where $(Boc)_2O$ traps aniline giving C_6H_4NHBoc to enhance the replacement. However, characterization of the reaction intermediate was hampered because of a slow ligand exchange reaction between the axial aniline ligands and TsN_3.

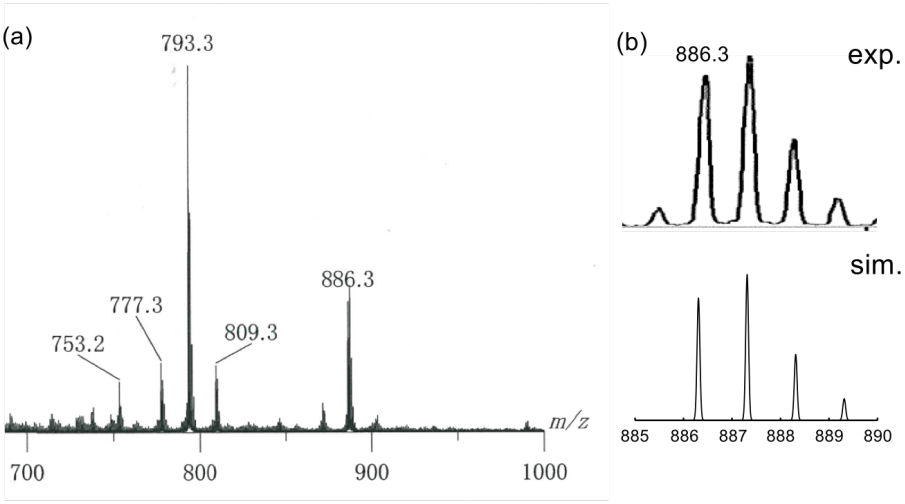

Figure 14. (a) FAB-mass spectrum (positive ion detection mode) of a reaction solution of $\mathbf{1}^{\mathbf{H}}$ with TsN_3 in the presence of $(Boc)_2O$. (b) Enlarged view of the peaks at m/z = 886.3. This isotope distribution patterns correspond to a 2:3 mixture of $[Rh+\mathbf{L}+NTs+PhNH_2+H]^+$ and $[Rh+\mathbf{L}+NTs+PhNH_2+2H]^+$.

Because the axial CH_3CN ligand of $^n Bu_4N[\mathbf{2}^{Cl/AN}]$ can be more easily replaced with the azide than $\mathbf{1}^{X}$, a direct reaction of $^n Bu_4N[\mathbf{2}^{Cl/AN}]$ and TsN_3 was examined. In a preparative-scale reaction, brown powder product $[\mathbf{3}]^-$ was obtained from the reaction in a 40 % yield as a $^n Bu_4N^+$ salt, and the yield was increased to 71%, when Ph_4P^+ was used as the counter cation. Single crystals suitable for X-ray crystallographic analysis was obtained by recrystallization of the brown power product from acetone/*n*-hexane. The crystal structure of the anionic part of the $Ph_4P[\mathbf{3}]$ is shown in Figure 15 together with the selected bond lengths and angles listed in Table 6.

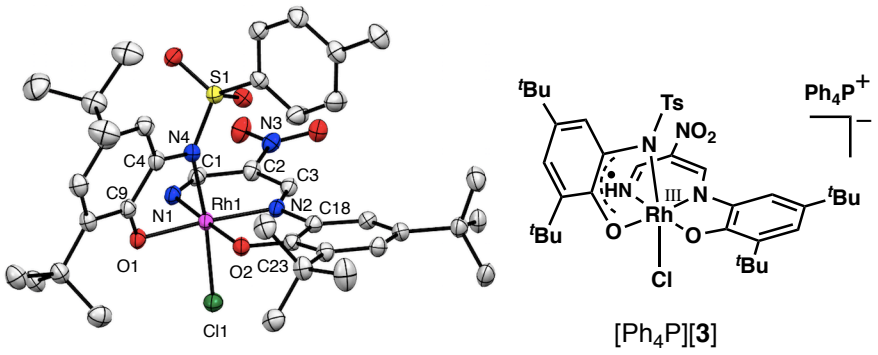

Figure 15. (left) Crystal structure of the anionic part of complex $Ph_4P[\mathbf{3}]$ showing 50% ellipsoids. Hydrogen atoms and counter cation are omitted for clarity. (right) A chemical structure of $Ph_4P[\mathbf{3}]$.

Table 6. Selected bond Lengths (Å) and angles (º) of Ph_4P[**3**] and **4**$^{(aniline\text{-}OMe)}$.

	Ph_4P[**3**]	**4**$^{(aniline\text{-}OMe)}$
Rh1−Cl1/N3	2.3318(8)	2.021(2)
Rh1−O1	2.031(2)	2.032(3)
Rh1−O2	2.000(2)	2.049(3)
Rh1−N1	2.005(3)	1.969(4)
Rh1−N2	1.972(2)	1.989(4)
Rh1−N4	2.073(2)	2.104(2)
Cl1/N3－Rh1－N4	173.10(7)	176.44(10)
O1－Rh1－O2	87.32(9)	99.45(13)
O1－Rh1－N1	94.72(10)	81.66(15)
N1－Rh1－N2	93.54(10)	95.89(16)
N1－Rh1－O2	177.95(9)	178.89(14)
N2－Rh1－O2	84.42(10)	83.00(14)
MOS*	−0.97(12)/ −1.64(23)	−1.61(23)/−2.03(13)

*Metrical oxidation states.[49]

As can be clearly seen, one of the phenolate moieties of $\mathbf{L}^{3-}$ is detached from the *β*-diketiminate unit, and the detached phenolate is aminated by TsN group. Thus, the Rh1 center is coordinated with two nitrogen atoms, N1 and N2, and one oxygen atom, O2, from the original ligand and one nitrogen atom, N4, and one oxygen atom, O1, from the newly formed aminated phenolate moiety. The Cl^- anion remained on the rhodium center to make a slightly distorted octahedral geometry. With respect to the structural parameters of the aminated phenolate moiety, the C9–O1 bond length of 1.289(3) Å is in a range of bond order of 1.5 and sum of the bond angles comprising S1–N4–C4, C4–N4–Rh1, and S1–N4–Rh1 is 359.8º. The metrical oxidation state (MOS) of the aminated phenolate moiety is − 0.97(12). These data indicate that the aminated phenolate moiety can be best described as iminosemiquinone radical, which is origin of the paramagnetic character of the complex as indicated by the EPR spectrum. The EPR spectrum of the solution of Ph_4P[**3**] showed a typical signal for an organic radical (g = 1.998, Figure 16). The DFT calculation (UB3LYP/def2-TZVP) also supported the iminosemiquinone radical structure. As clearly shown in Figure 17, most of the spin is located on the aminated phenolate moiety, indicating the iminosemiquinone radical structure.

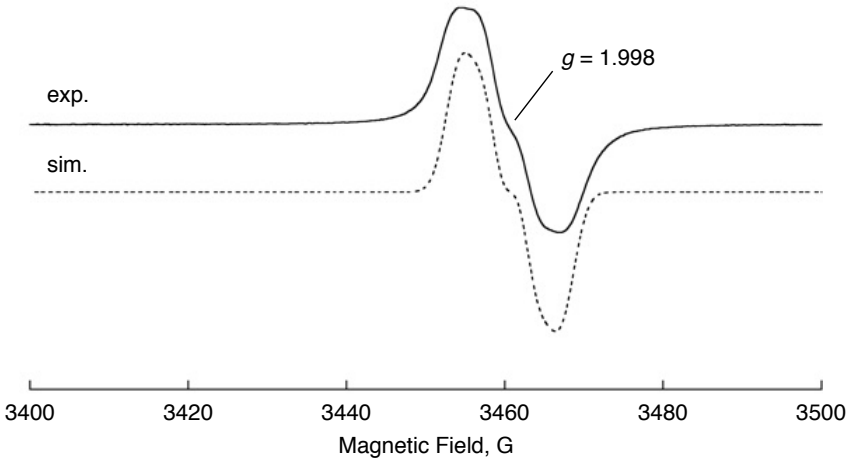

Figure 16. EPR spectrum of Ph_4P[**3**] (5.0 mM) in chlorobenzene at 60°C.

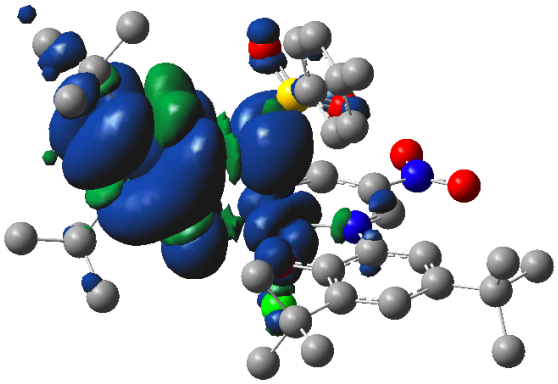

Figure 17. DFT (UB3LYP/def2-TZVP) calculated spin density plot for complex $[\mathbf{3}]^-$. Blue represents an excess of α spin density and green represents an excess of β spin density.

Regarding to the original ligand moiety, the C23–O2 and C18–N2 bond lengths of 1.323(4) Å and 1.433(4) Å, respectively, are in a range of the C–O and C–N single bonds that observed in the $[M^{II}(\mathbf{L}^{3-})]^-$ (M = Cu, Ni, and Pd) complexes.[30,31] The metrical oxidation state of the ring is –1.64(23), which is consistent with a value for a structure of an amidophenolato ring. The dianionic state of the tridentate ligand moiety may be stabilized due to strong electron-withdrawing nature of the nitro group at C2.

When the reaction of ^{n}Bu$_4$N[$\mathbf{2}^{\mathbf{Cl/AN}}$] (0.054 mM) and TsN_3 (2.5 mM) was monitored by UV-vis spectroscopy, the absorption band at 470 nm due to ^{n}Bu$_4$N[$\mathbf{2}^{\mathbf{Cl/AN}}$] (solid line)

disappeared with concomitant appearance of a new broad absorption band at 550 nm (dotted line) as shown in Figure 18. The UV-vis spectrum of the brown powder of [**3**]$^{-}$ was identical to that of a product generated in situ by treating ^{n}Bu$_4$N[**2**$^{\mathbf{Cl/AN}}$] with an excess amount of TsN$_3$ (Figure 18, dotted line). The absorption band at 550 nm and the broad band in the NIR region can be ascribed to the formation of iminosemiquinone radical of [**3**]$^{-}$, since the one-electron oxidized complex of ^{n}Bu$_4$N[**2**$^{\mathbf{Cl/AN}}$] has similar absorption bands at 660 nm and in a NIR region (Figure 10(a)). The ESI-MS of a solution containing ^{n}Bu$_4$N[**2**$^{\mathbf{Cl/AN}}$] and an excess amount of TsN$_3$ exhibited a peak cluster at m/z = 828.2, which is consistent with the molecular formula of [**3**]$^{-}$, [Rh + Cl + ^{t}Bu$_2$C$_6$H$_2$O(TsN)] + ^{t}Bu$_2$C$_6$H$_2$O(β-diketiminate)]$^{-}$.

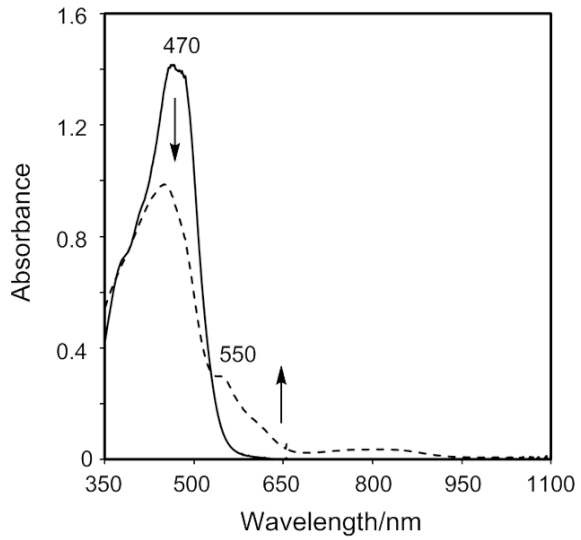

Figure 18. Absorption spectral change of ^{n}Bu$_4$N[**2**$^{\mathbf{Cl/AN}}$] (0.054 mM) upon addition of TsN$_3$ (2.5 mM) at room temperature in acetone.

Because [**3**]$^{-}$ was formed from [**2**$^{\mathbf{Cl/AN}}$]$^{-}$ by the reaction with TsN$_3$ in the absence of the substrate, [**3**]$^{-}$ might be a degradation product of the active species in the C–H bond amination. On the basis of DFT calculations, the author has proposed that the active species for the C–H amination is the diradical complex, [Rh$^{\mathrm{III}}$(Cl)(**L**$^{\bullet 2-}$)($^{\bullet}$NTs)] ([**2**$^{\mathbf{Cl}}$**-DR**]$^{-}$ in Scheme 4). Thus, [**3**]$^{-}$ might be formed from [**2**$^{\mathbf{Cl}}$**-DR**]$^{-}$ intermediate via intramolecular radical coupling between the radical moiety of **L**$^{\bullet 2-}$ and the nitrene radical moiety (N$^{\bullet}$Ts), as shown in Scheme 4.

To generate [**3**]$^{-}$ from [**2**$^{\mathbf{Cl}}$**-DR**]$^{-}$, hydrogen atom (H$^{\bullet}$) transfer or proton-coupled electron transfer (H^{+}/e^{-}) reduction should occur after the intramolecular C–N bond formation. To find such a reductant, the reaction of ^{n}Bu$_4$N[**2**$^{\mathbf{Cl/AN}}$] and TsN$_3$ was carried

out in acetone containing D_2O. In this case, a mono-deuterated complex, $^{n}Bu_4N$[**3**-D], was obtained as confirmed by ESI-MS (Figure 19). Thus, water contained in the solvent might be a reductant for the formation of [**3**]$^-$ from [**2**^{Cl}**-DR**]$^-$ (Scheme 4).

Scheme 4. A possible mechanism for the formation of [**3**]$^-$ from [**2**^{Cl}**-DR**]$^-$ intermediate.

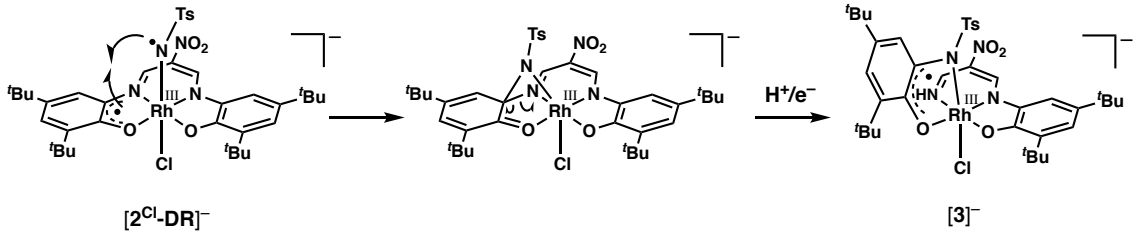

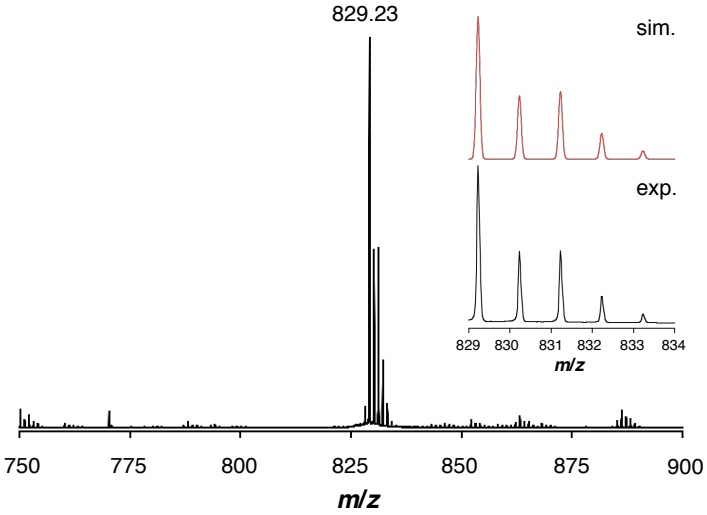

Figure 19. ESI-mass spectrum (negative ion detection mode) of reaction mixture of $^{n}Bu_4N$[**2**$^{Cl/AN}$] and TsN_3 in D_2O/acetone. Inset: Comparison of experimental spectrum (black) and simulated spectrum calculated as $C_{38}H_{49}D_1Rh_1S_1O_6N_4Cl$ (red).

Interestingly, the catalytic amination of xanthene also proceeded using Ph_4P[**3**] instead of Ph_4P[**2**$^{Y/Sol}$] as the catalyst, giving **A** (49 %) and **B** (5 %). Thus, the amination reactions by $^{n}Bu_4N$[**2**$^{Y/Sol}$] may involve not only the diradical intermediate [**2**^{Cl}**-DR**]$^-$ but also a different active intermediate derived from [**3**]$^-$, although mechanistic details are not clear at this stage.

van der Vlugt and co-workers reported an intramolecular amination-cyclization of 4-phenylbutaneazide by the reaction with palladium(II) of an amidophenolato-based pincer ligand in the presence of $(Boc)_2O$, giving a pyrrolidine derivative.[28, 29] Thus, the author

also examined the direct reaction of ^{n}Bu$_4$N[**2**$^{Cl/AN}$] and 4-phenylbutaneazide. In this reaction, a red powder of ^{n}Bu$_4$N[**4**^{Cl}] was isolated in a 60% yield. In the ^{1}H NMR spectrum in CD_3CN, the product showed one doublet at δ = 8.54 ppm with J = 21.2 Hz and one doublet of triplet at δ = 7.52 ppm with J = 21.2 Hz and J = 6.0 Hz (see the Experimental section). The appearance of such doublets having a large coupling constant suggests imine bond formation adopting an *E*-configuration. The author could not obtain single crystals of ^{n}Bu$_4$N[**4**^{Cl}]. However, when the methoxy-aniline derivative of **1**^{OMe} was treated with 4-phenylbutaneazide, the author was able to isolate red single crystals of the product, **4**$^{(aniline\text{-}OMe)}$. The ^{1}H NMR spectrum of **4**$^{(aniline\text{-}OMe)}$ also showed one doublet at δ = 7.77 ppm with J = 21.2 Hz and one doublet of triplet at 7.38 ppm with J = 21.2 Hz as in the case of ^{n}Bu$_4$N[**4**^{Cl}]. Crystal structure of **4**$^{(aniline\text{-}OMe)}$ is shown in Figure 20.

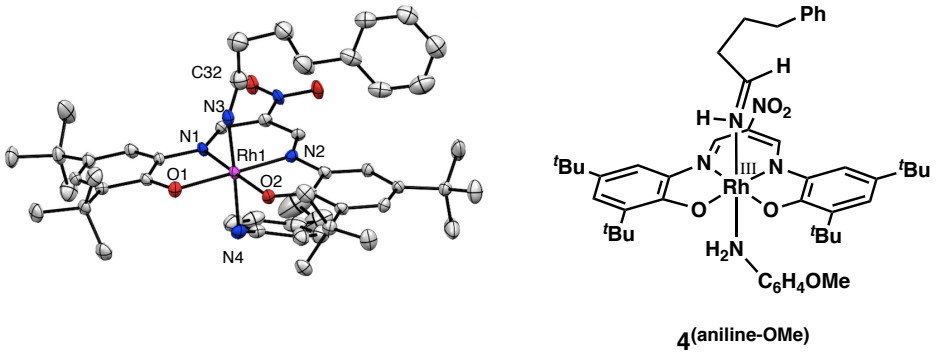

4$^{(aniline\text{-}OMe)}$

Figure 20. (Left) Crystal structure of the anionic part of complexes **4**$^{(aniline\text{-}OMe)}$ showing 50% ellipsoids. Hydrogen atoms and counter cation are omitted for clarity. (Right) Chemical structure of **4**$^{(aniline\text{-}OMe)}$.

The Rh1 atom is coordinated with two oxygen atoms, O1 and O2, and two nitrogen atoms, N1 and N2, from the tetradentate ligand, $\mathbf{L}^{3-}$, in the basal plane and one aniline nitrogen atom, N4, and one imine nitrogen atom, N3, from the axial positions, forming a distorted octahedral structure. As can be clearly seen, an intramolecular amination-cyclization of the azide did not occur, but an imine product having an *E*-configuration was formed, as suggested by the ^{1}H NMR data. The N3–C32 bond length of 1.275(4) Å is consistent with that of an N=C double bond. The dimensions of the tetradentate ligand are very close to those of **1**^{OMe}, ^{n}Bu$_4$N[**2**$^{Cl/AN}$], and ^{n}Bu$_4$N[**2**$^{Cl/H2O}$], and the metrical oxidation states of the two amidophenolato rings are –1.61(23) and –2.03(13), indicating that the ligand has trianionic form ($\mathbf{L}^{3-}$). Thus, it is safely concluded that ^{n}Bu$_4$N[**4**^{Cl}] generated from ^{n}Bu$_4$N[**2**$^{Cl/AN}$] also has an imine ligand derived from 4-phenylbutaneazide at the

axial position as in the case of **4**$^{(aniline\text{-}OMe)}$. Because Lewis acid catalyzed decomposition of alkyl azides to imines is well known,[53] the rhodium(III) complex ^{n}Bu$_4$N[**2**$^{Cl/H2O}$] might work as a Lewis acid in this reaction.

Conclusion

Werner type six-coordinate rhodium(III) complexes (**1**^{x}, ^{n}Bu$_4$N[**2**$^{Y/Sol}$]) coordinated by a redox-active tetradentate ligand **L**$^{3-}$ were synthesized and characterized. The remaining axial coordination sites were occupied with aniline derivatives (**1**^{x}) or halide anions (Y^{-}) and solvent molecules (Sol) (^{n}Bu$_4$N[**2**$^{Y/Sol}$]) to complete a distorted octahedral rhodium(III) center. The complexes were found to undergo the ligand-based oxidation with electrochemical and chemical methods to give a ligand radical complexes, formation of which was supported by CV, EPR, X-ray crystallography, and DFT calculation. The complexes are capable to catalyze the intermolecular C–H amination reaction of xanthene with tosyl azide. Possible reaction pathways are presented in Scheme 5.

Scheme 5. Reaction pathways in the catalytic amination reaction and formation of complex **3**.

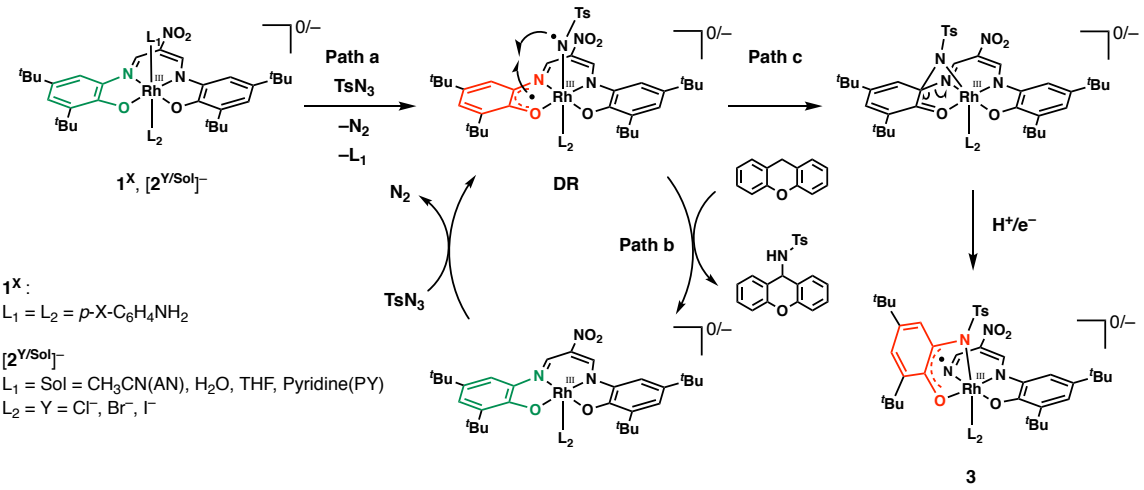

First of all, the active oxidant for the amination reaction, nitrene radical bound rhodium(III) complex **DR**, is formed via one-electron transfer from the redox-active tetradentate ligand **L**$^{3-}$ to the nitrene nitrogen atom as DFT calculation supported (path a). This intermediate induces the amination reaction of the external substrate (path b). In the absence of the substrate, on the other hand, intermediate **DR** decomposes to afford an NTs bound iminosemiquinone and a modified NNO tridentate ligand (path c). This

process may involve intramolecular radical coupling between the nitrene radical moiety and the phenoxyl radical moiety of $\mathbf{L}^{\bullet 2-}$. Thus, the present results strongly support the formation of nitrene radical complex supported by ligand radical (intermediate **DR**). The present study provides one of the rare examples of a nitrene radical metal complex generated by the combination of *a redox-active ligand* and a redox-innocent metal ion, that can be adopted for the catalytic C–H bond functionalization.

References

(1) Fantauzzi, S.; Caselli, A.; Gallo, E. *Dalton Trans.* **2009,** *28*, 5434–5443.

(2) Lu, H.; Zhang, X. P. *Chem. Soc. Rev.* **2011,** *40*, 1899–1909.

(3) Collet, F.; Lescot, C; Dauban, P. *Chem. Soc. Rev.* **2011,** *40*, 1926–1936.

(4) Che, C.-M.; Lo, V. K.-Y.; Zhou, C.-Y.; Huang, J.-S. *Chem. Soc. Rev.* **2011,** *40*, 1950–1975.

(5) Roizen, J. L.; Harvey, M. E.; Du Bois, J. *Acc. Chem. Res.* **2012,** *45*, 911–922.

(6) Intrieri, D.; Zardi, P.; Caselli, A.; Gallo, E. *Chem. Commun.* **2014,** *50*, 11440–11453.

(7) Park, Y.; Kim, Y.; Chang, S. *Chem. Rev.* **2017,** *117*, 9247–9301.

(8) Zhou, W.; Patrick, B. O.; Smith, K. M. *Chem. Commun.* **2014,** *50*, 9958–9960.

(9) Bagh, B.; Broere, D. L. J.; Sinha, V.; Kuijpers, P. F.; van Leest, N. P.; de Bruin, B.; Demeshko, S.; Siegler, M. A.; van der Vlugt, J. I. *J. Am. Chem. Soc.* **2017,** *139*, 5 117–5124.

(10) Ren, Y.; Cheaib, K.; Jacquet, J.; Vezin, H.; Fensterbank, L.; Orio, M.; Blanchard, S.; Desage-El Murr, M. *Chem. -Eur. J.* **2018,** *24*, 5086–5090.

(11) Romão, C. C.; Kühn, F. E.; Herrmann, W. A. *Chem. Rev.* **1997,** *97*, 3197–3246.

(12) Eikey, R. A.; Abu-Omar, M. M. *Coord. Chem. Rev.* **2003,** *243*, 83–124.

(13) *Comprehensive Coordination Chemistry II*. Elsevier Pergamon: Amsterdam, 2004; Vol. 4.

(14) *Comprehensive Coordination Chemistry II*. Elsevier Pergamon: Amsterdam, 2004; Vol. 5.

(15) Hazari, N.; Mountford, P. *Acc. Chem. Res.* **2005,** *38*, 839–849.

(16) Schrock, R. R. *Chem. Rev.* **2009,** *109*, 3211–3226.

(17) Ray, K.; Heims, F.; Pfaff, F. F. *Eur. J. Inorg. Chem.* **2013,** 2013, 3784–3807.

(18) Suarez, A. I. O.; Lyaskovskyy, V.; Reek, J. N. H.; van der Vlugt, J. I.; de Bruin, B. *Angew. Chem., Int. Ed.* **2013,** *52*, 12510–12529.

(19) Kuijpers, P. F.; van der Vlugt, J. I.; Schneider, S.; de Bruin, B. *Chem.–Eur. J.* **2017,** *23*, 13819–13829.

(20) Kuijpers, P. F.; Tiekink, M. J.; Breukelaar, W. B.; Broere, D. L. J.; van Leest, N.

P.; van der Vlugt, J. I.; Reek, J. N. H.; de Bruin, B. *Chem.–Eur. J.* **2017,** *23*, 7945–7952.

(21) Lyaskovskyy, V.; Suarez, A. I. O.; Lu, H.; Jiang, H.; Zhang, X. P.; de Bruin, B. *J. Am. Chem. Soc.* **2011,** *133*, 12264–12273.

(22) Goswami, M.; Lyaskovskyy, V.; Domingos, S. R.; Buma, W. J.; Woutersen, S.; Troeppner, O.; Ivanović-Burmazović, I.; Lu, H.; Cui, X.; Zhang, X. P.; Reijerse, E. J.; DeBeer, S.; van Schooneveld, M. M.; Pfaff, F. F.; Ray, K.; de Bruin, B. *J. Am. Chem. Soc.* **2015,** *137*, 5468–5479.

(23) Nurdin, L.; Spasyuk, D. M.; Piers, W. E.; Maron, L. *Inorg. Chem.* **2017,** *56*, 4157–4168.

(24) King, E. R.; Hennessy, E. T.; Betley, T. A. *J. Am. Chem. Soc.* **2011,** *133*, 4917–4923.

(25) Wilding, M. J. T.; Iovan, D. A.; Betley, T. A. *J. Am. Chem. Soc.* **2017,** *139*, 12043–12049.

(26) Wilding, M. J. T.; Iovan, D. A.; Wrobel, A. T.; Lukens, J. T.; MacMillan, S. N.; Lancaster, K. M.; Betley, T. A. *J. Am. Chem. Soc.* **2017,** *139*, 14757–14766.

(27) Kundu, S.; Miceli, E.; Farquhar, E.; Pfaff, F. F.; Kuhlmann, U.; Hildebrandt, P.; Braun, B.; Greco, C.; Ray, K. *J. Am. Chem. Soc.* **2012,** *134*, 14710–14713.

(28) Broere, D. L. J.; de Bruin, B.; Reek, J. N. H.; Lutz, M.; Dechert, S.; van der Vlugt, J. I. *J. Am. Chem. Soc.* **2014,** *136*, 11574–11577.

(29) Broere, D. L. J.; van Leest, N. P.; de Bruin, B.; Siegler, M. A.; van der Vlugt, J. I. *Inorg. Chem.* **2016,** *55*, 8603–8611.

(30) Takaichi, J.; Ohkubo, K.; Sugimoto, H.; Nakano, M.; Usa, D.; Maekawa, H.; Fujieda, N.; Nishiwaki, N.; Seki, S.; Fukuzumi, S.; Itoh, S. *Dalton Trans.* **2013,** *42*, 2438–2444.

(31) Morimoto, Y.; Takaichi, J.; Hanada, S.; Ohkubo, K.; Sugimoto, H.; Fujieda, N.; Fukuzumi, S.; Itoh, S. *J. Porphyrins. Phthalocyanines* **2015,** *19*, 377–387.

(32) Perrin, D. D.; Armarego, W. L. F.; Perrin, D. R. *Purification of Laboratory Chemicals 4th Edition*. 4th ed.; Pergamon Press: Elmsford, NY, 1996.

(33) Giordano, G.; Crabtree, R. H. *Inorg. Syn.*, **1990**, *28*, 88–90.

(34) Hajibabaei, K.; Boeini, H. Z. *Synlett*, **2014**, *25*, 2044–2048.

(35) Hennessy, E. T.; Betley, T. A. *Science*, **2013**, *340*, 591–595.

(36) Lewandowska-Andralojc, A.; Grills, D. C.; Zhang, J.; Bullock, R. M.; Miyazawa, A.; Kawanishi, Y.; Fujita, E. *J. Am. Chem. Soc.*, **2014**, *136*, 3572–3578.

(37) Frisch, M. J.; Trucks, G. W.; Schlegel, H. B.; Scuseria, G. E.; Robb, M. A.; Cheeseman, J. R.; Scalmani, G.; Barone, V.; Mennucci, B.; Petersson, G. A.;

Nakatsuji, H.; Caricato, M.; Li, X.; Hratchian, H. P.; Izmaylov, A. F.; Bloino, J.; Zheng, G.; Sonnenberg, J. L.; Hada, M.; Ehara, M.; Toyota, K.; Fukuda, R.; Hasegawa, J.; Ishida, M.; Nakajima, T.; Honda, Y.; Kitao, O.; Nakai, H.; Vreven, T.; Montgomery, J., J. A.; Peralta, J. E.; Ogliaro, F.; Bearpark, M.; Heyd, J. J.; Brothers, E.; Kudin, K. N.; Staroverov, V. N.; Kobayashi, R.; Normand, J.; Raghavachari, K.; Rendell, A.; Burant, J. C.; Iyengar, S. S.; Tomasi, J.; Cossi, M.; Rega, N.; Millam, J. M.; Klene, M.; Knox, J. E.; Cross, J. B.; Bakken, V.; Adamo, C.; Jaramillo, J.; Gomperts, R.; Stratmann, R. E.; Yazyev, O.; Austin, A. J.; Cammi, R.; Pomelli, C.; Ochterski, J. W.; Martin, R. L.; Morokuma, K.; Zakrzewski, V. G.; Voth, G. A.; Salvador, P.; Dannenberg, J. J.; Dapprich, S.; Daniels, A. D.; Farkas, O.; Foresman, J. B.; Ortiz, J. V.; Cioslowski, J.; Fox, D. J. Gaussian 09 (Revision D.01), Gaussian, Inc.: Wallingford CT, 2009.

(38) Becke, A. D. *J. Chem. Phys.,* **1993**, *98*, 5648–5652.

(39) Lee, C.; W. Yang, W.; Parr, R. G. *Phys. Rev. B*, **1988**, *37*, 785–789.

(40) Dolg, M.; Stoll, H.; Preuss, H.; Pitzer, R. M. *J. Phys. Chem.*, **1993**, *97*, 5852–5859.

(41) Dunning, T. H. Jr.; Hay, P. J. *In Modern Theoretical Chemistry*, Vol. 3; Schaefer, H. F., III, Ed.; Plenum Press: New York, 1976; pp 1.

(42) McQuarrie, D. A. Statistical Thermodynamics;University Science Book:MillValley, 1973.

(43) Weigend, F.; Ahrichs, R. *Phys. Chem. Chem. Phys.*, **2005**, *7*, 3297–3305.

(44) Dennington, I., R.; Keith, T.; Millam, J.; Eppinnett, K.; Hovell, W. L.; Gilliland, R. *GaussView, Semichem, Shawnee Mission, KS.* 2003.

(45) Burla, M. C., Caliandro, R., Camalli, M., Carrozzini, B., Cascarano, G. L., Giacovazzo, C., Mallamo, M., Mazzone, A., Polidori, G. and Spagna, R. (2012). *J. Appl. Cryst.* 45, 357–361.

(46) Crystal Structure Analysis Package, Rigaku Corporation (2000-2016). Tokyo 196-8666, Japan.

(47) Budzelaar, P. H. M.; Moonen, N. N. P.; de Gelder, R.; Smits, J. M. M.; Gal, A. W. *Eur. J. Inorg. Chem.*, **2000**, 753–769.

(48) Meier, G.; Steck, V.; Braun, B. ; Eißler, A.; Herrmann, R.; Ahrens, M.; Laubenstein, R.; Braun, T. *Eur. J. Inorg. Chem*., **2014**, 2793–2808.

(49) Brown, S. N. *Inorg. Chem.* **2012,** *51*, 1251–1260.

(50) Lincoln, S. F. *Helv. Chim. Acta* **2005,** *88*, 523–545.

(51) Geer, A. M.; Tejel, C.; López, J. A.; Ciriano, M. A. *Angew. Chem., Int. Ed*., **2014**, *53*, 5614–5618.

(52) The C–H amination profile with **1^{H}-DR-OSS** is identical with that with **1^{H}-DR-T**.

(53) L'Abbe, G. *Chem. Rev.* **1969,** *69*, 345–363.

Supporting Information for Chapter 1

(Table S1-S10, Figure S1-S5)

Table S1. Bond lengths in amidophenolato moieties (ring **a** and ring **b**) of $\mathbf{1^H}$ and [$\mathbf{1^H}$]SbF_6.

	$\mathbf{1^H}$	[$\mathbf{1^H}$]SbF_6
Ring **a**		
Rh1－O1	2.0190(11)	2.0383(16)
Rh1－N1	1.9817(13)	1.9842(17)
O1–C6	1.3332(19)	1.295(3)
N1–C1	1.4273(19)	1.383(3)
C1–C2	1.396(2)	1.407(3)
C2–C3	1.385(2)	1.376(3)
C3–C4	1.410(2)	1.437(3)
C4–C5	1.385(2)	1.369(3)
C5–C6	1.428(2)	1.448(3)
C6–C1	1.421(2)	1.440(3)
MOS*	−1.68(20)	−1.03(15)
Ring **b**		
Rh1－O2	2.0072(12)	2.0074(15)
Rh1－N2	1.9763(13)	1.9731(19)
O2–C15	1.3362(18)	1.320(3)
N2–C10	1.428(2)	1.415(3)
C10–C11	1.400(2)	1.396(3)
C11–C12	1.384(2)	1.379(3)
C12–C13	1.405(2)	1.417(3)
C13–C14	1.389(2)	1.370(3)
C14–C15	1.420(2)	1.433(3)
C15–C10	1.418(2)	1.417(3)
MOS*	−1.74(18)	−1.49(20)

*Metrical oxidation states. [49]

Table S2. Cartesian coordinates of $\mathbf{1^H}$ in the singlet state.

Atom	Coordinates (Å)		
	X	Y	Z
C	-1.928083	-2.306338	-2.914962
C	-0.555664	-2.429592	-2.662986
C	-0.006355	-3.575597	-2.071492
C	-0.864961	-4.617266	-1.716205
C	-2.253685	-4.520175	-1.926965
C	-2.767390	-3.358282	-2.536578
S	0.552404	-1.137616	-3.171663
O	0.211294	-0.638050	-4.511218
C	-3.164907	-5.634705	-1.473487
N	0.033449	0.255735	-2.057487
Rh	0.161248	0.704454	0.060342
N	-1.436606	-0.434130	0.496325
C	-1.321489	-1.684616	0.879861
C	-0.091439	-2.385963	1.017989
N	-0.207702	-3.774131	1.377025
O	0.829560	-4.469907	1.447388
C	1.237500	-1.907661	0.824425
N	1.551861	-0.693949	0.435202
C	2.873366	-0.198863	0.284332
C	2.944128	1.158080	-0.128636
C	4.227859	1.759338	-0.316485
C	5.349442	0.962629	-0.071036
C	5.295064	-0.389384	0.346481
C	4.035379	-0.956990	0.520675
O	1.806329	1.846259	-0.320092
C	6.602637	-1.168374	0.578414
C	6.347261	-2.620510	1.027720
C	4.357523	3.223017	-0.784497
C	3.680786	3.391126	-2.168009
O	-1.345825	-4.255645	1.581626
C	7.420584	-1.210227	-0.736337
C	7.439931	-0.467302	1.676828
C	3.685191	4.171316	0.240462
C	5.829719	3.661855	-0.927107
N	0.290701	1.521693	1.968810
C	0.262971	0.746083	3.191662
C	1.465004	0.286111	3.745515
C	1.433179	-0.453239	4.934133
C	0.210806	-0.731201	5.563395
C	-0.985524	-0.267234	4.996711
C	-0.965330	0.471281	3.807367
O	-1.287816	2.122996	-0.225390
C	-2.517399	1.636940	0.012024
C	-2.661826	0.272664	0.383336
C	-3.927667	-0.294247	0.623626
C	-5.081180	0.479858	0.514989
C	-4.919885	1.842609	0.168507
C	-3.687695	2.454838	-0.082364
C	-6.492575	-0.085049	0.760368
C	-7.350954	0.085021	-0.517512
C	-3.588774	3.952496	-0.439577
C	-2.962598	4.123175	-1.845204
O	1.926849	-1.477640	-2.798430
C	-6.468798	-1.583259	1.121670
C	-7.163806	0.678707	1.928773
C	-4.969360	4.641548	-0.455343
C	-2.713688	4.687489	0.607389
H	-3.998692	-1.341893	0.893586
H	-5.812398	2.453459	0.093926
H	6.327757	1.407882	-0.212587
H	-2.208906	-2.263858	1.115849
H	2.022101	-2.631971	1.021142
H	1.063189	-3.644616	-1.898401
H	-0.451895	-5.504052	-1.240703
H	-3.836957	-3.271603	-2.715012
H	-2.332585	-1.416154	-3.389565
H	-1.893101	0.826040	3.361418
H	-1.937259	-0.480631	5.478112

H	0.190398	-1.306551	6.486099	H	7.677684	-0.205115	-1.087740
H	2.364725	-0.811345	5.366580	H	8.357760	-1.761509	-0.587329
H	2.411881	0.499067	3.252029	H	6.853715	-1.706061	-1.532762
H	-7.436082	1.135812	-0.814159	H	8.382939	-1.004073	1.841443
H	-6.911457	-0.463415	-1.359282	H	7.687706	0.564261	1.404222
H	-8.365925	-0.298706	-0.352550	H	6.893248	-0.439055	2.627095
H	-6.028949	-2.188679	0.319831	H	3.777677	4.429026	-2.511531
H	-5.905888	-1.774130	2.043151	H	4.155035	2.741187	-2.913373
H	-7.492477	-1.941775	1.281112	H	2.618352	3.143870	-2.117260
H	-8.174652	0.291782	2.110301	H	4.154756	4.074027	1.227803
H	-6.584365	0.565983	2.852773	H	3.794923	5.214453	-0.082581
H	-7.250701	1.750160	1.718609	H	2.618412	3.954003	0.333153
H	-1.953099	3.709724	-1.876844	H	6.368269	3.062568	-1.670748
H	-3.570908	3.620255	-2.607060	H	5.863181	4.705569	-1.260689
H	-2.906517	5.187723	-2.106020	H	6.373010	3.603406	0.023939
H	-4.839419	5.700884	-0.705749	H	1.161637	2.053093	1.879336
H	-5.638983	4.207930	-1.207735	H	-0.480710	2.194178	1.933591
H	-5.467639	4.593298	0.520489	H	3.944010	-1.991322	0.832624
H	-3.139395	4.583363	1.613636	H	-4.204348	-5.451400	-1.761413
H	-1.694591	4.293174	0.610466	H	-2.853862	-6.595908	-1.899076
H	2.664499	5.758235	0.372253	H	-3.117444	-5.730257	-0.381723
H	5.787996	-3.188625	0.274948	N	-0.049955	1.319890	-2.737355
H	7.303642	-3.133378	1.183225	N	-0.143940	2.279715	-3.340426
H	5.793510	-2.665416	1.973449				

Table S3. Cartesian coordinates of **TS1** in the singlet state.

Atom	Coordinates (Å)		
	X	Y	Z
C	3.636139	-2.455376	-0.029753
C	2.474873	-1.620936	0.047548
C	2.639002	-0.254024	0.402607
C	3.909400	0.295379	0.659263
C	5.050364	-0.499316	0.582602
C	4.872293	-1.862117	0.240470
O	1.244140	-2.096113	-0.188679
Rh	-0.180001	-0.637311	0.006084
N	-0.303700	-1.380129	2.035566
C	-0.218650	-0.560546	3.223357
C	-1.384963	-0.004525	3.767350
C	-1.297416	0.792748	4.915077
C	-0.054034	1.036063	5.516750
C	1.106421	0.476746	4.962159
C	1.029789	-0.321371	3.814140
N	1.428795	0.481148	0.478695
C	1.318893	1.737777	0.837529
C	0.093608	2.457459	0.939666
C	-1.234795	1.992453	0.745454
N	-1.557819	0.776510	0.367239
C	-2.878335	0.289528	0.227762
C	-2.960772	-1.085425	-0.126947
C	-4.243752	-1.708911	-0.228485
C	-5.360443	-0.897145	-0.014361
C	-5.297077	0.480917	0.306306
C	-4.035123	1.058702	0.434341
O	-1.820165	-1.766983	-0.337206
C	-4.385948	-3.209544	-0.553343
C	-5.860533	-3.662534	-0.578526
C	-6.599612	1.277920	0.495798
C	-7.431132	0.653466	1.643807
C	6.465891	0.042379	0.853456
C	7.100653	-0.729046	2.037109
C	3.520069	-3.948385	-0.399509
C	2.615080	-4.680482	0.623667
N	0.088120	-0.284869	-1.928836
N	-0.524512	-1.692827	-2.658451
N	-0.265715	-2.647583	-3.185468
S	-0.624867	0.966005	-2.986907
O	-1.925722	1.478330	-2.523097
C	0.639854	2.197212	-2.696543
C	1.967347	1.929277	-3.061510
C	2.926912	2.929023	-2.874974
C	2.577315	4.185734	-2.344244
C	1.231114	4.427235	-2.006648
C	0.257088	3.440759	-2.173385
C	3.616585	5.261539	-2.132520
O	-0.500798	0.410006	-4.347739
N	0.220516	3.852006	1.285441
O	1.361442	4.321506	1.487435
O	0.811991	4.552723	1.351233
C	-6.337264	2.756290	0.844131
C	-7.422939	1.232264	-0.815776
C	-3.778894	-3.513086	-1.945070
C	-3.657171	-4.051764	0.524694
C	7.345389	-0.147031	-0.407214
C	6.460469	1.542011	1.209560
C	2.918103	-4.090847	-1.818942
C	4.889544	-4.659316	-0.398073
H	3.992987	1.345175	0.916858
H	5.756140	-2.487403	0.183327
H	-6.341070	-1.350597	-0.099728
H	2.208252	2.309626	1.084969
H	-2.013359	2.725167	0.934601
H	-0.781872	3.627497	-1.919139
H	0.943749	5.391989	-1.593553
H	3.961066	2.727791	-3.146484
H	2.241398	0.963970	-3.477662

H	1.931305	-0.751142	3.380398	H	-7.291680	3.280784	0.968397
H	2.075117	0.660863	5.421520	H	-5.779464	2.863891	1.782289
H	0.010047	1.657062	6.407236	H	-7.683834	0.206560	-1.097807
H	-2.202491	1.223742	5.337398	H	-8.357980	1.794400	-0.698440
H	-2.349715	-0.190351	3.297937	H	-6.859277	1.673377	-1.645857
H	7.418457	-1.200284	-0.698399	H	-8.369131	1.206381	1.779282
H	6.930935	0.405475	-1.258872	H	-7.688241	-0.391764	1.441071
H	8.363275	0.220374	-0.224199	H	-6.877943	0.684157	2.590166
H	6.048700	2.152563	0.396881	H	-3.919259	-4.572695	-2.193830
H	5.881433	1.745663	2.118291	H	-4.266814	-2.914250	-2.723389
H	7.486631	1.883044	1.389929	H	-2.710033	-3.297225	-1.961218
H	8.114051	-0.358553	2.237459	H	-4.079229	-3.860794	1.519659
H	6.505045	-0.603646	2.949139	H	-3.774611	-5.121201	0.309376
H	7.173704	-1.802514	1.831855	H	-2.588030	-3.826115	0.543643
H	1.924756	-3.641231	-1.868722	H	-6.437492	-3.147109	-1.355443
H	3.558526	-3.603234	-2.564080	H	-5.901654	-4.735297	-0.799347
H	2.831511	-5.151329	-2.088050	H	-6.359671	-3.506386	0.385433
H	4.747214	-5.713651	-0.662546	H	-1.187860	-1.890834	2.003194
H	5.579647	-4.228632	-1.133364	H	0.448694	-2.071919	2.001523
H	5.370323	-4.629718	0.587265	H	-3.940907	2.109111	0.683593
H	3.024809	-4.593803	1.638197	H	4.619997	4.909298	-2.389724
H	1.602550	-4.270133	0.614945	H	3.397643	6.142685	-2.748098
H	2.554258	-5.747866	0.376105	H	3.622899	5.589531	-1.086301
H	-5.780685	3.269907	0.051508				

Table S4. Cartesian coordinates of $\mathbf{1^{H}}$-$\mathbf{TsN_3}$ in the singlet state.

Atom	Coordinates (Å)		
	X	Y	Z
C	1.503342	3.921971	0.326649
C	0.344095	3.473044	-0.325256
C	-0.876393	4.140243	-0.139590
C	-0.931547	5.262906	0.695422
C	0.222748	5.722285	1.346471
C	1.437599	5.046594	1.158125
N	0.402605	2.305747	-1.165695
Rh	0.062018	0.236642	-0.383363
S	0.680609	-2.840501	-0.290297
C	-0.313060	-4.086976	0.552918
C	-0.183571	-4.249661	1.936978
C	-0.951013	-5.226799	2.583007
C	-1.846161	-6.039583	1.864581
C	-1.955537	-5.851919	0.471749
C	-1.196335	-4.882977	-0.190015
O	-1.505725	0.371217	-1.769776
C	-2.655035	0.566544	-1.164872
C	-2.666630	0.864362	0.237875
C	-3.861538	1.224340	0.902484
C	-5.065333	1.234200	0.215062
C	-5.046936	0.867197	-1.164840
C	-3.906194	0.519014	-1.876235
N	-1.419607	0.737437	0.861386
C	-1.241093	0.814672	2.169507
C	0.009313	0.667617	2.810136
C	1.289346	0.499965	2.245408
N	1.518380	0.376008	0.944997
C	2.803166	0.346159	0.382204
C	3.994577	0.592039	1.098880
C	5.220221	0.494609	0.457633
C	5.217168	0.155930	-0.927362
C	4.076898	-0.086297	-1.686958
C	2.815537	0.022911	-1.009515
C	-6.404388	1.599010	0.877062
C	-7.034650	2.807179	0.139704
C	-3.949629	0.108905	-3.359925
C	-3.124471	1.103591	-4.215580
C	6.560934	0.729862	1.172776
C	7.322755	1.891006	0.486215
C	4.146346	-0.441320	-3.184173
C	5.597323	-0.449304	-3.708497
O	1.663285	-0.144337	-1.634615
C	-7.367178	0.388014	0.791813
C	-6.240351	1.976860	2.361858
C	-3.369811	-1.319958	-3.514984
C	-5.389422	0.099684	-3.913789
C	6.375846	1.091775	2.659344
C	7.415760	-0.560046	1.095016
C	3.547865	-1.850926	-3.412476
C	3.356775	0.602618	-4.015037
N	-0.023343	0.758871	4.276032
O	1.045587	0.642715	4.895525
O	-1.118990	0.947169	4.828747
H	-3.834484	1.483988	1.954122
H	-5.993996	0.861529	-1.692360
O	0.928565	-3.323237	-1.670135
H	6.177333	0.089107	-1.426118
H	-2.089359	0.982400	2.823967
H	2.120423	0.469785	2.941125
H	0.518672	-3.630854	2.489547
H	-0.849619	-5.358913	3.658801
C	-2.654708	-7.111788	2.560792
H	-2.641055	-6.474977	-0.100837
H	-1.270268	-4.748652	-1.265895
H	-1.774554	3.785971	-0.642747
H	-1.878821	5.779864	0.833160
H	0.176510	6.596131	1.992188
H	2.339169	5.394705	1.657678

H	2.446323	3.396632	0.184593	H	8.379033	-0.408804	1.598126
H	-7.560685	0.089384	-0.244085	H	6.902606	-1.398115	1.580282
H	-6.951032	-0.479376	1.317188	H	8.286474	2.059973	0.982701
H	-8.331579	0.636412	1.252018	H	7.526471	1.680679	-0.569237
H	-5.836471	1.146783	2.953470	H	6.746214	2.822538	0.536415
H	-5.583855	2.845543	2.492945	H	3.578807	-2.096674	-4.481977
H	-7.216913	2.236455	2.786234	H	4.128037	-2.609344	-2.873636
H	-7.999255	3.067005	0.593041	H	2.513617	-1.920400	-3.071642
H	-6.382438	3.686571	0.199163	H	3.754669	1.614098	-3.856981
H	-7.212957	2.594352	-0.919812	H	3.445782	0.371209	-5.083637
H	-2.341315	-1.377972	-3.152343	H	2.296058	0.591207	-3.754232
H	-3.974157	-2.044816	-2.956025	H	6.216367	-1.195596	-3.196390
H	-3.381064	-1.612941	-4.572418	H	5.590284	-0.709422	-4.773052
H	-5.367943	-0.220696	-4.961575	H	6.082423	0.530506	-3.612857
H	-6.035314	-0.600762	-3.370767	O	1.838992	-2.530428	0.590773
H	-5.853298	1.093584	-3.885447	H	1.305428	2.211075	-1.631398
H	-3.509862	2.125865	-4.109744	H	-0.325478	2.313328	-1.882561
H	-2.071271	1.091162	-3.926741	H	3.947441	0.855626	2.148920
H	-3.190680	0.827201	-5.275180	H	-3.682410	-7.144729	2.181830
H	5.873046	0.291770	3.215467	H	-2.212923	-8.102652	2.391811
H	7.355510	1.249173	3.124968	H	-2.693236	-6.945852	3.642009
H	5.799556	2.016249	2.787440	N	-0.440540	-1.596013	-0.325425
H	7.623540	-0.851601	0.059922				

Table S5. Cartesian coordinates of **1^{H}-DR-T** in the triplet state.

Atom	Coordinates (Å)		
	X	Y	Z
C	2.981637	-2.794824	0.407333
C	1.530448	-2.797988	0.370405
C	0.812127	-4.009851	0.292349
C	1.489667	-5.218524	0.252374
C	2.924563	-5.199057	0.309306
C	3.694980	-4.054569	0.387139
N	0.966495	-1.534358	0.427067
C	-0.340001	-1.294255	0.394424
C	-0.912974	-0.011604	0.479449
N	-2.373984	0.013451	0.424158
O	-2.949863	1.113619	0.510414
C	0.770250	-6.570236	0.143658
C	1.231964	-7.288733	-1.150161
C	5.232660	-4.088812	0.428622
C	5.744568	-3.397174	1.718859
O	3.601341	-1.657068	0.475820
Rh	2.311388	-0.039302	0.537611
N	2.151169	0.302738	-1.414989
S	3.153897	-0.537835	-2.457908
O	2.677020	-1.947418	-2.529048
N	2.571754	-0.217289	2.739658
C	1.462106	-0.318174	3.654028
C	0.969653	-1.580227	4.018103
C	-0.124009	-1.673050	4.888108
C	-0.728651	-0.513750	5.395231
C	-0.230423	0.744015	5.024619
C	0.862060	0.846910	4.154769
O	3.649759	1.492492	0.776309
C	3.048867	2.665038	0.811747
C	1.617311	2.722468	0.789545
C	0.928786	3.953935	0.861706
C	1.634829	5.144622	0.946903
C	3.060478	5.072519	0.949494
C	3.793650	3.894127	0.879677
N	0.997828	1.470015	0.686924
C	-0.297820	1.270539	0.613348
C	0.950782	6.519986	1.018452
C	-0.586127	6.410210	1.020702
C	5.333396	3.878904	0.847724
C	5.926477	5.300700	0.923484
C	2.768095	0.237573	-4.040597
C	1.671615	-0.216466	-4.784938
C	1.382661	0.392916	-6.009786
C	2.174441	1.448556	-6.503635
C	3.270272	1.879982	-5.735815
C	3.574274	1.280858	-4.505954
C	1.861516	2.082138	-7.841747
O	4.586055	-0.265898	-2.178078
C	1.383121	7.248740	2.315397
C	1.371119	7.367486	-0.208804
C	5.886021	3.075908	2.052769
C	5.815932	3.231370	-0.476060
C	1.126340	-7.444357	1.373148
C	-0.762039	-6.419072	0.088306
C	5.770422	-5.534639	0.430321
C	5.807344	-3.364314	-0.815229
O	-2.985580	-1.062570	0.295598
H	-0.154767	3.963307	0.841604
H	3.608098	6.006960	1.001713
H	3.435187	-6.154523	0.281770
H	-0.981701	2.111677	0.649632
H	-1.041399	-2.116087	0.299600
H	1.068585	-1.040195	-4.412017
H	0.531698	0.042649	-6.592239
H	3.896693	2.691535	-6.102281
H	4.428913	1.604892	-3.917873
H	1.245464	1.824637	3.866868
H	-0.691676	1.649651	5.412601

H	-1.578260	-0.589222	6.069769
H	-0.501257	-2.653701	5.170159
H	1.437241	-2.482584	3.626748
H	2.455280	7.517644	-0.250287
H	1.065345	6.881071	-1.142345
H	0.899113	8.357146	-0.167764
H	-0.963994	5.940618	0.104840
H	-0.953837	5.836015	1.879697
H	-1.027733	7.411535	1.081739
H	0.914629	8.239318	2.368700
H	1.081219	6.680968	3.203532
H	2.467902	7.392307	2.363559
H	5.450743	2.207803	-0.584438
H	5.470050	3.815534	-1.338044
H	6.913028	3.210858	-0.501398
H	7.019793	5.234039	0.890190
H	5.611473	5.924653	0.078493
H	5.656496	5.814510	1.854547
H	5.546376	3.509352	3.002416
H	5.570524	2.031242	2.006443
H	6.982881	3.100688	2.045513
H	-1.084157	-5.835715	-0.782142
H	-1.225804	-7.408780	0.009413
H	-1.160685	-5.941752	0.991561
H	2.311282	-7.473877	-1.156551
H	0.727630	-8.258518	-1.240959
H	0.990114	-6.691884	-2.036817
H	0.630716	-8.419849	1.296829
H	2.203455	-7.625467	1.452958
H	0.795750	-6.966782	2.303155
H	6.903649	-3.412291	-0.789908
H	5.466748	-3.847865	-1.737935
H	5.508697	-2.315657	-0.857630
H	5.333574	-3.878816	2.615980
H	6.837547	-3.473374	1.769192
H	5.481616	-2.336954	1.729370
H	5.490967	-6.079203	-0.479479
H	6.864974	-5.507008	0.468159
H	5.425117	-6.107819	1.300135
H	3.194766	-1.021547	2.819799
H	3.129506	0.620960	2.911141
H	-0.270028	-3.991517	0.254142
H	2.407946	3.020745	-7.977076
H	2.139662	1.412216	-8.665724
H	0.790476	2.292883	-7.941031
C	-10.152748	1.660634	-0.155838
C	-8.888618	0.827389	-0.107395
C	-11.390735	0.816164	-0.375642
H	-10.256687	2.228072	0.780340
H	-10.071360	2.410200	-0.956013
C	-12.663308	1.403877	-0.467333
C	-13.815819	0.636377	-0.667445
C	-13.703302	-0.759212	-0.780376
C	-12.448314	-1.367071	-0.693190
C	-11.303166	-0.579773	-0.492300
H	-12.745319	2.487056	-0.379298
H	-14.789107	1.117061	-0.735031
H	-14.589338	-1.371215	-0.936271
H	-12.331512	-2.444756	-0.777621
O	-10.113767	-1.267873	-0.419768
C	-8.935603	-0.567569	-0.237908
C	-7.769298	-1.346304	-0.189899
C	-6.529263	-0.727682	-0.008934
C	-6.455162	0.669320	0.123371
C	-7.630120	1.426541	0.072389
H	-7.857414	-2.424948	-0.296283
H	-5.617409	-1.318682	0.029751
H	-5.487932	1.144843	0.263351
H	-7.578492	2.510624	0.173752

Table S6. Cartesian coordinates of **TS2** in the triplet state.

Atom	Coordinates (Å)		
	X	Y	Z
C	-2.325546	3.724199	0.916694
C	-0.943600	3.849461	0.711492
C	-0.402426	5.028354	0.195005
C	-1.258112	6.092586	-0.131521
C	-2.645993	5.991120	0.054221
C	-3.164193	4.790916	0.584746
S	0.163302	2.500979	1.208956
O	1.539468	2.932979	0.825988
C	-3.570103	7.136023	-0.299048
N	-0.404801	1.221890	0.301391
Rh	0.132558	-0.647966	0.929332
O	-1.469692	-0.630505	2.219729
C	-2.595894	-0.895421	1.598896
C	-2.563454	-1.268044	0.212288
C	-3.747328	-1.569025	-0.496615
C	-4.975677	-1.523693	0.145151
C	-4.992415	-1.163138	1.527176
C	-3.866500	-0.846620	2.276404
N	-1.277448	-1.312439	-0.333979
C	-0.986486	-1.753160	-1.540170
C	0.329508	-1.798446	-2.082794
C	1.555132	-1.370579	-1.535972
N	1.692575	-0.839447	-0.325938
C	2.912846	-0.480168	0.228625
C	2.830503	-0.093286	1.621680
C	4.045322	0.233128	2.337404
C	5.224329	0.169761	1.617182
C	5.319763	-0.193168	0.232306
C	4.154422	-0.515480	-0.443776
O	1.667603	-0.086897	2.202111
C	4.003808	0.628998	3.824209
C	5.415457	0.913031	4.377560
C	6.701448	-0.202780	-0.438492
C	7.632660	-1.189734	0.310142
C	-6.304492	-1.822585	-0.568336
C	-7.027073	-2.992479	0.145234
C	-3.947516	-0.440715	3.760042
C	-3.118418	-1.423842	4.625339
O	-0.116191	2.243509	2.645084
N	0.454587	-2.629197	1.841255
C	0.606501	-3.846146	1.084443
C	1.885526	-4.270036	0.694493
C	2.027021	-5.441122	-0.060134
C	0.899490	-6.189738	-0.427824
C	-0.375529	-5.758159	-0.033628
C	-0.526948	-4.588194	0.720616
N	0.429016	-2.424481	-3.404364
O	-0.615442	-2.825386	-3.946738
O	1.552363	-2.542535	-3.922887
C	6.635348	-0.635214	-1.915826
C	7.307855	1.222187	-0.376872
C	3.149565	1.908118	4.008974
C	3.396401	-0.527725	4.659646
C	-7.205822	-0.562868	-0.524771
C	-6.100423	-2.215571	-2.044295
C	-3.398429	0.997488	3.939767
C	-5.397161	-0.465743	4.286743
C	-0.067988	2.113951	-2.211894
C	-1.239287	1.620486	-2.973094
C	-1.056758	0.772407	-4.083539
O	0.193414	0.423044	-4.540090
C	1.306037	1.034726	-4.006795
C	1.234396	1.868295	-2.873129
C	-2.562035	1.947598	-2.610573
C	-3.653670	1.443536	-3.319771
C	-3.441785	0.584002	-4.414114
C	-2.140946	0.246997	-4.798562
C	2.517059	0.784621	-4.665014

C	3.687460	1.387107	-4.194536	H	6.011063	0.039994	-2.511844
C	3.643931	2.224918	-3.064284	H	7.642937	-0.622779	-2.347297
C	2.431461	2.452898	-2.410873	H	6.242648	-1.653050	-2.026713
H	-3.690152	-1.812972	-1.550868	H	7.420402	1.576801	0.653123
H	-5.956667	-1.124199	2.021535	H	8.300475	1.231151	-0.843920
H	6.146344	0.416453	2.130868	H	6.672240	1.939901	-0.908340
H	-1.770342	-2.133009	-2.186547	H	8.628780	-1.190361	-0.149275
H	2.425678	-1.521301	-2.164713	H	7.754782	-0.923736	1.365387
H	0.673167	5.109748	0.063093	H	7.236610	-2.211169	0.265405
H	-0.835129	7.012126	-0.532472	H	3.157137	2.200978	5.067039
H	-4.237582	4.695000	0.743894	H	3.560009	2.738176	3.422402
H	-2.730725	2.805404	1.331705	H	2.114061	1.760329	3.698766
H	-1.518039	-4.253826	1.023414	H	3.975026	-1.452564	4.534413
H	-1.256829	-6.331278	-0.313400	H	3.412337	-0.263465	5.724098
H	1.012868	-7.097162	-1.016243	H	2.357850	-0.713445	4.376186
H	3.020474	-5.766811	-0.360859	H	5.897558	1.752549	3.862247
H	2.762660	-3.690448	0.978467	H	5.335066	1.184815	5.435905
H	-7.422981	-0.250243	0.502313	H	6.074696	0.038115	4.311871
H	-6.722491	0.278712	-1.034918	H	1.264540	-2.456798	2.437974
H	-8.163319	-0.761226	-1.022370	H	-0.370654	-2.657455	2.443041
H	-5.620317	-1.414123	-2.618072	H	4.186987	-0.777987	-1.493798
H	-5.490697	-3.121495	-2.144630	H	-4.143550	7.464461	0.576505
H	-7.071774	-2.419450	-2.509636	H	-3.012115	7.997215	-0.679363
H	-7.982010	-3.208460	-0.350025	H	-4.293343	6.836692	-1.067813
H	-6.416716	-3.902935	0.119736	H	-0.183587	3.147057	-1.873217
H	-7.242201	-2.763899	1.194580	H	-1.944483	-0.411118	-5.640717
H	-2.362298	1.086348	3.605770	H	-4.287064	0.184853	-4.971107
H	-4.010331	1.714797	3.377471	H	-4.665135	1.713739	-3.024636
H	-3.442913	1.282388	4.998767	H	-2.719889	2.601324	-1.755585
H	-5.400089	-0.168900	5.341685	H	2.517271	0.129537	-5.532075
H	-6.044125	0.237922	3.748929	H	4.628712	1.207238	-4.710352
H	-5.845370	-1.465423	4.225631	H	4.553814	2.692479	-2.694478
H	-3.481403	-2.453068	4.506997	H	2.394258	3.065544	-1.512815
H	-2.060944	-1.385868	4.355074	H	-0.132003	1.563512	-1.059989
H	-3.208244	-1.154659	5.685070				

Table S7. Cartesian coordinates of $\mathbf{1^{H}}$-**TsNH** in the triplet state.

Atom	Coordinates (Å)		
	X	Y	Z
C	3.125279	-2.680716	0.064510
C	1.772001	-2.694438	0.601995
C	1.146247	-3.910681	0.941837
C	1.812257	-5.112271	0.754755
C	3.148056	-5.081863	0.224529
C	3.829233	-3.933576	-0.126813
N	1.212213	-1.437951	0.732996
C	-0.040676	-1.221349	1.123354
C	-0.602979	0.053088	1.300431
N	-2.000380	0.059111	1.719285
O	-2.561040	1.157270	1.895109
C	1.177511	-6.471179	1.079327
C	1.113597	-7.320873	-0.216021
C	5.249616	-3.955174	-0.716128
C	6.209235	-3.117255	0.168270
O	3.668375	-1.540281	-0.216552
Rh	2.437388	0.072082	0.226725
N	1.563945	0.265609	-1.632066
S	1.738509	-0.905411	-2.805853
O	1.251750	-2.185217	-2.231063
N	3.499342	0.074482	2.140419
C	2.821412	0.102228	3.415162
C	2.528912	-1.099628	4.075715
C	1.857176	-1.068828	5.304507
C	1.476121	0.154581	5.874289
C	1.771660	1.351336	5.204920
C	2.442540	1.330618	3.976038
O	3.687959	1.633435	-0.205466
C	3.116673	2.805383	0.038046
C	1.790043	2.839298	0.565140
C	1.140916	4.059123	0.855683
C	1.786487	5.266734	0.628454
C	3.105574	5.217980	0.094737
C	3.793390	4.047024	-0.213415
N	1.212835	1.567410	0.745712
C	-0.018130	1.350016	1.136788
C	1.137678	6.631134	0.918794
C	-0.288306	6.492477	1.486723
C	5.214223	4.061682	-0.810084
C	5.748350	5.495929	-0.999946
C	0.537789	-0.354310	-4.042630
C	-0.831694	-0.387561	-3.741880
C	-1.752614	0.011007	-4.713343
C	-1.327643	0.443854	-5.986603
C	0.049874	0.468524	-6.259567
C	0.988289	0.069127	-5.295610
C	-2.339588	0.850239	-7.035664
O	3.064106	-0.893730	-3.477046
C	1.994499	7.402525	1.953275
C	1.054289	7.453122	-0.391609
C	6.193532	3.316884	0.132291
C	5.203188	3.371927	-2.198113
C	2.042118	-7.204659	2.136145
C	-0.252797	-6.336398	1.636431
C	5.814675	-5.388732	-0.787283
C	5.220277	-3.378173	-2.154398
O	-2.581358	-1.030184	1.884326
H	0.132908	4.047214	1.254262
H	3.607235	6.162086	-0.086420
H	3.648567	-6.033254	0.089176
H	-0.675874	2.184671	1.355014
H	-0.701171	-2.058421	1.322181
H	-1.164456	-0.722376	-2.762838
H	-2.816598	-0.012889	-4.482136
H	0.397739	0.799280	-7.236833
H	2.054405	0.076017	-5.505991
H	2.667702	2.260266	3.456019
H	1.480896	2.305631	5.638701

H	0.955052	0.175364	6.828571	H	5.923305	-2.063227	0.175057
H	1.634774	-2.002684	5.816281	H	5.214778	-6.035842	-1.438077
H	2.824662	-2.051250	3.636359	H	6.824877	-5.352614	-1.209877
H	2.042608	7.621768	-0.832778	H	5.887598	-5.858416	0.201856
H	0.439405	6.936801	-1.137909	H	4.109797	-0.740638	2.068800
H	0.604639	8.434931	-0.197751	H	4.084104	0.902287	2.008476
H	-0.960129	5.983318	0.785523	H	0.138409	-3.903571	1.337832
H	-0.300449	5.943339	2.436064	H	-1.862704	1.374061	-7.870132
H	-0.706999	7.487073	1.678689	H	-2.853151	-0.030025	-7.443711
H	1.551336	8.384752	2.159998	H	-3.108290	1.507718	-6.613401
H	2.056391	6.850812	2.898930	C	-9.656484	1.479815	0.332676
H	3.016657	7.568005	1.596025	C	-8.421181	0.866766	0.691281
H	4.877531	2.332091	-2.124895	C	-10.775970	0.661574	0.009334
H	4.532862	3.899805	-2.887675	H	-9.743415	2.562833	0.306028
H	6.211499	3.386884	-2.631206	C	-12.050177	1.170263	-0.361610
H	6.756050	5.449180	-1.428358	C	-13.107969	0.315728	-0.666965
H	5.126913	6.079629	-1.689565	C	-12.928949	-1.080390	-0.612099
H	5.819609	6.041133	-0.050720	C	-11.683254	-1.614855	-0.249455
H	6.218671	3.788551	1.123111	C	-10.627635	-0.754789	0.055090
H	5.906620	2.268810	0.245012	H	-12.186271	2.249533	-0.402890
H	7.209186	3.349560	-0.281461	H	-14.074933	0.727276	-0.948419
H	-0.927439	-5.855569	0.918687	H	-13.753455	-1.748431	-0.850055
H	-0.657565	-7.331896	1.850443	H	-11.518613	-2.688352	-0.199709
H	-0.278188	-5.764995	2.572173	O	-9.432074	-1.337544	0.402978
H	2.106311	-7.497365	-0.643336	C	-8.341828	-0.554289	0.716574
H	0.665521	-8.298385	-0.000301	C	-7.164260	-1.220319	1.057262
H	0.504297	-6.824529	-0.979553	C	-6.020298	-0.477757	1.384993
H	1.604522	-8.184112	2.364179	C	-6.065805	0.931143	1.369589
H	3.066800	-7.373028	1.788274	C	-7.245264	1.589908	1.029319
H	2.093600	-6.630049	3.068612	H	-7.156152	-2.307589	1.061137
H	6.236148	-3.382867	-2.569981	H	-5.093675	-0.980363	1.649867
H	4.584270	-3.989885	-2.804409	H	-5.169464	1.491219	1.624122
H	4.837406	-2.356897	-2.185960	H	-7.284132	2.677933	1.016306
H	6.224147	-3.491917	1.200427	H	1.972350	1.115529	-2.034310
H	7.229619	-3.187497	-0.227379				

Table S8. Cartesian coordinates of **TS3** in the singlet state.

Atom	Coordinates (Å)		
	X	Y	Z
O	-0.129010	0.115704	4.334420
C	1.113739	0.437119	3.892062
C	1.323711	1.433620	2.909627
C	0.182911	2.052994	2.279723
C	-1.118022	1.715745	2.794616
C	-1.221747	0.749410	3.824688
C	-2.453701	0.426775	4.410541
C	-3.597437	1.083498	3.964028
C	-3.524598	2.054303	2.938288
C	-2.303274	2.364141	2.359638
C	2.185769	-0.227706	4.508767
C	3.485203	0.131146	4.164800
C	3.727445	1.154464	3.218025
C	2.661776	1.792168	2.600669
N	0.366440	1.410124	0.144062
S	0.123035	2.825063	-0.826804
O	0.362449	2.573487	-2.256728
Rh	-0.218885	-0.424382	-0.801839
N	1.138876	-1.398014	0.329756
C	0.816818	-1.995896	1.454337
C	-0.489187	-2.028478	2.016555
N	-0.604194	-2.706365	3.278654
O	-1.730439	-2.796961	3.819608
C	-1.704868	-1.514196	1.475594
N	-1.803659	-0.808372	0.374819
C	-3.029708	-0.369370	-0.189650
C	-2.887572	0.274528	-1.447898
C	-4.066035	0.714188	-2.136519
C	-5.292848	0.501880	-1.503876
C	-5.447162	-0.125273	-0.242344
C	-4.292573	-0.562787	0.401871
O	-1.669337	0.429690	-1.966242
C	-6.856138	-0.299951	0.353585
C	-6.831221	-1.015532	1.718666
C	-3.971201	1.383466	-3.522249
C	-3.141158	2.686812	-3.426277
O	0.428234	-3.171570	3.816031
C	-7.512863	1.088720	0.553076
C	-7.733063	-1.140201	-0.607939
C	-3.293962	0.416813	-4.527398
C	-5.360054	1.744759	-4.089486
N	-0.628259	-2.125400	-2.016334
C	-0.885648	-3.452920	-1.511345
C	-2.202343	-3.850892	-1.239965
C	-2.444910	-5.138443	-0.746077
C	-1.381496	-6.024811	-0.520781
C	-0.067749	-5.614730	-0.792054
C	0.185446	-4.329416	-1.286132
O	1.413542	-0.252995	-2.046908
C	2.504404	-0.824749	-1.535280
C	2.434231	-1.429364	-0.249464
C	3.564662	-2.014449	0.351851
C	4.788874	-2.034322	-0.313856
C	4.837331	-1.461022	-1.608280
C	3.747128	-0.865322	-2.248916
C	6.059936	-2.658039	0.291673
C	7.172022	-1.584728	0.392598
C	3.856493	-0.291015	-3.675786
C	3.531326	1.223052	-3.668936
O	-1.153862	3.425163	-0.376652
C	1.450994	3.943411	-0.290892
C	1.141741	5.061814	0.489460
C	2.166119	5.947660	0.852881
C	3.493166	5.732905	0.441334
C	3.772606	4.603795	-0.354965
C	2.761580	3.714960	-0.733614
C	4.589155	6.709857	0.804275
C	5.818629	-3.227109	1.703611

C	6.553754	-3.816099	-0.610850	H	-6.248410	-0.456430	2.460870
C	5.268835	-0.468297	-4.271147	H	-7.852324	-1.113377	2.106064
C	2.860025	-1.020920	-4.612166	H	-6.408483	-2.024623	1.644444
H	3.476000	-2.450777	1.340466	H	-7.593790	1.639773	-0.390035
H	5.782728	-1.491194	-2.138642	H	-8.524204	0.982567	0.966489
H	-6.189615	0.835615	-2.013778	H	-6.923550	1.702661	1.245237
H	1.572585	-2.532551	2.019551	H	-8.744353	-1.263070	-0.199044
H	-2.596745	-1.753373	2.046005	H	-7.826529	-0.667678	-1.591504
H	0.111355	5.246262	0.783519	H	-7.301702	-2.137141	-0.757341
H	1.925113	6.820770	1.456672	H	-3.098124	3.172887	-4.410068
H	4.790890	4.426683	-0.697258	H	-3.599245	3.388738	-2.718987
H	2.983062	2.870808	-1.381471	H	-2.121472	2.485705	-3.095479
H	1.205474	-4.007605	-1.489900	H	-3.856617	-0.522802	-4.608048
H	0.763769	-6.294306	-0.618095	H	-3.259228	0.875027	-5.524072
H	-1.574100	-7.023492	-0.135370	H	-2.268951	0.195912	-4.220508
H	-3.466896	-5.446617	-0.536169	H	-5.890262	2.463516	-3.452885
H	-3.026430	-3.159204	-1.406833	H	-5.235023	2.210541	-5.073959
H	7.423284	-1.165632	-0.587583	H	-5.998747	0.862329	-4.221499
H	6.855537	-0.755705	1.037377	H	-1.413129	-1.766086	-2.565195
H	8.087926	-2.017140	0.815618	H	0.201415	-2.099886	-2.614250
H	5.485579	-2.451769	2.404626	H	-4.360479	-1.053409	1.366343
H	5.068846	-4.027075	1.699262	H	5.532216	6.193316	1.013419
H	6.750243	-3.651094	2.096862	H	4.774853	7.405562	-0.024358
H	7.463832	-4.267896	-0.195372	H	4.321276	7.305796	1.682438
H	5.790426	-4.598903	-0.691930	H	1.385777	1.284389	0.156786
H	6.785445	-3.471110	-1.624215	H	0.310268	3.034874	1.849661
H	2.523130	1.411520	-3.292817	H	1.971482	-1.008443	5.232943
H	4.258894	1.765743	-3.049672	H	4.322611	-0.378041	4.636917
H	3.597319	1.627618	-4.687269	H	4.748209	1.432524	2.969007
H	5.287515	-0.045552	-5.282381	H	2.842189	2.572599	1.865163
H	6.034094	0.053834	-3.683793	H	-2.486445	-0.335749	5.182963
H	5.555555	-1.524021	-4.350670	H	-4.559043	0.839957	4.411111
H	3.061220	-2.099725	-4.631944	H	-4.429731	2.544005	2.589191
H	1.830522	-0.854816	-4.286385	H	-2.232540	3.069790	1.537176
H	2.958037	-0.640621	-5.636928				

Table S9. Cartesian coordinates of **1^{H}-TsN(Xan)** in the singlet state.

Atom	Coordinates (Å)		
	X	Y	Z
C	2.977902	0.249331	1.252496
C	3.076448	-0.492016	0.046732
C	4.314151	-0.714084	-0.584581
C	5.491262	-0.236856	-0.012547
C	5.384725	0.446455	1.223000
C	4.180540	0.699732	1.886106
N	1.835794	-0.993753	-0.426953
C	1.718099	-1.871105	-1.395857
C	0.497507	-2.465917	-1.821617
N	0.604345	-3.398155	-2.918437
O	-0.430564	-3.960141	-3.336658
C	6.873971	-0.425030	-0.663086
C	7.505640	0.960986	-0.945602
C	4.146037	1.420952	3.249428
C	3.478820	0.505596	4.307759
O	1.767650	0.481834	1.775843
Rh	0.271379	-0.419771	0.700393
N	-0.359821	1.500312	-0.371315
S	0.273894	2.961511	0.499670
O	1.638297	3.179534	-0.003464
N	0.596250	-1.942129	2.085801
C	0.815014	-3.333765	1.754208
C	2.119273	-3.794924	1.531016
C	2.325048	-5.143964	1.218966
C	1.237604	-6.025520	1.130309
C	-0.063051	-5.550964	1.354750
C	-0.280056	-4.203719	1.667414
O	-1.362589	0.028348	1.864473
C	-2.465132	-0.630425	1.472308
C	-2.405084	-1.443802	0.310013
C	-3.536921	-2.137189	-0.156438
C	-4.750491	-2.050144	0.524206
C	-4.789266	-1.250758	1.691007
C	-3.695219	-0.539965	2.195100
N	-1.119719	-1.498372	-0.291657
C	-0.803772	-2.302276	-1.284409
C	-6.023332	-2.779062	0.055194
C	-5.787751	-3.604659	-1.224862
C	-3.798005	0.304842	3.481430
C	-5.210834	0.257770	4.098893
C	-0.737298	4.349638	-0.059775
C	-0.264764	5.191174	-1.075572
C	-1.031354	6.300912	-1.445712
C	-2.255236	6.586557	-0.810270
C	-2.694011	5.730575	0.217627
C	-1.941819	4.615565	0.604116
C	-3.057093	7.807672	-1.198940
O	-0.047276	2.751090	1.913978
C	-6.512207	-3.744626	1.162999
C	-7.134754	-1.742311	-0.242614
C	-2.802765	-0.228087	4.543370
C	-3.464864	1.786390	3.172534
C	7.799660	-1.219413	0.291497
C	6.795110	-1.193148	-1.997065
C	5.560782	1.764347	3.761246
C	3.347049	2.741857	3.141493
O	1.729013	-3.609597	-3.420900
H	-3.462161	-2.734286	-1.058293
H	-5.728233	-1.185720	2.229210
H	6.300385	0.799081	1.683915
H	-1.568795	-2.920550	-1.744144
H	2.601884	-2.206484	-1.929272
H	0.694186	4.991214	-1.546392
H	-0.668856	6.957106	-2.234871
H	-3.629719	5.942576	0.731388
H	-2.269539	3.977721	1.420888
H	-1.289341	-3.831220	1.834644
H	-0.911723	-6.227675	1.284599

H	1.402048	-7.071991	0.883890	H	2.439790	0.297863	4.039529
H	3.336204	-5.503725	1.042397	H	6.084109	2.455933	3.090105
H	2.960833	-3.107155	1.592878	H	5.479732	2.255985	4.737715
H	-7.378386	-1.141801	0.640637	H	6.184452	0.871450	3.892788
H	-6.819406	-1.054551	-1.036401	H	1.392496	-1.540113	2.590278
H	-8.053900	-2.245540	-0.569254	H	-0.230065	-1.824333	2.678165
H	-5.468448	-2.974456	-2.063426	H	4.342881	-1.248849	-1.527126
H	-5.031132	-4.384214	-1.075786	H	-4.103520	7.714250	-0.892743
H	-6.718720	-4.102255	-1.521309	H	-2.648586	8.705263	-0.716774
H	-7.428991	-4.259082	0.847704	H	-3.027991	7.975591	-2.280782
H	-5.752257	-4.504634	1.380202	H	-1.300360	1.402692	0.031811
H	-6.731143	-3.216151	2.097024	C	-0.538064	1.732758	-1.889420
H	-2.440002	1.884222	2.807197	H	-0.481741	2.818362	-2.017727
H	-4.159129	2.186900	2.421420	C	0.531021	1.114679	-2.767557
H	-3.565854	2.391773	4.082806	C	-1.929609	1.297466	-2.308875
H	-5.228070	0.870538	5.007790	C	-2.117921	0.302882	-3.280039
H	-5.972550	0.657188	3.418289	C	-3.404257	-0.103364	-3.670097
H	-5.503211	-0.760030	4.383864	C	-4.523721	0.502367	-3.101179
H	-3.011958	-1.279150	4.779921	C	-4.362268	1.522261	-2.147743
H	-1.773045	-0.139576	4.188616	C	-3.076613	1.908039	-1.766540
H	-2.894147	0.350887	5.471224	H	-3.494452	-0.881897	-4.423303
H	6.176105	-0.667845	-2.734380	H	-5.519877	0.189725	-3.407073
H	7.799423	-1.297632	-2.424305	H	-5.229676	2.007498	-1.707596
H	6.386409	-2.202233	-1.865689	H	-2.961016	2.710931	-1.041223
H	7.624969	1.547999	-0.028554	C	0.195732	0.161332	-3.741678
H	8.497607	0.847311	-1.401616	C	1.156021	-0.371180	-4.613194
H	6.877999	1.542485	-1.631440	C	2.478288	0.062147	-4.527647
H	8.794091	-1.347376	-0.155229	C	2.836869	1.029991	-3.573981
H	7.929365	-0.709048	1.251940	C	1.869414	1.546913	-2.710855
H	7.386950	-2.214504	0.496121	O	-1.083344	-0.309786	-3.928462
H	3.367067	3.268188	4.105147	H	0.845602	-1.120511	-5.336405
H	3.785459	3.401054	2.382881	H	3.223894	-0.353554	-5.201554
H	2.307721	2.552535	2.871375	H	3.865131	1.374637	-3.497057
H	4.022492	-0.443272	4.405138	H	2.155914	2.276645	-1.959958
H	3.482290	0.998318	5.288413				

Table S10. Cartesian coordinates of [**3**]$^{-}$.

Atom	Coordinates (Å)		
	X	Y	Z
Rh	0.0659	-1.7633	0.1551
Cl	0.8679	-3.3845	1.6482
S	-0.5757	0.2941	-2.4985
O	-1.8423	-1.9849	0.8607
O	0.4672	-0.3055	1.5102
O	2.5488	-4.7562	-3.6441
O	4.1503	-3.4510	-2.9964
O	-1.6811	0.2258	-3.4278
O	0.6723	-0.3217	-2.8505
N	-0.1802	-3.1997	-1.2326
H	-1.0768	-3.6594	-1.3156
N	1.9654	-1.4299	-0.3767
N	2.9732	-3.8304	-2.9376
N	-1.0213	-0.3422	-1.0273
C	0.7520	-3.6588	-2.0060
H	0.5241	-4.4657	-2.6929
C	2.0809	-3.1859	-2.0291
C	2.6170	-2.1366	-1.2509
H	3.6644	-1.9310	-1.4242
C	-2.2697	-0.1253	-0.5133
C	-3.1923	0.8614	-0.9229
H	-2.9170	1.5261	-1.7207
C	-4.4241	0.9775	-0.3221
C	-4.7686	0.0736	0.7214
H	-5.7367	0.1903	1.1838
C	-3.9429	-0.9265	1.1702
C	-2.6546	-1.0466	0.5403
C	-5.4419	2.0499	-0.7336
C	-4.9297	2.9376	-1.8770
H	-4.7125	2.3553	-2.7740
H	-5.6922	3.6760	-2.1354
H	-4.0251	3.4791	-1.5957
C	-6.7446	1.3695	-1.2071
H	-7.1919	0.7552	-0.4249
H	-7.4797	2.1239	-1.5003
H	-6.5539	0.7269	-2.0688
C	-5.7525	2.9587	0.4751
H	-6.1674	2.3961	1.3123
H	-4.8479	3.4592	0.8254
H	-6.4801	3.7253	0.1948
C	-4.3425	-1.8854	2.3020
C	-5.7410	-1.5650	2.8544
H	-5.9762	-2.2671	3.6568
H	-5.7954	-0.5575	3.2730
H	-6.5180	-1.6643	2.0927
C	-3.3393	-1.7724	3.4713
H	-3.6391	-2.4450	4.2797
H	-2.3309	-2.0362	3.1628
H	-3.3238	-0.7547	3.8684
C	-4.3694	-3.3397	1.7808
H	-4.6846	-4.0134	2.5822
H	-5.0798	-3.4420	0.9563
H	-3.3875	-3.6547	1.4370
C	2.5496	-0.4019	0.4029
C	3.8480	0.0796	0.2222
H	4.4499	-0.3242	-0.5770
C	4.3630	1.0677	1.0462
C	3.5314	1.5523	2.0707
H	3.9324	2.3090	2.7292
C	2.2314	1.1175	2.2896
C	1.7054	0.1241	1.4107
C	5.7845	1.6299	0.8860
C	5.7217	3.1501	0.6260
H	6.7286	3.5653	0.5204
H	5.1688	3.3612	-0.2919
H	5.2266	3.6777	1.4425
C	6.5406	0.9836	-0.2845
H	7.5414	1.4158	-0.3600

H	6.6550	-0.0932	-0.1479
H	6.0344	1.1522	-1.2368
C	6.5965	1.3735	2.1733
H	7.6103	1.7738	2.0756
H	6.1335	1.8438	3.0419
H	6.6699	0.3032	2.3755
C	1.3761	1.6607	3.4470
C	0.1059	2.3462	2.8988
H	-0.4886	1.6534	2.3085
H	-0.5071	2.7164	3.7264
H	0.3696	3.1993	2.2683
C	0.9754	0.4985	4.3823
H	0.4299	-0.2715	3.8419
H	1.8633	0.0406	4.8248
H	0.3457	0.8722	5.1957
C	2.2194	2.6986	4.2951
H	1.4787	3.0393	5.1041
H	3.0296	2.2802	4.7506
H	2.4167	3.5769	3.7120
C	-0.2400	2.0319	-2.2218
C	-0.9040	2.9840	-2.9842
H	-1.6466	2.6666	-3.7031
C	-0.5951	4.3308	-2.8245
H	-1.1129	5.0688	-3.4266
C	0.3685	4.7444	-1.9071
C	1.0255	3.7676	-1.1528
H	1.7819	4.0610	-0.4343
C	0.7339	2.4217	-1.3059
H	1.2624	1.6843	-0.7184
C	0.6986	6.2024	-1.7241
H	0.1466	6.8264	-2.4277
H	0.4528	6.5379	-0.7131
H	1.7652	6.3875	-1.8730

E(UB3LYP):–3118.50288735 hartree, $<S^2>$: 0.7575

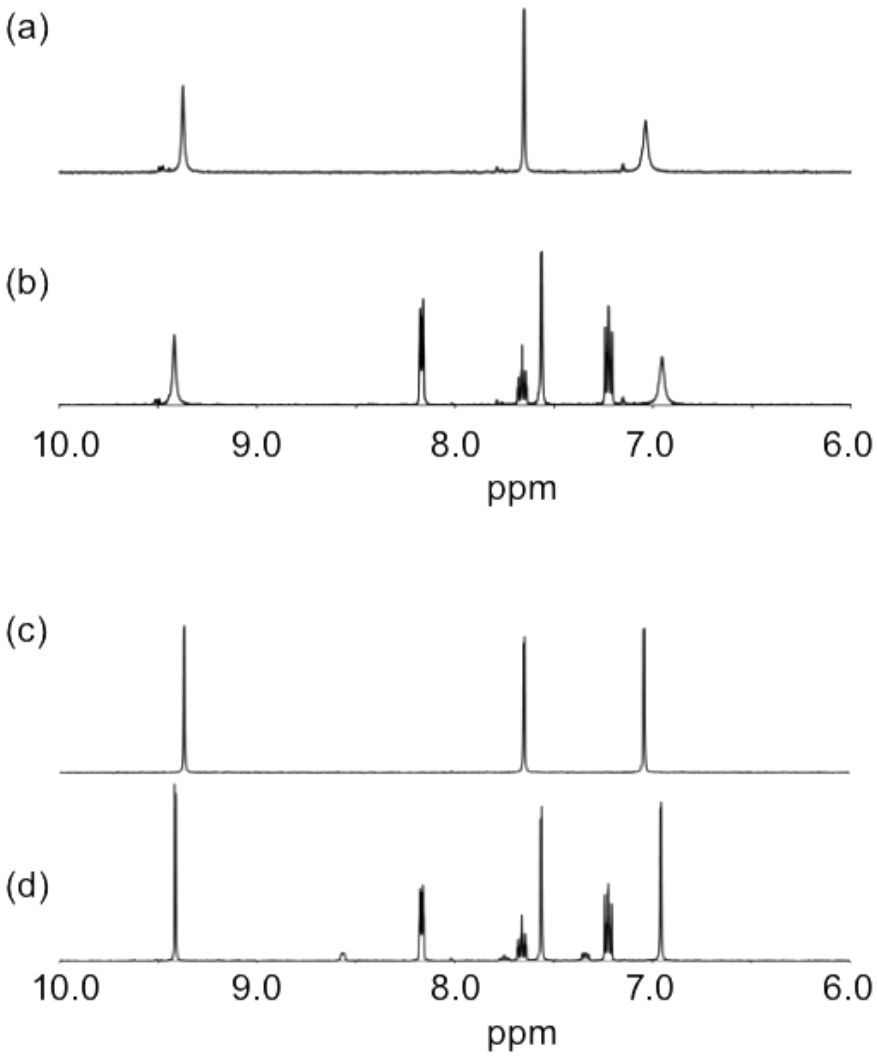

Figure S1. (a) ^{1}H NMR spectrum of ^{n}Bu$_4$N[**2**$^{\mathbf{Cl/H2O}}$] in acetone-d_6 and (b) that obtained upon addition of 1 equiv. of pyridine. (c) ^{1}H NMR spectrum of ^{n}Bu$_4$N[**2**$^{\mathbf{Cl/THF}}$] in acetone-d_6 and (d) that obtained upon addition of 1 equiv. of pyridine.

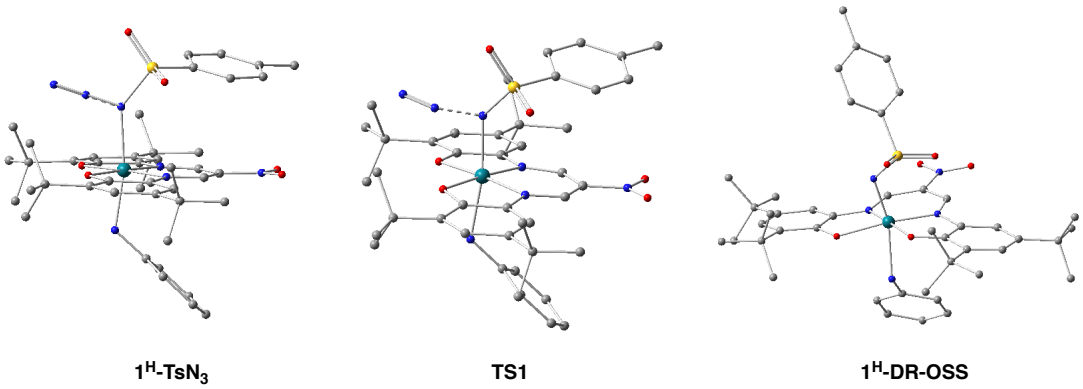

Figure S2. DFT optimized structures (B3LYP/ SDD(for Rh atom), D95**(for the other atoms)) of intermediates and transition states in the formation of **1^{H}-TsN**.

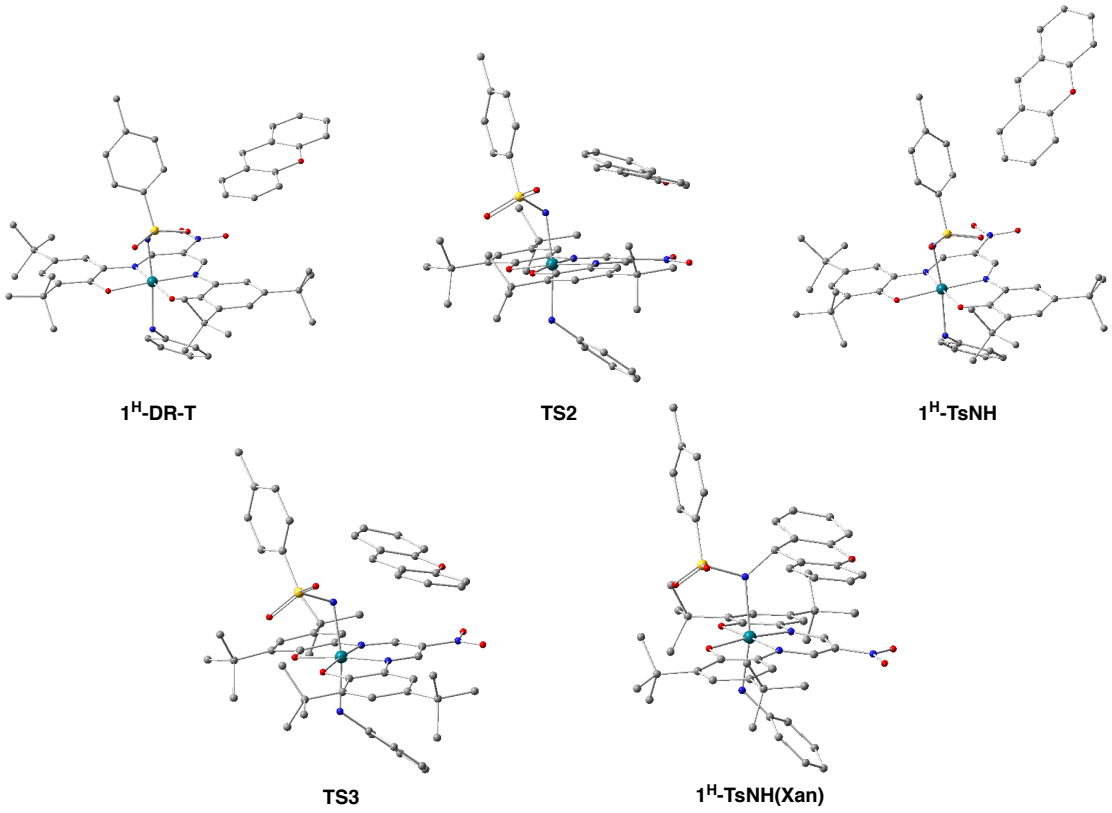

Figure S3. DFT optimized structures (B3LYP/ SDD(for Rh atom), D95**(for the other atoms)) of intermediates and transition states in the amination reaction of xanthene.

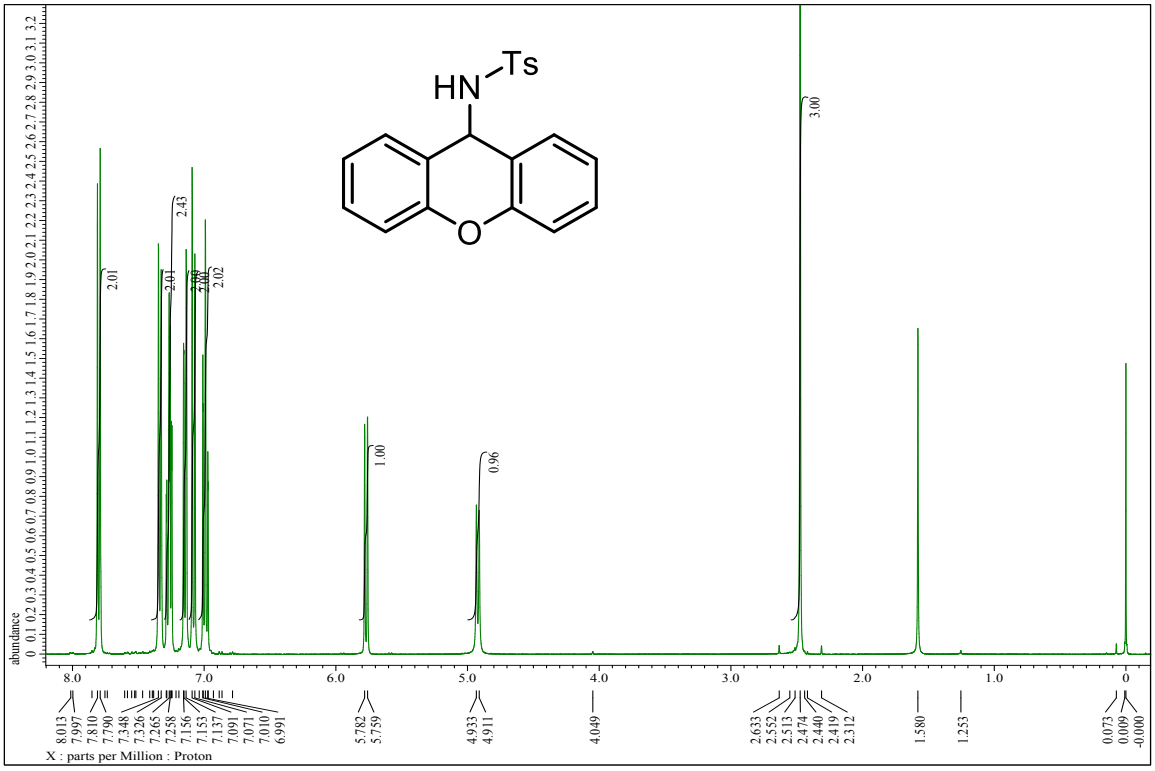

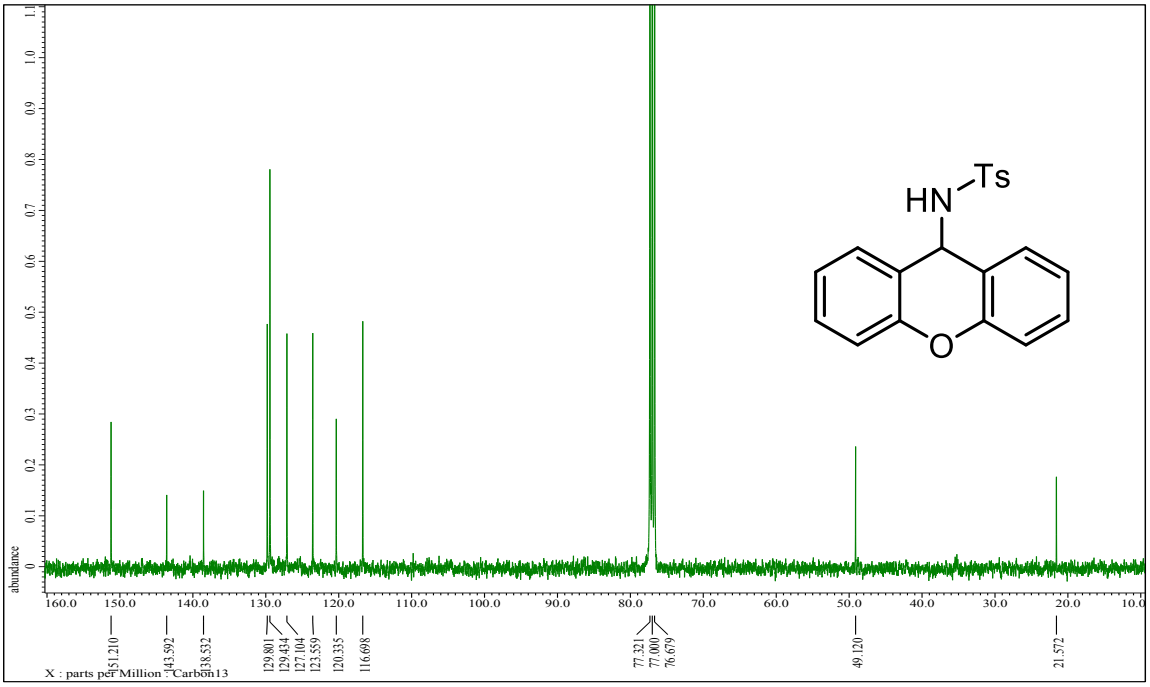

Figure S4. ^{1}H NMR (above) and ^{13}C NMR (below) chart of *N*-xanthyl-*p*-toluenesulfonamide (Solvent: $CDCl_3$).

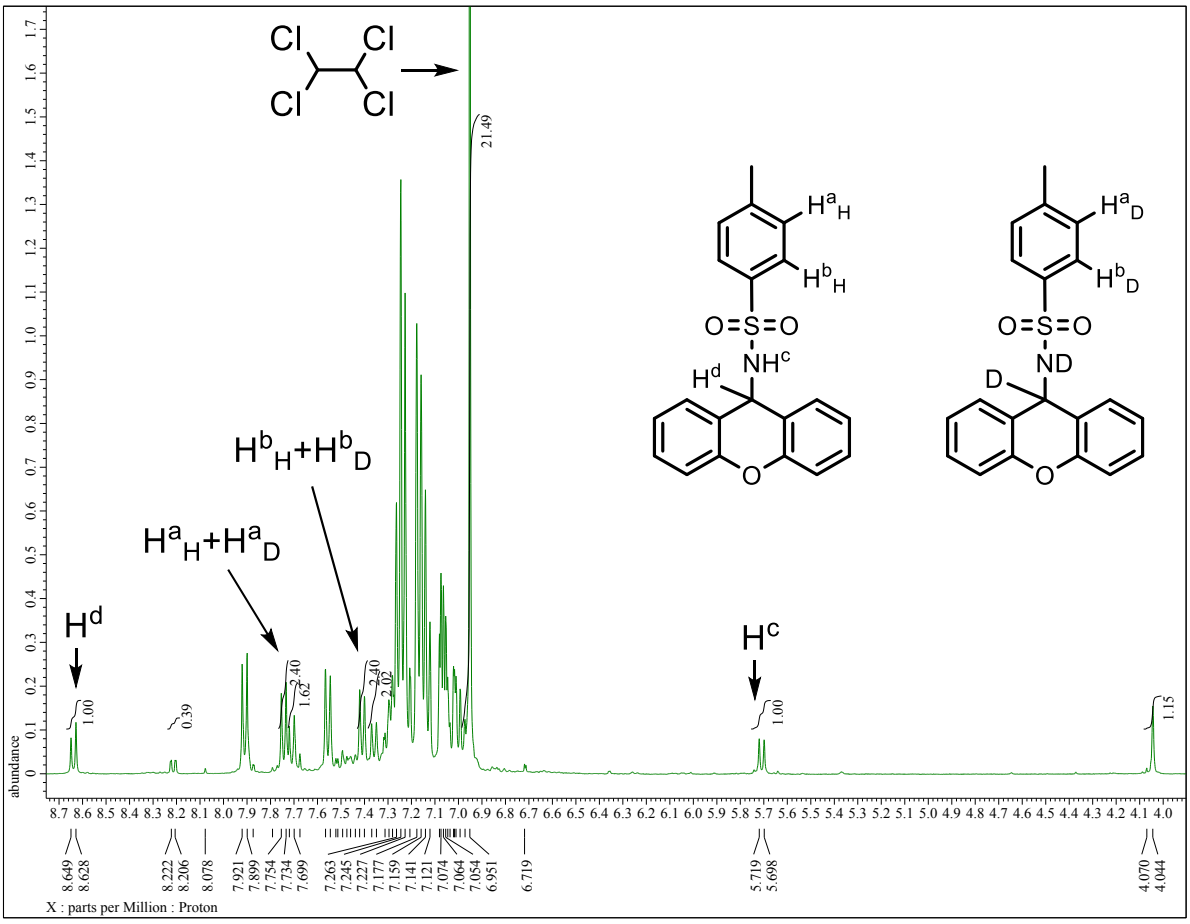

Figure S5. ^{1}H NMR chart of kinetic isotope effect experiment (Solvent: DMSO-d_6).

Chapter 2

C–H Iodination and Pseudo Oxidative Addition of Iodine at the Metal Center in the Rhodium(III) Complex with a Redox-active ligand

Introduction

C–H activation is an essential step for efficient functionalization of unreactive hydrocarbons. Such transformations are attractive from a synthetic point of view due to the possibility of transforming abundant and simple organic compounds into more useful and complex products. Rhodium complexes are one of the most prominent catalysts for the C–H functionalization. Numerous catalytic systems using rhodium(I) complexes,[1,2] piano-stool type rhodium(III) complexes ($CpRhX_3$),[2-4] and paddle-wheel type rhodium(II) complexes ($[Rh_2(RCOO)_4]$)[5,6] have so far been developed for C–H functionalization. Rhodium-porphyrin complexes have been reported to exhibit stoichiometric C(sp^2 and sp^3)–H activation.[7-26] On the other hand, however, the examples of C–H activation and functionalization by non-heme rhodium(III) complexes are very limited.[27,28]

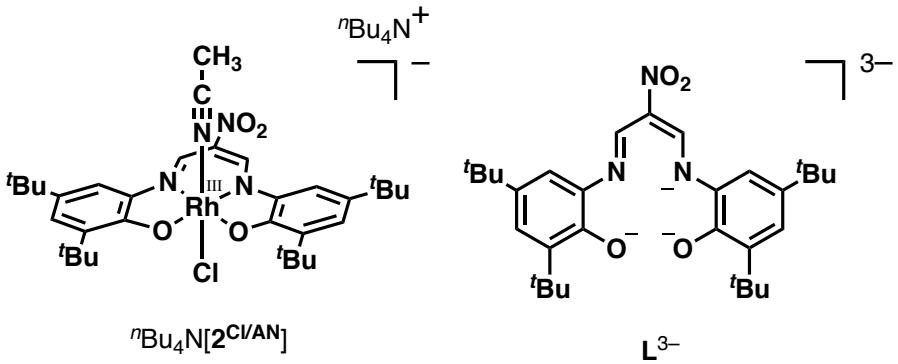

Figure 1. Chemical structure of rhodium(III) complex (^{n}Bu$_4$N[**2**$^{\mathbf{Cl/AN}}$]$^{\mathbf{I}}$) and the tetradentate ligand (**L**$^{3-}$).

In chapter 1, the author synthesized the rhodium(III) complex with a trianionic tetradentate ligand (**L**$^{3-}$), ^{n}Bu$_4$N[Rh^{III}(**L**$^{3-}$)(MeCN)(Cl)] (^{n}Bu$_4$N[**2**$^{\mathbf{Cl/AN}}$]) (Figure 1), and found that the ligand was redox-active to reach the dianionic radical **L**$^{\bullet 2-}$ and monoanionic **L**$^-$ states upon oxidation (Scheme 1).[29,30] In this chapter, C(sp^2)–H metalation of toluene and iodine atom insertion between the rhodium(III)-carbon bond are examined. The complex products as well as iodinated toluenes are characterized, based on which the

reaction mechanism is discussed.

Scheme 1. Ligand-based redox behavior of ^{n}Bu$_4$N[**2**$^{Cl/AN}$].

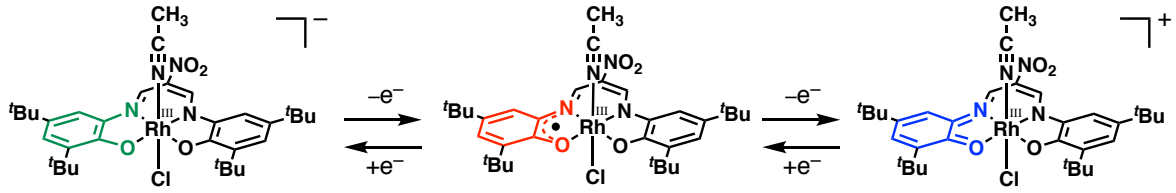

Experimental

General. The reagents used in this study, except the compounds mentioned below, were commercial products of the highest available purity and were used as received without further purification, unless otherwise noted.[31] **L**H$_3$ (*N*-(2-hydroxy-3,5-di-tert-butylphenyl)-3-(2-hydroxy-3,5-di-tert-butyl-phenyl)amino-2-nitro-2-propeneimine),[32] ^{n}Bu$_4$N[Rh^{III}(**L**$^{3-}$)(MeCN)(Cl)] (^{n}Bu$_4$N[**2**$^{Cl/AN}$]), and ^{n}Bu$_4$N[Rh^{III}(**L**$^{3-}$)(MeCN)(I)] (^{n}Bu$_4$N[**2**$^{I/AN}$])[30] were synthesized according to the reported procedures. ^{1}H NMR spectra were recorded at 400 MHz on a JEOL-ECP 400 or a JEOL-ECS 400 spectrometer. EPR spectra were taken on a Bruker X-band spectrometer (EMX-Micro). UV-visible spectra were taken on a Hewlett-Packard HP8453 photo diode array spectrophotometer. Electrospray ionization mass spectra (ESI-MS) were recorded with a Bruker micrOTOF II spectrometer. Elemental analyses were carried out on a Yanaco CHN-Corder MT-5.

Synthesis. ^{n}Bu$_4$N[Rh^{III}(**L**$^{3-}$)(*κ*-*C*-C$_6$H$_4$CH$_3$)(H$_2$O)] (**5**). Toluene (10 mL) was added to the mixture of ^{n}Bu$_4$N[Rh^{III}(**L**$^{3-}$)(MeCN)(Cl)] (^{n}Bu$_4$N[**2**$^{Cl/AN}$]) (100 mg, 0.106 mmol) and K$_2$CO$_3$ (147 mg, 1.06 mmol) in the 50 mL Schlenk tube. The mixture was stirred for 24 h at 100°C under dinitrogen atmosphere. After the reaction, inorganic solid was removed by filtration. The red filtrate was concentrated to 5 mL and the solution was added to excess hexane with vigorous stirring. The red precipitation (64.1 mg) was collected by centrifugation. The precipitation was dissolved in chloroform and *n*-hexane was diffused into the chloroform solution to give red crystals of **5** as a mixture of *p*-isomer and *m*-isomer. Yield: 32.3 mg (31%). Anal. Calcd for C$_{54}$H$_{87}$N$_4$O$_5$Rh·2H$_2$O: C, 64.14; H, 9.07; N, 5.54. Found: C, 63.96; H, 9.18; N, 5.71. ^{1}H NMR (400 MHz, CDCl$_3$): δ 9.60 (s, 4H), 7.59 (s, 4H), 7.05 (s, 4H), 6.67 (s, 1H), 6.45–6.30 (m, 6H), 5.97 (d, 1H, J = 7.2 Hz), 3.01–2.89 (m, 8H), 2.23 (s, 3H), 1.99 (s, 3H), 1.66–1.41 (m, 26 H), 1.40–1.21 (m, 26 H), 0.94 (t, 12H, J = 7.6 Hz). UV-vis (CHCl$_3$,

30°C) λ_{max}/nm (ε/M^{-1} cm^{-1}): 435 (20000). ESI-MS (negative ion detection mode): m/z = 714.30 ([Rh**L**(C_7H_7)]$^-$).

^{n}Bu$_4$N[Rh^{III}(**L**$^{2\bullet-}$)(I)$_2$] (**6**). **Method A**: Diiodine (76.1 mg, 0.300 mmol) was added to a $CDCl_3$ solution (600 μL) of ^{n}Bu$_4$N[Rh^{III}(**L**$^{3-}$)(κ-*C*-$C_6H_4CH_3$)(H_2O)] (**5**) (5.99 mg, 6.14 μmol) and the mixture was stirred for 2 h at room temperature. Tetrachloroethane (7.99 mg, 47.6 μmol) was added to the mixture as internal standard and the ^{1}H NMR measurement was carried out. After the measurement, the solution was passed through a silica-gel column (eluent: $CHCl_3$) and excess diiodine was quenched by saturated Na_2SO_3 aqueous solution. The collected chloroform solution was dried over Na_2SO_4 and was concentrated to about 600 μL. Black crystals suitable for X-ray crystallographic analysis were obtained by slow diffusion of *n*-hexane into the chloroform solution. Yield: 1.03 mg (15%). **Method B:** Diiodine (4.34 mg, 17.1 μmol) and ^{n}Bu$_4$N[Rh^{III}(**L**$^{3-}$)(MeCN)(I)] (^{n}Bu$_4$N[**2**$^{I/AN}$]) (34.2 mg, 33.1 μmol) were dissolved in chloroform (3 mL) and the solution was stirred for 10 min. Black crystals suitable for X-ray crystallographic analysis were obtained by slow diffusion of *n*-hexane into the chloroform solution. Yield: 36.6 mg (99%). Anal. Calcd for $C_{47}H_{78}N_4O_4Rh_1 \cdot 2CHCl_3$: C, 43.32; H, 5.94; N, 4.12. Found: C, 43.53; H, 6.08; N, 4.26. UV-vis ($CHCl_3$, 30°C) λ_{max}/nm (ε/M^{-1} cm^{-1}): 554 (15000). ESI-MS (negative ion detection mode): m/z = 877.05 ([Rh**L**I_2]$^-$), 750.14([Rh**L**I]$^-$).

C–H Iodination. Diiodine (76.1 mg, 0.300 mmol) was added to a $CDCl_3$ solution (600 μL) of ^{n}Bu$_4$N[Rh^{III}(**L**$^{3-}$)(κ-*C*-$C_6H_4CH_3$)(H_2O)] (**5**) (5.99 mg, 6.14 μmol) and the mixture was stirred for 2 h at room temperature. Tetrachloroethane (7.99 mg, 47.6 μmol) was added to the mixture as internal standard, and the ^{1}H NMR measurement was carried out. Iodination products (*p*- and *m*-iodotoluene) were identified by comparing its ^{1}H NMR chemical shifts with those reported in literature.[33]

EPR measurement. EPR spectrum of a chloroform solution of **6** in thin EPR tube (ϕ=ca.2 mm) was recorded with X-band microwave (9.636 GHz) at room temperature. Microwave power of 1.0 mW and modulation amplitude of 10 G were employed in the measurement.

X-ray Crystallography. A single crystal of **6** suitable for X-ray crystallographic analysis was obtained by slow diffusion of *n*-hexane into the $CHCl_3$ solution. The single crystal was mounted on a loop with a mineral oil, and X-ray data were collected at 110 K on a Rigaku R-AXIS RAPID diffractometer using filtered Mo-Kα radiation. The structure was solved by direct method (SHELXT[34]) and expanded using Fourier techniques. The non-hydrogen atoms were refined anisotropically by full-matrix least squares on F^2. The hydrogen atoms were attached at idealized positions on

carbon atoms and were not refined. The structure in the final stage of refinement showed no movement in the atom position. All calculations were performed using the CrystalStructure 4.2 crystallographic software package[35] except for refinement, which was performed using SHELXL.[36] Crystallographic parameters are summarized in Table 1.

Table 1. Crystallographic data for **6**.

	6·2$CHCl_3$
formula	$C_{49}H_{80}Cl_6I_2N_4O_4Rh$
fw	1358.63
crystal system	triclinic
space group	*P*-1 (#2)
a, Å	14.6266(6)
b, Å	15.4756(6)
c, Å	15.6599(6)
α, deg	60.520(4)
β, deg	74.155(5)
γ, deg	81.564(6)
V, Å^3	2968.2(2)
Z	2
D_{calced}, g cm^{-3}	1.520
F(000)	1374.00
μ, cm^{-1}	16.394
cryst size, mm	0.60× 0.30 ×0.20
T, K	110
$2\theta_{max}$, deg	55.0
reflns. obsd	13385
no. of params	592
*R*1[a]	0.0560
*wR*2[b]	0.1521
GOF	1.041
max./min. $\Delta\rho$, e Å^{-3}	2.19/-1.21

[a] $R1 = \Sigma(|F_o| - |F_c|)/\Sigma|F_o|$. [b] $wR2 = (\Sigma(w(F_o^2 - F_c^2)^2)/\Sigma w(F_o^2)^2)^{1/2}$.

Results and Discussion

First of all, reactivity of $^{n}Bu_4N[Rh^{III}(\mathbf{L}^{3-})(MeCN)(Cl)]$ ($^{n}Bu_4N[\mathbf{2}^{Cl/AN}]$) with toluene was examined. A mixture of $^{n}Bu_4N[\mathbf{2}^{Cl/AN}]$ and 10 equiv of K_2CO_3 was heated in toluene at 100°C for 24 h under dinitrogen atmosphere (Scheme 2). As a result, a toluene adduct $^{n}Bu_4N[Rh^{III}(\mathbf{L}^{3-})(\kappa\text{-}C\text{-}C_6H_4CH_3)(H_2O)]$ (**5**) was obtained as a microcrystalline powder by the slow diffusion of *n*-hexane to a chloroform solution of the product. The elemental analysis data suggest that **5** contains one H_2O molecule presumably as an axial ligand. In the ^1H NMR spectrum of **5**, two methyl protons due to the toluene moiety were observed and sum of the integration of the protons at the *p*- and *m*-positions was 3. This observation indicates that **5** was a mixture of the *p*-isomer and *m*-isomer with respect to the positions of carbon atoms coordinating to the rhodium center. The ratio of *p*-isomer to *m*-isomer was 1.5 : 1. There was no signal assignable to the *o*-isomer. In this case, the product derived from -CH_3 (methyl group) activation was not obtained, which is different from Chan's rhodium(III) porphyrin system in which rhodium(II) species was generated *in situ* to perform the C(sp^3)–H activation.[24-26] Therefore, it is suggested that the +III oxidation state of the rhodium center was kept during the C(sp^2)–H (aromatic carbon) metalation and the metalation might involve electrophilic aromatic substitution mechanism.

Scheme 2. C(sp^2)–H activation of toluene by rhodium(III) complex $^{n}Bu_4N[\mathbf{2}^{Cl/AN}]$ giving rhodium(III) complex **5**.

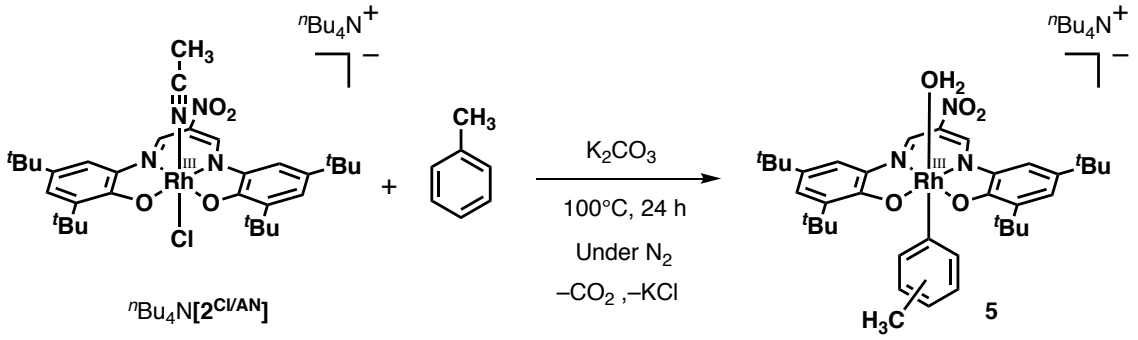

Since σ-alkyl and σ-aryl metal complexes have been often reactive toward oxidants such as dihalogens, **5** was treated with diiodine (I_2).[37] A treatment of **5** (*p* : *m* = 1.5 :1) with 50-fold excess diiodine gave *p*- and *m*-iodotoluene in a 84% ^1H NMR yield (*p* : *m* = 1.3 :1) (Scheme 3). After quenching the remaining excess amount of diiodine by addition of a Na_2SO_3 aqueous solution, slow diffusion of *n*-hexane into the chloroform solution of the reaction mixture gave black single crystals of **6** in a 15% yield (Scheme

3). In 1986, Ogoshi and co-workers reported iodination of σ-aryl rhodium(III)-porphyrin complexes.[9] Although porphyrins are known as a redox-active ligand, a rhodium complex with a porphyrin radical was not discussed as a product in the system.

Scheme 3. Iodination of complex **5** by the addition of diiodine giving complex **6**.

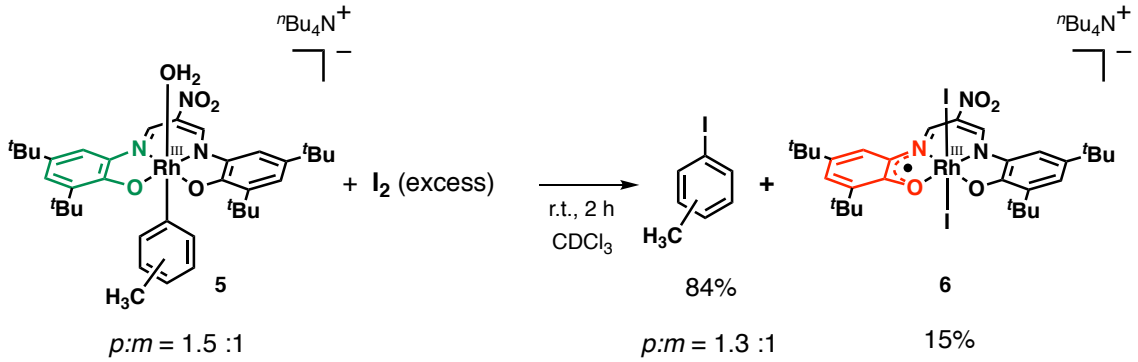

The ORTEP diagram of **6** is depicted in Figure 2. According to the charge balance, it can be concluded that the tetradentate ligand one-electron oxidation took place at the ligand moiety to give a rhodium(III)-dianion/radical ligand $\mathbf{L}^{\bullet 2-}$ complex. The dimension of the amidophenolato moieties (**a** and **b**) showed structural distortion due to the contribution of a quinonoid canonical structure.[38] In other words, C1–N1(C10–N2), C6–O1(C15–O2), C2–C3(C11–C12), and C4–C5(C13–C14) is shortened whereas C1–C2(C10–C11), C3–C4(C12–C13), C5–C6(C14–C15), and C1–C6(C10–C15) is lengthened compared to $\mathbf{1^H}$ bearing the fully reduced ligand ($\mathbf{L}^{3-}$) (see Table S1).[29] The metrical oxidation state (MOS) values proposed by Brown was –1.17 (13) for the amidophenolato moiety **a** and –1.06 (16) for the amidophenolato moiety **b**, supporting the dianionic structure of ligand $\mathbf{L}^{\bullet 2-}$.[38] The result of the EPR measurement indicates that **6** is a paramagnetic species, which is consistent with the above conclusion (Figure 3). The absorption band at 554 nm in the UV-vis spectrum of **6** is similar in energy to that of $^{n}Bu_4N[Rh^{III}(\mathbf{L}^{\bullet 2-})(MeCN)(Cl)]$ which is the one-electron oxidized product of $^{n}Bu_4N[\mathbf{2}^{\mathbf{Cl/AN}}]$ by $[(4\text{-bromophenyl})_3N^{\bullet +}]SbCl_6$.[30] These results indicate that complex **6** is $^{n}Bu_4N[Rh^{III}(\mathbf{L}^{\bullet 2-})(I)_2]$, which suggests that the iodination involves pseudo oxidative addition of diiodine to the rhodium(III) center, concomitant with ligand-based oxidation as reported in $Zr^{IV}(ap)_2(THF)_2$ (ap = 2,4-di-*tert*-butyl-6-*tert*-butylamidophenolato)[39], $Zr^{IV}(pda)_2$ (pda = *N, N'*-bis(*neo*-pentyl)-*o*-phenylenediamido),[40] and $Cu^{II}(sq)_2$ (sq = 2,4-di-*tert*-butyl-*N*-phenyl-*o*-iminobenzosemiquinonato).[41]

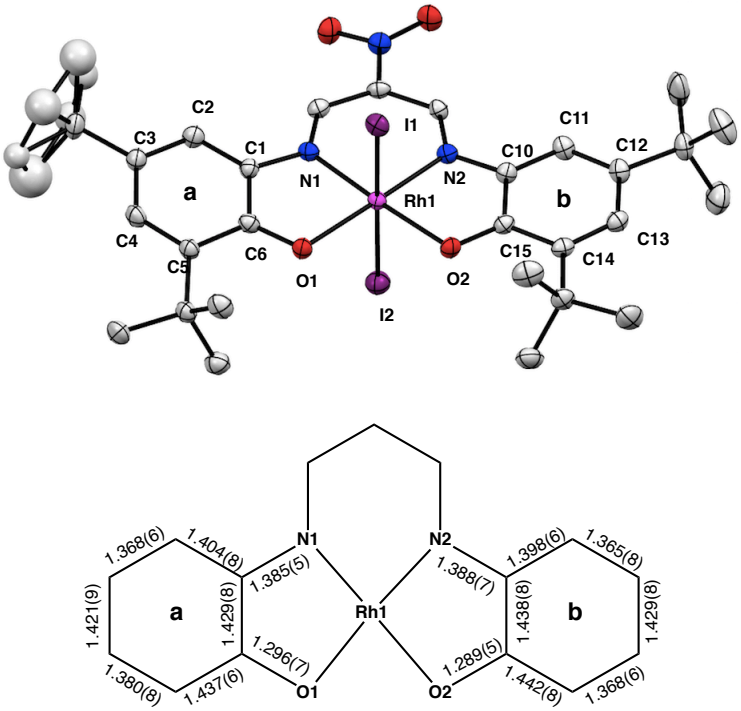

Figure 2. ORTEP diagram of **6** showing 50% ellipsoids. Hydrogen atoms, solvent molecules, and counter ion are omitted for clarity (above). The chemical structure including the selected bond lengths of the iminobenzosemiquinonato ligand moiety (below).

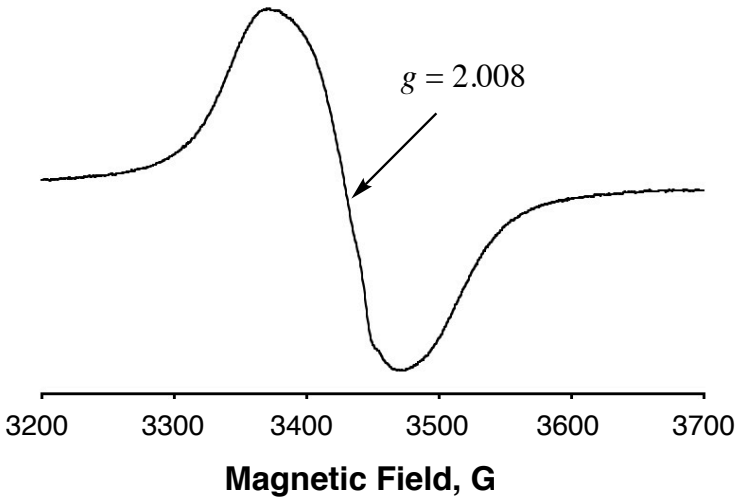

Figure 3. EPR spectrum of **6** in $CHCl_3$ (1.0 mM) at 298 K.

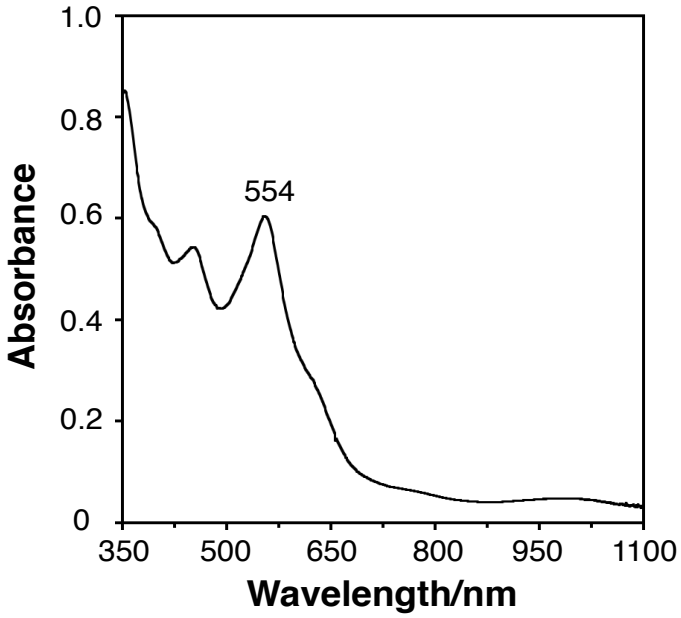

Figure 4. UV-vis spectrum of **6** (0.041 mM) in $CHCl_3$ at 30°C.

In order to obtain further mechanistic insights for the iodidation reaction, the reaction of **5** (^{n}Bu$_4$N[Rh^{III}(**L**$^{3-}$)(κ-*C*-C$_6$H$_4$CH$_3$)(H$_2$O)]) with diiodine was monitored by UV-vis spectroscopy. Figure 5 shows the UV-vis spectral change of **5** observed upon addition of various amounts of diiodine, where the intense absorption band at 435 nm due to **5** disappeared with concomitant appearance of a new absorption band at 547 nm. The spectral change completed when 0.5 equivalents of diiodine was added as shown in Figure 5 (inset). Given that the complex **6** containing the oxidized ligand **L**$^{\bullet 2-}$ (^{n}Bu$_4$N[Rh^{III}(**L**$^{\bullet 2-}$)(I)$_2$]) is formed by the reaction of ^{n}Bu$_4$N[Rh^{III}(**L**$^{3-}$)(MeCN)(I)] (^{n}Bu$_4$N[**2**$^{\mathbf{I/AN}}$]) with 0.5 equivalent of diiodine (see Method B in Experimental), the pseudo oxidative addition of diiodine to **5** might occur to yield ^{n}Bu$_4$N[Rh^{III}(**L**$^{\bullet 2-}$)(κ-*C*-C$_6$H$_4$CH$_3$)(I)] (intermediate **A** in Scheme 3). The absorption band at 547nm shown in Figure 5 may be due to intermediate **A**. In fact, the ESI-mass spectrum of a chloroform solution containing **5** and diiodine (0.5 equiv.) showed peak clusters at *m*/*z* = 714.29 ([Rh+**L**+C$_7$H$_7$])$^-$, 750.14 ([Rh+**L**+I]$^-$), 841.19 ([Rh+**L**+C$_7$H$_7$+I]$^-$), 877.04 ([Rh+**L**+I+I]$^-$), which shows formation of ^{n}Bu$_4$N[Rh**L**$^{\bullet 2-}$(κ-*C*-C$_6$H$_4$CH$_3$)(I)] (Figure 6).

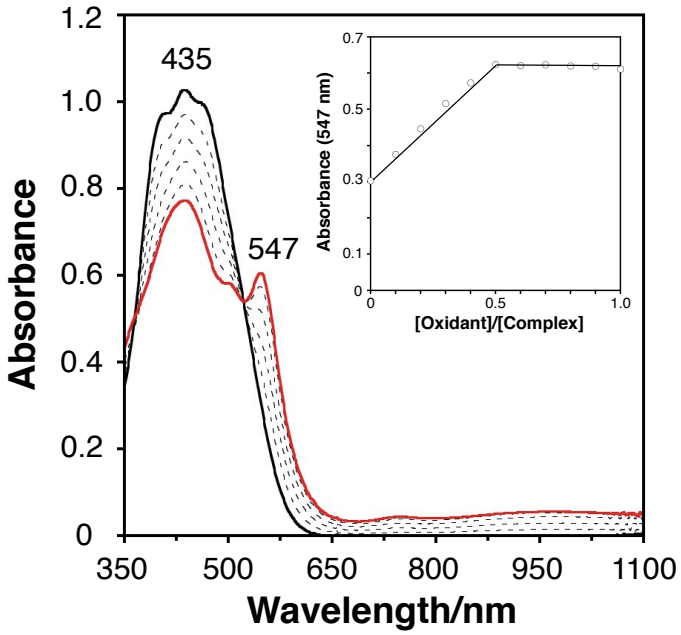

Figure 5. Spectral change observed upon the addition of diiodine to **5** (0.050 mM) in chloroform at 30°C (black → red). (Inset) Absorbance change at 547 nm against the [Oxidant]/[**5**] ratio.

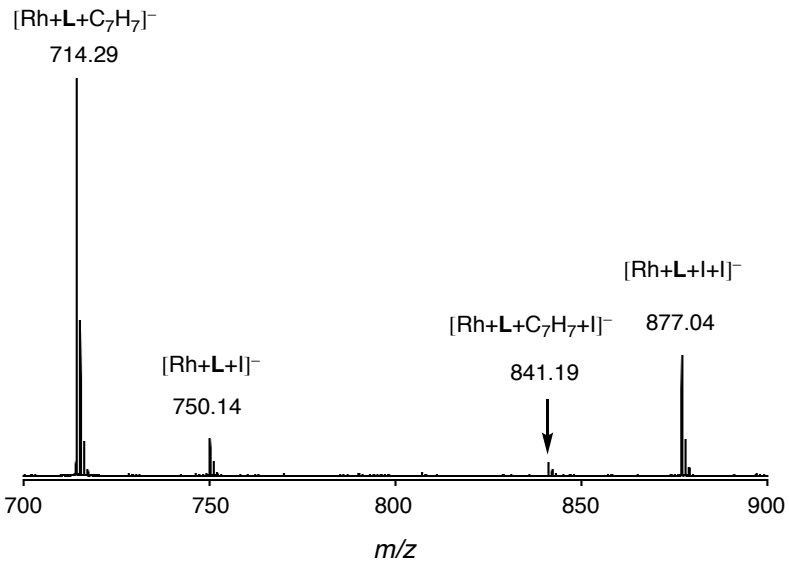

Figure 6. ESI-mass spectrum (negative ion detection mode) of the mixture of **5** and 0.5 equivalent of diiodine.

Summary and Mechanistic Consideration

The author synthesized the rhodium(III)-toluene adduct **5** by electrophilic metalation of toluene to ^{n}Bu$_4$N[Rh^{III}(**L**$^{3-}$)(MeCN)(Cl)] (^{n}Bu$_4$N[**2**$^{Cl/AN}$]). The ^{1}H NMR measurement showed that the adduct gave a mixture of regioisomers with respect to the position of the carbon coordinating to the rhodium (*p*-isomer : *m*-isomer = 1.5 : 1). The reaction of the rhodium(III)-toluene adduct with 50-fold excess diiodine gave *p*- and *m*-iodotoluene and the oxidized rhodium complex **6**. Based on the X-ray crystal structure analysis and EPR data, the complex **6** was assigned as ^{n}Bu$_4$N[Rh^{III}(**L**$^{\bullet 2-}$)(I)$_2$] containing the one-electron oxidized ligand. Titration experiments for a reaction **5** with diiodine showed that 0.5 equiv of diiodine was required for the oxidation of complex **5**. The possible reaction pathway in the iodination is depicted in Scheme 3. First of all, 0.5 equivalent of diiodine oxidize the complex **5** to yield an intermediate complex **A** (^{n}Bu$_4$N[Rh^{III}(**L**$^{\bullet 2-}$)(I)(κ-*C*-C$_6$H$_4$CH$_3$)]), which was detected by the UV-vis titration shown in Figure 5 and the ESI-MS shown in Figure 6. In the presence of an excess amount of diiodine, the intermediate complex **A** further reacts with diiodine to give the final product **6**. In the C–I bond formation step from **A** to **6**, there are two possible pathways; the C–I bond forms via heterolysis (Scheme 3, through **B**) or homolysis (Scheme 3, through **C**) of Rh–C and I–I bonds. This study provides the first example of C–H iodination involving pseudo oxidative addition of diiodine to the rhodium(III) center concomitant with ligand-based oxidation.

Scheme 3. Possible reaction pathways for the iodination reaction of **5** giving **6**.

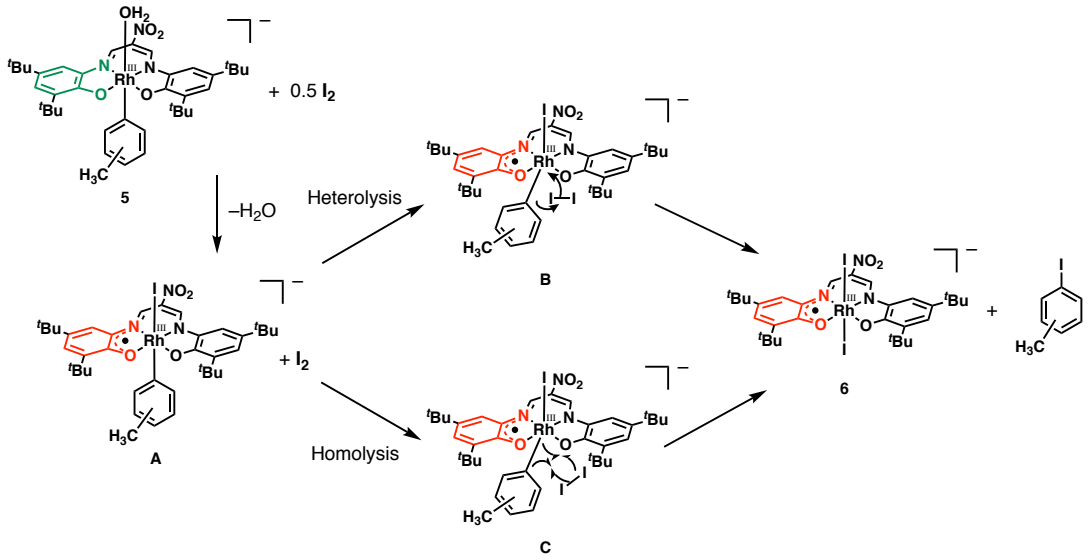

References

(1) Colby, D. A.; Bergmann, R. G.; Elman, J. A. *Chem. Rev*., **2010**, *110*, 624–655.

(2) Colby, D. A.; Tsai, A. S.; Bergman, R. G.; Ellman, J. A. *Acc. Chem. Res.*, **2012**, *45*, 814–825.

(3) Rej, S.; Chatani, N. *Angew. Chem. Int. Ed*., **2019**, *58*, 8304–8329.

(4) Song, G.; Wang, F.; Li, X. *Chem. Soc. Rev.*, **2012**, *41*, 3651–3678.

(5) Doyle, M. P.; Duffy, R.; Ratnikov, M.; Zhou, L. *Chem. Rev.*, **2010**, *110*, 704–724.

(6) Roizen, J. L.; Harvey, M. E.; Du Bois, J. *Acc. Chem. Res.*, **2012**, *45*, 911–922.

(7) Fleischer, E. B.; Lavallee, D. *J. Am. Chem. Soc.*, **1967**, *89*, 7132–7133.

(8) Aoyama, Y.; Yoshida, T.; Sakurai, K.; Ogoshi, H. *J. Chem. Soc., Chem. Commun.*, **1983**, 478–479.

(9) Aoyama, Y.; Yoshida, T.; Sakurai, K.; Ogoshi, H. *Organometallics*, **1986**, *5*, 168–173.

(10) Zhou, X.; Tse, M. K.; Wu, D.-D.; Mak, T. C. W.; Chan, K. S. *J. Organomet. Chem.*, **2000**, *598*, 80–86.

(11) Yang, W.; Zhang, H.; Li, L.; Tam, C. M.; Feng, S.; Wong, K. L.; Lai, W. Y.; Ng, S. H.; Chen, C.; Chan, K. S. *Organometallics*, **2016**, *35*, 3295–3300.

(12) Collman, J. P.; Boulatov, R. *Inorg. Chem.*, **2001**, *40*, 2461–2464.

(13) Choi, K. S.; Chiu, P. F.; Chan, K. S. *Organometallics*, **2010**, *29*, 624–629.

(14) Aoyama, Y.; Yoshida, T.; Ogoshi, H. *Tetrahedron Lett.*, **1985**, *26*, 6107–6108.

(15) Aoyama, Y.; Yamaguchi, A.; Tanaka, Y.; Toi, H.; Ogoshi, H. *J. Am. Chem. Soc.*, **1987**, *109*, 4735–4737.

(16) Wayland, B. B.; Del Rossi, K. J. *J. Organomet. Chem.*, **1984**, *276*, c27–c30.

(17) Del Rossi, K. J.; Wayland, B. B. *J. Am. Chem. Soc.*, **1985**, *107*, 7941–7944.

(18) Sherry, A. E.; Wayland, B. B. *J. Am. Chem. Soc.*, **1990**, *112*, 1259–1261.

(19) Del Rossi, K. J.; Zhang, X.-X.; Wayland, B. B. *J. Organomet. Chem.*, **1995**, *504*, 47-56.

(20) Cui, W.; Zhang, X. P.; Wayland, B. B. *J. Am. Chem. Soc.*, **2003**, *125*, 4994–4995.

(21) Cui, W.; Wayland, B. B. *J. Am. Chem. Soc.*, **2004**, *126*, 8266–8274.

(22) Li, S.; Cui, W.; Wayland, B. B. *Chem. Commun.*, **2007**, 4024-4025.

(23) Sarkar, S.; Li, S.; Wayland, B. B. *J. Am. Chem. Soc.*, **2010**, *132*, 13569–13571.

(24) Chan, K. S.; Chiu, P. F.; Choi, K. S. *Organometallics*, **2007**, *26*, 1117–1119.

(25) Chan, Y. W.; Chan, K. S. *Organometallics*, **2008**, *27*, 4625–4635.

(26) Chan, K. S.; Chan, Y. W. *Organometallics*, **2014**, *33*, 3702–3708.

(27) Kovach, J.; Brennessel, W. W.; Jones, W. D. *J. Organomet. Chem*., **2015**, *793*, 192–199.

(28) Ito, J.; Nishiyama, H. *Eur. J. Inorg. Chem.*, **2007**, 1114–1119.
(29) Fujita, D.; Sugimoto, H.; Shiota, Y.; Morimoto, Y.; Yoshizawa, K.; Itoh, S. *Chem. Commun.* **2017,** *53*, 4849-4852.
(30) Fujita, D.; Sugimoto, H.; Morimoto, Y.; Itoh, S. *Inorg. Chem.* **2018,** *57*, 9738–9747.
(31) Perrin, D. D.; Armarego, W. L. F.; Perrin, D. R. *Purification of Laboratory Chemicals 4th Edition*. 4th ed.; Pergamon Press: Elmsford, NY, 1996.
(32) Takaichi, J.; Ohkubo, K.; Sugimoto, H.; Nakano, M.; Usa, D.; Maekawa, H.; Fujieda, N.; Nishiwaki, N.; Seki, S.; Fukuzumi, S.; Itoh, S. *Dalton Trans.* **2013**, *42*, 2438−2444.
(33) Dong, C.-P.; Nakamura, K.; Taniguchi, T.; Mita, S.; Kodama, S.; Kawaguchi, S.; Nomoto, A.; Ogawa, A.; Mizuno, T. *ACS Omega*, **2018**, *3*, 9814-9821.
(34) Sheldrick, G. *Acta Crystallogr., Sect. A* **2015,** *71*, 3–8.
(35) Crystal Structure Analysis Package, Rigaku Corporation (2000-2017). Tokyo 196-8666, Japan.
(36) Sheldrick, G. *Acta Crystallogr., Sect. A* **2008,** *64*, 112–122.
(37) Petrone, D. A.; Ye, J.; Lautens, M. *Chem. Rev.*, **2016**, *116*, 8003–8104.
(38) Brown, S. N. *Inorg. Chem.*, **2012**, *51*, 1251–1260.
(39) Blackmore, K. J.; Ziller, J. W.; Heyduk, A. F. *Inorg. Chem.* **2005**, *44*, 5559–5561.
(40) Ketterer, N. A.; Fan, H.; Blackmore, K. J.; Yang, X.; Ziller, J. W.; Baik, M.-H.; Heyduk, A. F. *J. Am. Chem. Soc.*, **2008**, *130*, 4364–4374.
(41) Mukherjee, C.; Weyhermüller, T.; Bothe, E.; Chaudhuri, P. *Inorg. Chem.*, **2008**, *47*, 2740–2746.

Supporting Information for Chapter 2

(Table S1, Figure S1)

Table S1. Comparison of bond lengths in amidophenolato moieties (ring **a** and ring **b**) of $\mathbf{1^H}$ and **6**.

	$\mathbf{1^H}$	**6**
Ring **a**		
Rh1－O1	2.0190(11)	2.047(3)
Rh1－N1	1.9817(13)	1.973(5)
O1–C6	1.3332(19)	1.296(7)
N1–C1	1.4273(19)	1.385(5)
C1–C2	1.396(2)	1.404(8)
C2–C3	1.385(2)	1.368(6)
C3–C4	1.410(2)	1.421(9)
C4–C5	1.385(2)	1.380(8)
C5–C6	1.428(2)	1.437(6)
C6–C1	1.421(2)	1.429(8)
MOS*	–1.68(20)	–1.17 (13)
Ring **b**		
Rh1－O2	2.0072(12)	2.050(4)
Rh1－N2	1.9763(13)	1.979(3)
O2–C15	1.3362(18)	1.289(5)
N2–C10	1.428(2)	1.388(7)
C10–C11	1.400(2)	1.398(6)
C11–C12	1.384(2)	1.365(8)
C12–C13	1.405(2)	1.429(8)
C13–C14	1.389(2)	1.368(6)
C14–C15	1.420(2)	1.442(8)
C15–C10	1.418(2)	1.438(8)
MOS*	–1.74(18)	–1.06 (16)

*Metrical oxidation states.[38]

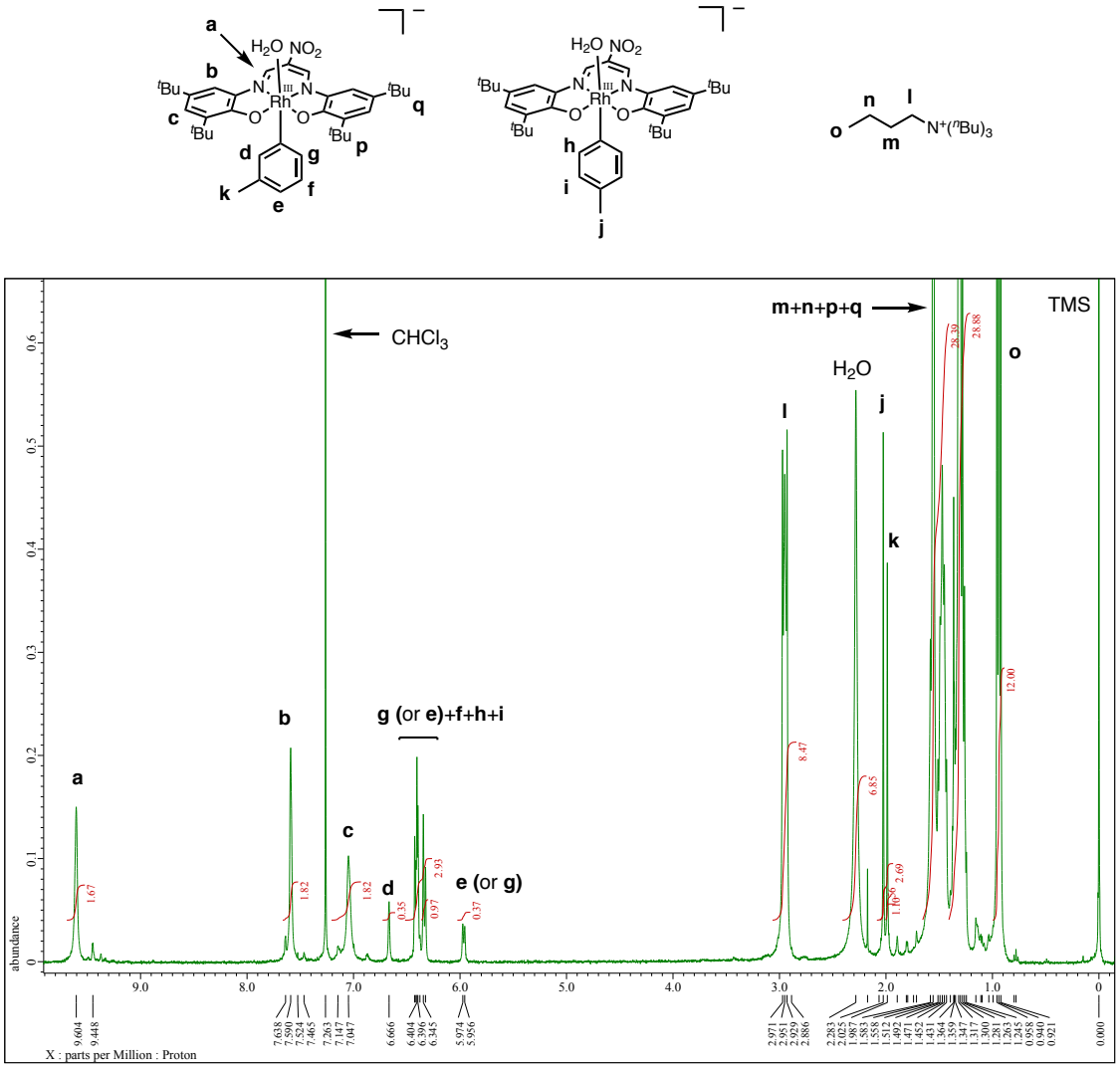

Figure S1. ^{1}H NMR chart of **2** at room temperature (400 MHz, $CDCl_3$).

Chapter 3

Controlling Coordination Number of Rhodium(III) Complex by Ligand-based Redox for Catalytic C–H Amination

Introduction

Redox-active ligands play important roles in catalytic reactions and material functions involving transition-metal complexes.[1,2] Typically, redox-active ligands serve as electron reservoirs or finely tune the redox potentials of the complexes to facilitate the reactions. *o*-Phenylene derivatives constitute one of the large families of such redox-active ligands that can chelate to a transition metal ions to donate or accept electrons to or from substrates depending on their redox state,[3] the substrates of which include organic azides,[4-11] disulfides,[12] trifluoromethyl cation,[13,14] and dioxygen.[15-23] *o*-Phenylene ligand based redox events of the metal complexes are found in magnetism,[24,25] photo-[26,27] and electro-chemical[28] behavior in functional materials, and catalytic cycles in metalloenzymes.[29,30]

Combination of redox-active ligands and redox-innocent metal ions has attracted much recent attention, since such a combination will provide a new type of reactive intermediates including a ligand radical species.[31,32] Such a strategy has been adopted for catalytic C–H amination, where a nitrene radical active species is generated via an electron transfer from the redox-active supporting ligand to the coordinated organic azide oxidant. For instance, van der Vlugt and co-workers reported an intramolecular C–H amination of 4-phenylbutaneazide to Boc-protected 2-phenylpyrrolidine by a palladium(II) complex supported by a redox-active pincer ligand (2,4-di-*tert*-butyl-6-((2-(pyridin-2-yl)propan-2-yl)amido)phenolato) (Scheme 1(a)).[4] In this system, the putative active species is a nitrene radical bound palladium(II) complex that is generated via an intramolecular electron transfer from the pincer ligand to the azide compound bound to the metal center. In chapter 1, the author demonstrated a catalytic intermolecular C–H amination with tosyl azide by the six-coordinate rhodium(III) complexes of a redox-active tetradentate ligand,[9] where a nitrene radical active intermediate is generated via a similar way; an intramolecular electron transfer from the ligand to the coordinated azide compound with keeping the rhodium(III) oxidation state (Scheme 1(b)).

Scheme 1. (a) Intramolecular amination using the palladium(II) complex bearing a redox-active pincer ligand.[4] (b) Intermolecular amination using the rhodium(III) complexes bearing a redox-active tetradentate ligand.[9]

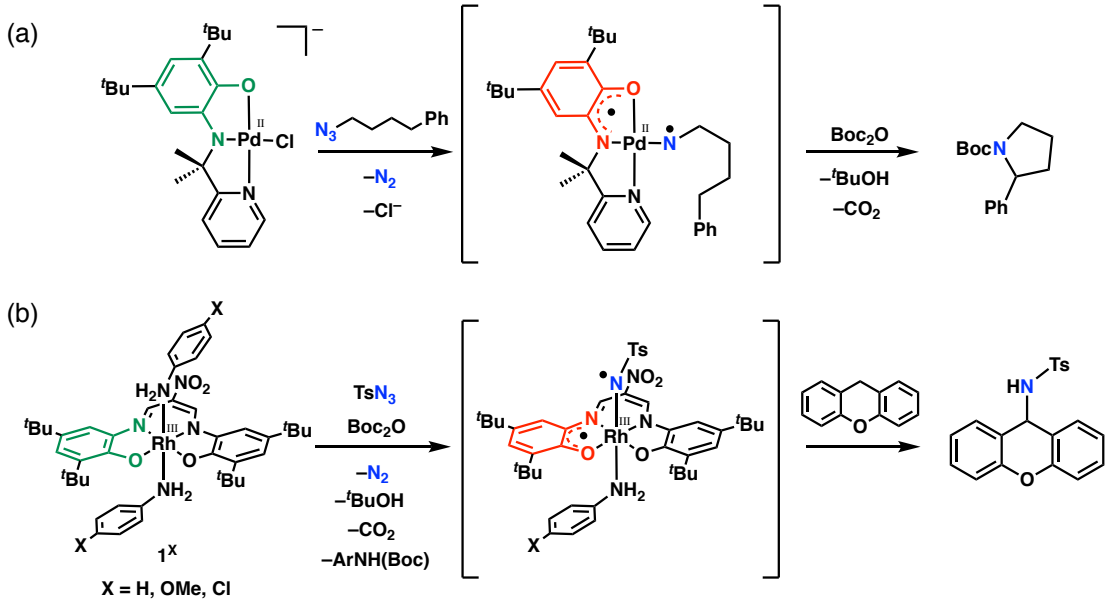

In this chapter, the author presents another example of a C–H amination catalyzed by a rhodium(III) complex supported by an *o*-phenylenediamine ligand and Cp* (1,2,3,4,5-pentamethylcyclopentadienido). In this system, the coordination number of rhodium(III) center is altered depending on the redox state of *o*-phenylenediamido ligand; $C_6H_4N_2{}^{t\mathrm{Bu2}}Ph_2{}^{2-}$ (reduced dianion form; **L'**$^{2-}$) vs. $C_6H_4N_2{}^{t\mathrm{Bu2}}Ph_2{}^{\bullet-}$ (*o*-diminobenzosemiquinone radical anion form; **L'**$^{\bullet-}$) vs. $C_6H_4N_2{}^{t\mathrm{Bu2}}Ph_2{}^{0}$ (oxidized neutral form; **L'**^{0}), where $^{t\mathrm{Bu2}}$Ph is 3,5-di-*tert*-butyphenyl. In this case, association and dissociation of the external substrate and product are controlled by the redox state of the supporting ligand, which is different from the case of former examples shown in Scheme 1, where ligand displacement is necessary to induce the reactions (Cl^- in Scheme 1a and *p*-X-$C_6H_4NH_2$ in Scheme 1b).

In this study, the author synthesized and characterized [Cp*Rh$^{\mathrm{III}}$(**L'**$^{2-}$)] (**7**), [Cp*Rh$^{\mathrm{III}}$(**L'**$^{\bullet-}$)(CN)] (**8**), and [Cp*Rh$^{\mathrm{III}}$(**L'**^{0})(CN)](PF$_6$) (**9**) shown in Figure 1, and examined their catalytic activity in the intramolecular amination of trisylazide (2,4,6-triisopropylphenylsulfonyl azide) to find that complex **8** exhibited the highest reactivity. Mechanistic details are discussed on the basis of the structure-reactivity relationship.

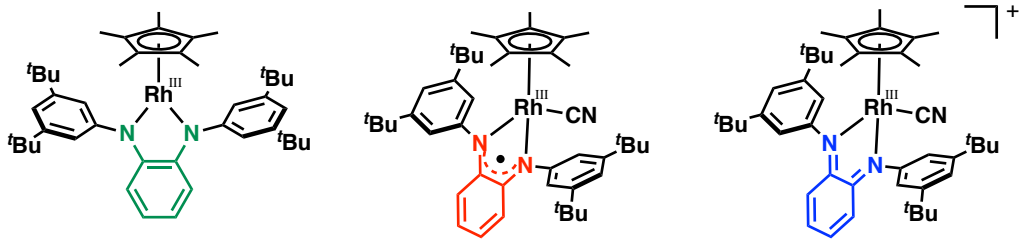

Figure 1. Rhodium(III) complexes **7**, **8**, and **9** synthesized in this work.

Experimental

General. The reagents used in this study, except the compounds mentioned below, were commercial products of the highest available purity and were used as received without further purification, unless otherwise noted.[33] H_2**L'** (*N,N*-di-(3,5-di-*tert*-butylphenyl)benzene-1,2-diamine)),[34,35] $[Cp^*Rh^{III}Cl_2]_2$,[36] and trisylazide[37] were synthesized according to the reported procedures. ^{1}H NMR and ^{13}C NMR spectra were recorded at 400 MHz and 101 MHz, respectively, on a JEOL-ECP 400 or a JEOL-ECS 400 spectrometer. EPR spectra were taken on a Bruker X-band spectrometer (EMX-Micro). UV-visible spectra were taken on a Jasco V-650 spectrophotometer or a Hewlett-Packard HP8453 photodiode array spectrophotometer. Electrospray ionization mass spectra (ESI-MS) were recorded with a Bruker micrOTOF II spectrometer. Elemental analyses were carried out on a Yanaco CHN-Corder MT-5. Electrochemical measurements were performed with a Hokuto Denko HZ-7000. A set of a carbon working electrode, an $Ag^+/AgNO_3/CH_3CN$ reference electrode, and a platinum counter electrode was employed in these experiments. All potentials were referenced versus the ferrocene/ferrocenium redox couple (Fc/Fc^+).

Synthesis. $[Cp^*Rh^{III}(L'^{2-})]$ (**7**·THF). A 0.25 mL (0.40 mmol) of 1.6 M ^{n}BuLi solution in *n*-hexane was added to H_2**L'**(97 mg, 0.20 mmol) in 5.0 mL of THF at –78°C. The resulting mixture was warmed to room temperature and stirred for 1 h before addition of $[Cp^*Rh^{III}Cl_2]_2$ (62 mg, 0.10 mmol). The reaction mixture was stirred for 20 h at room temperature and then the solvents were removed *in vacuo*. The crude complex was dissolved in THF (2 mL), and methanol (8 mL) was diffused into the solution to give purple crystals of **7**. Yield: 89 mg (62%). Anal. Calcd for $C_{44}H_{61}N_2Rh$·THF: C, 72.70; H, 8.77; N, 3.53. Found: C, 72.89; H, 8.79; N, 3.81. ^{1}H NMR (400 MHz, $CDCl_3$): δ 7.31 (t, 2H, J = 2.0 Hz), 7.12 (d, 4H, J = 2.0 Hz), 6.70-6.66 (m, 2H), 6.65-6.61 (m, 2H),

1.39 (s, 36H), 1.37 (s, 15H). ^{13}C NMR (101 MHz, $CDCl_3$, ppm): 154.45, 151.18, 149.09, 120.38, 118.37, 117.31, 111.88, 91.43 (d, $J_{Rh\text{-}C}$ = 7.8 Hz, $C_5(CH_3)_5$), 35.20, 31.80, 9.14. UV-vis (CH_2Cl_2) λ_{max}/nm (ε/M^{-1} cm^{-1}): 542 (28000).

[Cp*Rh^{III}(L'$^{\bullet-}$)(CN)] (8·0.8H$_2$O). A dichloromethane solution (10 mL) of **7** (41 mg, 0.058 mmol) was added to a slurry of AgCN (8.1 mg , 0.060 mmol) and CH_3CN (10 mL). After stirring for 3 h, the color of the reaction solution was changed from purple to cherry red. The precipitated silver was removed by filtration with Celite. The solvents were then removed *in vacuo* to yield a crude complex, which was recrystallized from benzene and *n*-hexane to give brown crystals of **8**. Yield: 7.8 mg (18%). Anal. Calcd for $C_{45}H_{61}N_3Rh\cdot0.8H_2O$: C, 70.99; H, 8.29; N, 5.52. Found: C, 71.27; H, 8.65; N, 5.60. UV-vis (CH_2Cl_2) λ_{max}/nm (ε/M^{-1} cm^{-1}): 398 (9300), 472 (4700), 809 (2800). FT-IR (KBr) ν/cm^{-1}: 2116 (CN).

[Cp*Rh^{III}(L'^{0})(CN)][PF$_6$] ([9]PF$_6$·1.3H$_2$O). KCN (3.0 mg, 40 μmol) and $NOPF_6$ (13 mg, 74 μmol) were added to a dichloromethane solution (4 mL) of **7** (23 mg, 38 μmol), and the resulting mixture was stirred for 1 h at room temperature. The solution was added to *n*-hexane (20 mL) to yield a dark brown precipitate, which was collected by filtration. The solid was dissolved in dichloromethane (20 mL) and insoluble materials were removed by filtration using Celite. The solvent was removed *in vacuo* to give green solid of **9**. Pale green crystals of **9** were obtained after recrystallization from benzene and *n*-hexane. The collected crystals were dried in air. Yield: 15 mg (44%). Anal. Calcd for $C_{45}H_{61}N_3PF_6Rh\cdot1.3H_2O$: C, 59.05; H, 7.00; N, 4.59. Found: C, 58.86; H, 6.93; N, 4.84.^{1}H NMR (400 MHz, $CDCl_3$): δ 7.49 (t, 2H, J = 2.0 Hz), 7.39 (t, 2H, J = 2.0 Hz), 7.35 (t, 2H, J = 2.0 Hz,), 6.96-6.90 (m, 2H,), 6.70-6.64 (m, 2H), 1.41 (s, 18H), 1.40 (s, 18H), 1.32 (s, 15H). ^{13}C NMR (101 MHz, $CDCl_3$, ppm): 165.73, 153.68, 152.50, 146.67, 135.56, 122.89, 120.77, 117.69, 117.20, 103.77 (d, $J_{Rh\text{-}C}$ = 5.9 Hz, $C_5(CH_3)_5$), 35.51, 31.50, 31.43, 8.81. UV-vis (CH_2Cl_2) λ_{max}/nm (ε/M^{-1} cm^{-1}): 379 (8500), 470 (7800), 588 (2700). ESI-MS (positive ion detection mode): *m/z* = 746.36 ([Cp*Rh(L'^{0})(CN)]$^+$). FT-IR (KBr) ν/cm^{-1}: 2130 (CN).

Intramolecular C–H Amination of Trisylazide. A toluene solution (1 mL) of trisylazide (11 mg, 35 μmol) was added to complex **7**, **8**, or **9** (3.5 μmol, 10 mol%) in a 4 mL vial covered with aluminum foil. The solution was stirred at 50°C for 24, 48, and 72 h. After the reaction, all volatiles were evaporated *in vacuo* and the crude products were analyzed by ^{1}H NMR spectroscopy ($CDCl_3$, 400 MHz). The aminated product **10** (5,7-di-isopropyl-2,3-dihydro-3,3-dimethyl-1,2-benzothiazole-1,1-dioxyde) was identified by comparing its ^{1}H NMR chemical shifts to those of the known product.[38] Yield of **10** was calculated from the integrated ratio of **10** and remaining trisylazide.

Theoretical Calculations. DFT calculations were performed using Gaussian 09, revision D.01 on "ultrafine" grid.[39] Geometry optimizations was conducted with the UB3LYP functional.[40] The convergence criterions for Maximum Force, RMS Force, Maximum Displacement, and RMS displacement were set to 1.5 x 10^{-5}, 1.0 x 10^{-5}, 6.0 x 10^{-5}, and 4.0 x 10^{-5} in atomic units, respectively. For the Rh atom, the SDD basis set was employed, and 6-31G+(d,p) basis set were used for the other atoms.[41-43] Graphical outputs of the computational results were generated with the GaussView software program.[44]

EPR Measurement. EPR spectrum of a toluene solution of **8** in a thin EPR tube (ϕ = ca.2 mm) was recorded with X-band microwave (9.640 GHz) at room temperature. Microwave power of 1.0 mW and modulation amplitude of 0.50 G were employed in the measurement. The obtained spectrum was simulated with a software SimFonia.[45]

X-ray Crystallography. A single crystal of **7** suitable for X-ray crystallographic analysis was obtained by slow diffusion of methanol into a THF solution of **7**. Single crystal of **9** suitable for X-ray crystallographic analysis was obtained by slow diffusion of *n*-hexane into a benzene solution of **9**. The single crystal was mounted on a loop with a mineral oil, and X-ray data were collected at 133 K for **7** and 110 K for **9** on a Rigaku R-AXIS RAPID diffractometer using filtered Mo-Kα radiation. The structures were solved by direct method (SHELXT)[46] and expanded using Fourier techniques. The non-hydrogen atoms were refined anisotropically by full-matrix least squares on F^2. The hydrogen atoms were attached at idealized positions on carbon atoms and were not refined. All structures in the final stage of refinement showed no movement in the atom position. All calculations were performed using the CrystalStructure 4.2 crystallographic software package[47] except for refinement, which was performed using SHELXL.[48] Crystallographic parameters are summarized in Table 1.

Table 1. Crystallographic data for **7** and **9**.

	7	**9**·benzene·0.5 *n*-hexane
formula	$C_{44}H_{61}N_2Rh$	$C_{108}H_{150}F_{12}N_6P_2Rh_2$
fw	720.88	2028.15
crystal system	orthorhombic	monoclinic
space group	*P*bca (#61)	$P2_1/n$ (#14)
a, Å	12.7157(3)	19.2754(6)
b, Å	18.9268(5)	17.1742(5)
c, Å	31.9174(7)	32.6144(11)
α, deg	90	90
β, deg	90	105.190(7)
γ, deg	90	90
V, Å^3	7681.5(3)	10419.4(7)
Z	8	4
D_{calced}, g cm^{-3}	1.247	1.293
F(000)	3072.00	4272.00
μ, cm^{-1}	4.753	4.166
cryst size, mm	0.50 × 0.50 × 0.40	0.30 × 0.30 × 0.10
T, K	133	110
$2\theta_{max}$, deg	55.0	55.0
reflns. obsd	8803	23831
no. of params	424	1165
*R*1[a]	0.0474	0.0686
*wR*2[b]	0.1136	0.1915
GOF	1.074	1.009
max./min. $\Delta\rho$, e Å^{-3}	1.04/ –0.65	1.85/ –1.11

[a] $R1 = \Sigma(||F_o| - |F_c||)/\Sigma|F_o|$. [b] $wR2 = (\Sigma(w(F_o^2 - F_c^2)^2)/\Sigma w(F_o^2)^2)^{1/2}$.

Results and Discussion

Synthesis and Characterization of Complex 7 Complex **7** ([Cp*Rh^{III}(**L'**$^{2-}$)]) was obtained as a purple solid from the reaction of [Cp*Rh^{III}Cl$_2$]$_2$ and the neutral ligand H$_2$**L'** (*N,N*-di-(3,5-di-*tert*-butylphenyl)benzene-1,2-diamine)) in a 1 : 2 ratio in the presence of 2 equiv of *n*-BuLi. In the ^{1}H NMR spectrum in $CDCl_3$, no peak assignable to the NH protons was observed, indicating **7** has deprotonated diamido ligand **L'**$^{2-}$. The elemental analysis data indicated that the product was a rhodium(III) complex involving Cp* and deprotonated diamido ligand **L'**$^{2-}$, [Cp*Rh^{III}(**L'**$^{2-}$)]. The single crystals were obtained by slow diffusion of methanol into a THF solution of **7**. An ORTEP drawing of the X-ray crystal structure is depicted in Figure 2 (left) and the selected bond lengths are given in Figure 2 (right). The complex consists of one rhodium ion (Rh1), one pentamethyl cyclopentadienyl ligand (Cp*), and **L'**$^{2-}$ ligand, where Cp* coordinates to Rh1 in an η^5-fashion and **L'**$^{2-}$ chelates to Rh1 to complete a formally five-coordinate rhodium center. Strong π-donation of *o*-phenylenediamido ligand (**L'**$^{2-}$) to the metal center stabilizes the five-coordinate structure (*vide infla*).[49,50] Similar five-coordinate metal centers can be found in organometallic complexes having *o*-phenylenediamido and *o*-amidophenolato ligands, such as [(η^6-cymene)M^{II}(C$_6$H$_4$ONAr^{2-})] (M = Ru, Os, C$_6$H$_4$ONAr^{2-} = 4,6-di-*tert*-butyl-*N*-aryl-*o*-amidophenolato), [(η^5-Cp*)Ir^{III}(C$_6$H$_4$ONAr^{2-})] (C$_6$H$_4$ONAr^{2-} = 4,6-di-*tert*-butyl- *N*-aryl-*o*-amidophenolato)[51,52] , [(η^5-Cp*)Rh^{III}(C$_6$H$_4$N$_2$R$_2^{2-}$)] (R = Ts or H), [53] [(η^5-Cp*)Ir^{III}(C$_6$H$_2$Me$_2$N$_2$Ph$_2^{2-}$)].[49] The Rh1–N1 and Rh1–N2 bond lengths of **1** are close to the Rh-amido bond lengths (1.9833(18) and 1.9722(19) Å) of [(η^5-Cp*)Rh^{III}(C$_6$H$_4$N$_2$H$_2^{2-}$)] but shorter than the Rh-amine bond length (2.1456(14) Å) of [(η^5-Cp*)Rh^{III}Cl(C$_6$H$_4$N$_2$H$_2$Ts^{2-})].[53] This comparison also indicates that **7** has deprotonated dianionic **L'**$^{2-}$. The C–C bond lengths of **L'**$^{2-}$ lie between 1.381(4) and 1.422(4) Å and the C1–N1 and C2–N2 bond lengths are 1.362(3) and 1.364 (3) Å, respectively. These dimensional values of the **L'**$^{2-}$ ligand are very close to those of the complexes mentioned above, being consistent with the assigned as [(η^5-Cp*)Rh^{III}(**L'**$^{2-}$)], where **L'**$^{2-}$ has a fully reduced state, benzene-1,2-diamido structure.

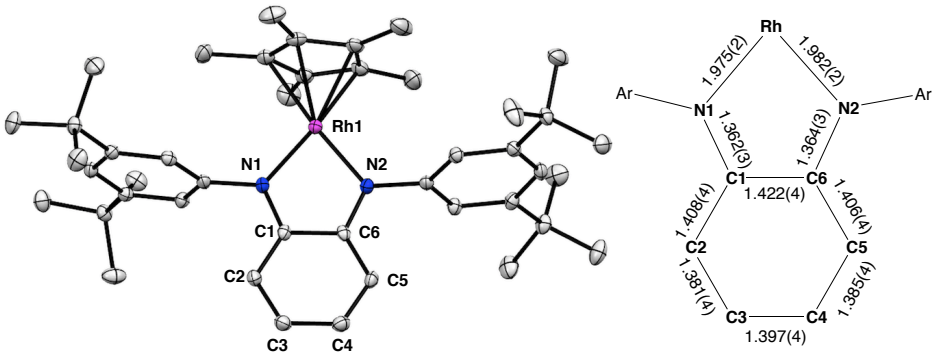

Figure 2. ORTEP diagram of **7** showing 50% ellipsoids (left). Hydrogen atoms are omitted for clarity. The chemical structure including the selected bond lengths of *o*-phenylenediamido ligand moiety (right).

The cyclic voltammogram (CV) of **7** (1.0 mM) was measured at room temperature in CH_2Cl_2 containing $^nBu_4NPF_6$ (0.10 M) and shown in Figure 3. One quasi-reversible redox wave was observed at –0.18 V. No additional wave corresponding to further oxidation was observed up to +1.2 V (Figure S1). Bulk electrolysis of the solution at 0.02 V consumed 0.8 electron, which showed that the redox wave corresponded to one-electron oxidation process. Then, the author tried to isolate the one-electron oxidized complex of **7** by the oxidation with $(NH_4)_2[Ce(NO_3)_6]$ (CAN). However, it was found that stability of the one-electron oxidized complex was insufficient for isolation under the employed conditions.

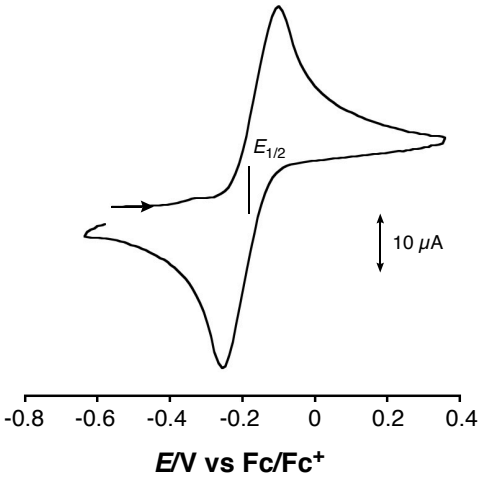

Figure 3. Cyclic voltammogram of **7** (1.0 mM) at room temperature in CH_2Cl_2 containing $^nBu_4PF_6$ (0.10 M). Working electrode: glassy carbon. Counter electrode: Pt wire. Scan rate: 100 mV s^{-1}.

Figure 4 shows the UV-vis spectral change of **7** observed upon addition of various amounts of $(NH_4)_2[Ce(NO_3)_6]$ (CAN), where the intense absorption band at 542 nm due to **7** disappeared with concomitant appearance of absorption bands at 410 nm and 933 nm keeping two isosbestic points at 465 and 611 nm. The spectral change completed when 2 equiv of CAN was added as shown in the inset of Figure 4. The result indicates that the one-electron oxidized species of **7** itself is unstable as mentioned above and easily undergoes disproportionation to give the reduced complex and the two-electron oxidized species under this condition.

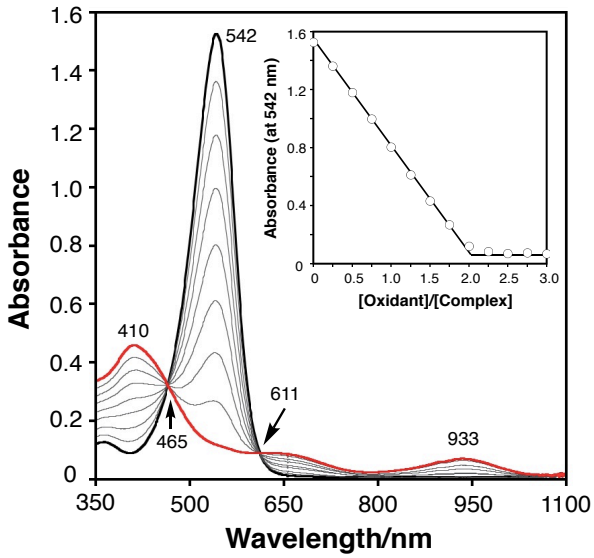

Figure 4. Spectral change observed upon addition of CAN ($(NH_4)_2[Ce(NO_3)_6]$) to **7** (0.050 mM) in THF at 25°C (black → red). Inset: Absorbance change at 542 nm against the [Oxidant]/[**7**] ratio.

Synthesis and Characterization of Cyanide Bound One-electron Oxidized Complex 8. One-electron oxidized form of the five-coordinate complexes such as $[(\eta^6\text{-cymene})M^{II}(C_6H_4ONAr^{2-})]$ (M = Ru, Os, $C_6H_4ONAr^{2-}$ = 4,6-di-*tert*-butyl-*N*-aryl-*o*-amidophenolato) and $[(\eta^5\text{-Cp*})Ir^{III}(C_6H_4ONAr^{2-})]$ ($C_6H_4ONAr^{2-}$ = 4,6-di-*tert*-butyl-*N*-aryl-*o*-amidophenolato) can be stabilized by the coordination of external ligands to the metal centers.[51,52] To see whether the one-electron oxidized form of **7** can be stabilized by coupling with an anion coordination, CV of **7** was measured in the presence of cyanide anion. As shown in Figure S2, one quasi-reversible redox wave was newly observed at –0.59 V, indicating that one-electron oxidation coupled with coordination of the added cyanide anion to the rhodium center occurred. Then, oxidation of **7** with

dioxygen in the presence of cyanide anion was monitored by UV-visible spectroscopy. Notably, complex **7** was oxidized efficiently by dioxygen, when (^{n}Bu$_4$N)CN was added into a toluene solution of **7**. Figure 5 shows the spectral change of **7** in the presence of (^{n}Bu$_4$N)CN under dioxygen atmosphere, where the intense absorption band at 545 nm due to **7** disappeared and new broad absorption bands around 800–900 nm appeared concomitantly. Such a spectral change was not observed under dinitrogen atmosphere.

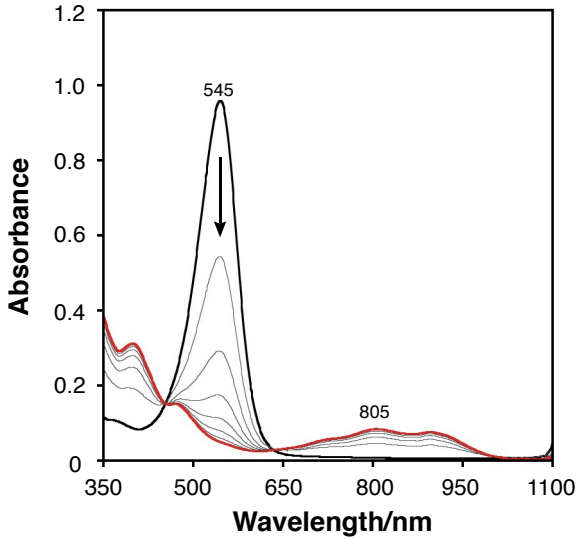

Figure 5. Spectral change observed upon the addition of (^{n}Bu$_4$N)CN (0.175 mM) to **7** (0.035 mM) in toluene at 25°C under aerobic conditions (black → red). The spectra were measured every 20 seconds.

Then, the generated species in the presence of cyanide ion under dioxygen was characterized. The ESI-MS (positive ion detection mode) of the toluene solution exhibited a peak cluster at m/z = 746.39, the isotope distribution pattern of which matched with that of ([Cp*Rh^{III}(**L'**^{0})] + CN)$^+$ containing one cyanide anion (Figure 6). The oxidized species in toluene at 298 K showed an EPR signal with g-value at 1.991 with splitting to six peaks (Figure 7). The g-value is typical for an organic radical species coordinated to rhodium(III) ion.[9,10,54] The structure of the spectrum was nicely simulated assuming hyperfine coupling of an unpaired electron with two-equivalent ^{14}N nuclei, two-sets of equivalent ^{1}H nuclei, and a ^{1}H nucleus using the hyper-fine coupling constants shown in the caption of Figure 7. The spin densities on each atom estimated from the EPR spectrum are reasonably consistent with those calculated by DFT calculations (Figure 8a). The spin density plot (99.6 % total spin density) based on DFT calculation indicated that most part of spin density localized on the **L'**$^{\bullet-}$ ligand (Figure

8b). All these results are consistent with the assignment of the oxidized species as [Cp*Rh^{III}(**L'**$^{\bullet-}$)(CN)] (**8**).

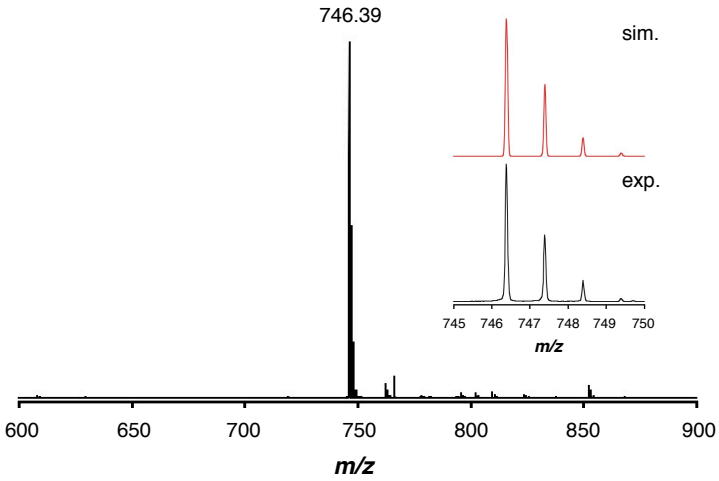

Figure 6. ESI-mass spectrum (positive ion detection mode) of **8**. Inset: Comparison of experimental spectrum (black) and simulated spectrum calculated as $C_{45}H_{61}N_3Rh$ (red).

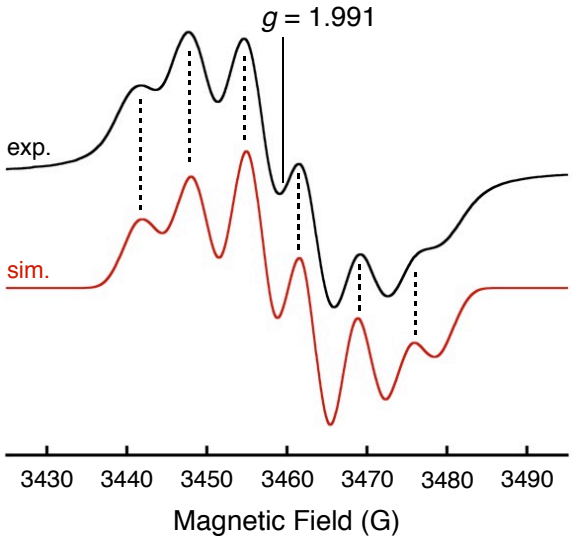

Figure 7. EPR spectrum of **8** in toluene (1.0 mM) at 298 K (black: experimental spectrum, red: simulation). Simulated hyperfine splitting constant values (A, G) of ^{14}N and ^{1}H nuclei: A^{N} 6.80; A^{H1} 1.80; A^{H2} 2.20; A^{H3} 4.70.

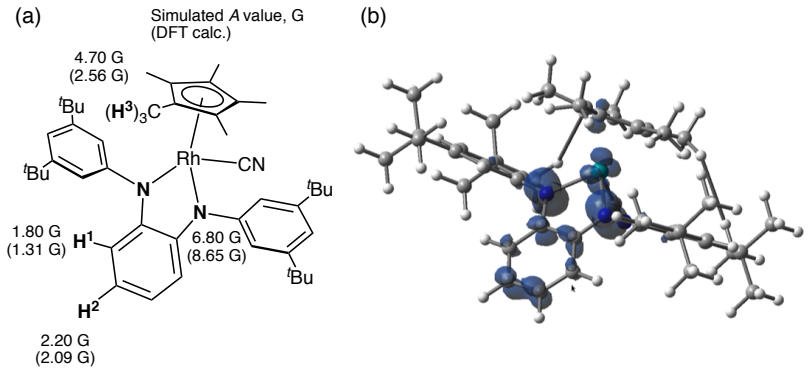

Figure 8. (a) Simulated and DFT calculated (in brackets) hyperfine splitting constant values (A, G) of ^{14}N and ^{1}H nuclei. (b) DFT calculated spin density plot of **8** (UB3LYP/SDD (on Rh), 6-31G+(d,p) (on C, H, N))**.**

In a preparative scale experiment, **8** was obtained by a reaction of **7** with 1 equiv of AgCN and was purified by recrystallization from benzene/*n*-hexane (see Experimental Section). The UV-vis and ESI-mass spectra of the isolated **8** were identical with those of **8** generated from **7** and CN^- under dioxygen atmosphere (Figure S2). The CV of **8** exhibited one quasi-reversible redox wave ($E_{1/2}$ = –0.59 V) as shown in Figure 9. Appearance of the quasi-reversible redox wave indicates that **8** can be oxidized further to $[Cp^*Rh^{III}(\mathbf{L'}^0)(CN)]^+$ or $[Cp^*Rh^{IV}(\mathbf{L'}^{\bullet-})(CN)]^+$).

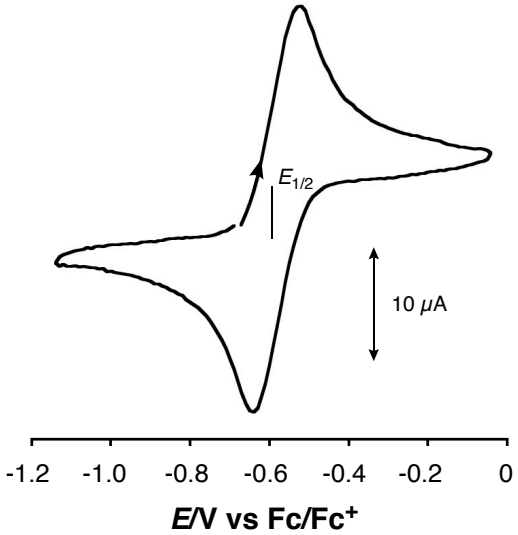

Figure 9. Cyclic voltammogram of isolated **8** (1.0 mM) at room temperature in CH_2Cl_2 containing ^{n}Bu$_4$PF$_6$ (0.10 M). Working electrode: glassy carbon. Counter electrode: Pt wire. Scan rate: 100 mV s^{-1}.

Synthesis and Characterization of Cyanide Bound Two-electron Oxidized Complex 9. To examine importance of the oxidation state of the supporting ligand in the catalytic amination reaction (see below), the author also synthesized the two-electron oxidized complex **9**. The reaction of **7** with 2 equiv of $NOPF_6$ as an oxidant was carried out in the presence of an equimolar amount of KCN. Single crystals suitable for X-ray diffraction analysis were obtained by slow diffusion of *n*-hexane into a benzene solution of the product. The X-ray crystal structure is shown in Figure 10 (left) together with the selected bond lengths of the ligand moiety of the oxidized complex shown in Figure 10 (right).

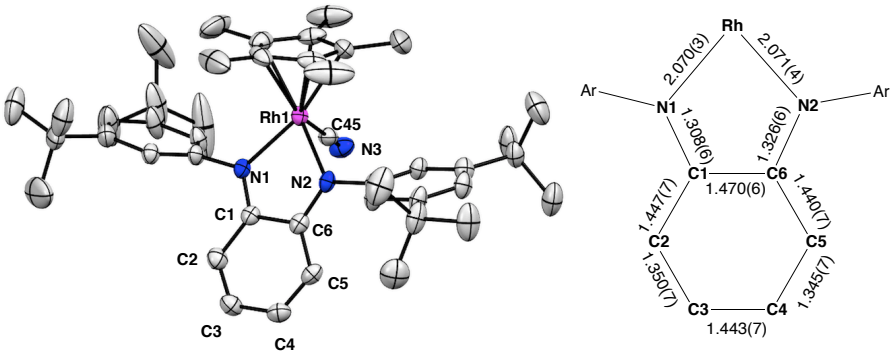

Figure 10. ORTEP diagrams of **9** showing 50% ellipsoids (left). Hydrogen atoms, a counter ion, and solvent molecules are omitted for clarity. The chemical structure including the selected bond lengths of *o*-diiminobenzoquinone ligand moiety (right).

The rhodium center in **9** exhibits a six-coordinate structure with the oxidized ligand, η^5-Cp*, and a cyanide anion. The Rh–N, C–N, and C–C bond lengths of the *o*-phenylenediamine moiety are significantly altered from those of **7** upon the oxidation. Namely, the C1–N1, C6–N2, C2–C3 and C4–C5 bonds in **9** became shortened, whereas its Rh1–N1, Rh1–N2, C1–C2, C3–C4, C5–C6, and C6–C1 bonds were elongated (Figure 10, Table S1). The elongated rhodium-nitrogen bonds are reflection of the decrease of π-donation from the imine nitrogen atoms to the Rh1 atom in **9**.[49] The dimension of the *o*-diiminobenzoquinone moiety of **9** is similar to those of [(η^5-Cp*)Ir^{III}($C_6H_2Me_2N_2Ar_2^0$)Cl]$SbCl_4$ that contained an *o*-diiminobenzoquinone form ($C_6H_2Me_2N_2Ar_2^0$ = 4,5-dimethyl-*N,N*-diphenyl-1,2-diiminobenzoquinone).[49] These structural data unambiguously indicate that the supporting ligand is fully oxidized to $\mathbf{L}^0$. By the one-electron oxidation from **8** to **9**, ν_{CN} stretching frequency became larger (2116

$\rightarrow$ 2130 cm^{-1}), consistent with less electron density of the rhodium(III) center in **9**. Figure 11 shows a UV-vis spectral change for the oxidation of **8** to **9** by adding ferrocenium hexafluorophosphate ($FcPF_6$), where a broad absorption band at 809 nm due to **8** disappears with concomitant increase of the absorption bands at 470 nm and 588 nm due to **9**. The spectral change completed when an equimolar amount of the oxidant was added as shown in the inset of Figure 11. It has been reported that metal complexes having *o*-diiminobenzoquinone type ligands show absorption bands around 500 and 600 nm.[49]

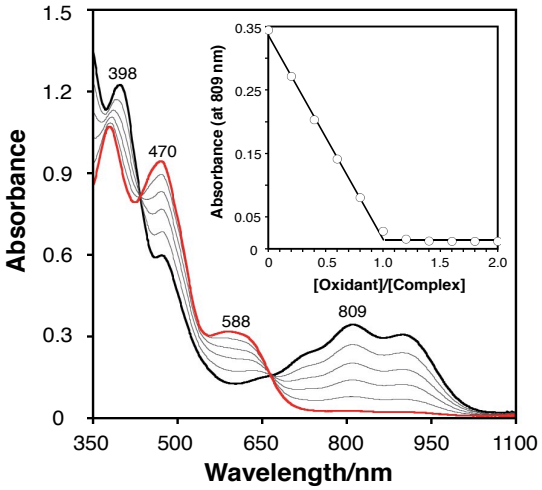

Figure 11. Spectral change observed upon the addition of $FcPF_6$ to **8** (0.12 mM) in CH_2Cl_2 at 25°C (black $\rightarrow$ red). Inset: Absorbance change at 809 nm in the titration experiment.

DFT Calculation of 7. The complex **7** prefers to have five-coordinate structure, although the rhodium center has enough space to accommodate the third ligand to finalize its coordination sphere (Figure 2). This result is somewhat interest because trivalent ion of group 9 elements (Co^{III}, Rh^{III}, Ir^{III}) generally prefer to have octahedral geometries due to maximize ligand field splitting. Kaim and co-workers studied iridium(III) complex in a five-coordinate structure. They have concluded that the five-coordinate structure is largely stabilized by donation of π-electrons of its ligand. The DFT calculation of the iridium complex suggested that 6π-electron system emerged on the Rh–N–C–C–N 5 membered ring to stabilize its coordinatively unsaturated structure.[50] The author also conducted DFT calculation of **7**. The highest occupied Corn–Sham orbital (HOMO) of **7** is delocalized over the *o*-phenylenediamido ligand to the d_{xy} orbital of rhodium center (Figure 12). Bond formation energy of this π-bond seems larger than the stabilization of their d-electron by having an octahedral structure.

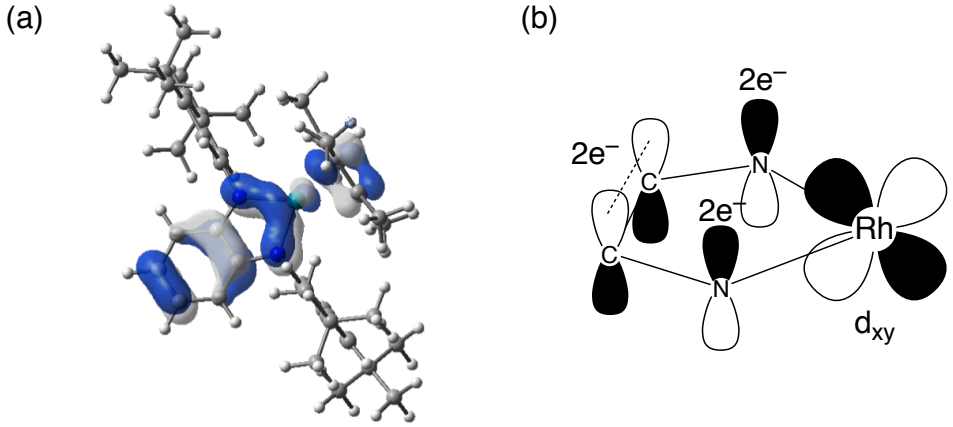

Figure 12. (a) Calculated HOMO of **7** shown in 99.6% probability and (b) schematic diagram of 6π-electron system emerged on the 5-membered chelate ring of **7**.

Catalytic Activity of Complexes 7, 8, and 9 in Intramolecular Amination of Trisylazide. In Chapter 1, the author describes the C–H amination of xanthene with tosyl azide by six-coordinate rhodium(III) complexes with a trianionic redox-active tetradentate ligand ($\mathbf{L}^{3-}$), [$Rh^{III}(\mathbf{L}^{3-})(ArNH_2)_2$] and $^{n}Bu_4N[Rh^{III}(\mathbf{L}^{3-})(Sol)(Cl)]$ ($\mathbf{L}H_3$ = *N*-(2-hydroxy-3,5-di-*tert*-butylphenyl)-3-(2-hydroxy-3,5-di-*tert*-butyl-phenyl)amino-2-nitro-2-propeneimine, solv = MeCN, H_2O, THF, or pyridine), where the amination started after replacement of one of the axial ligands, $ArNH_2$ or solv, with TsN_3 to afford [$Rh^{III}(\mathbf{L}^{3-})(ArNH_2$ or Cl)(TsN_3)] (Scheme 1b).[9,10] Since the rhodium center in **7** can be regarded as a five-coordinate structure, the amination of xanthene with TsN_3 in the presence of **7** was expected to proceed more smoothly than the cases of the six-coordinate rhodium(III) complexes of $\mathbf{L}^{3-}$. However, the expected intermolecular amination did not proceed at all, which indicates that reactivity of **7** in amination is lower than the rhodium(III) complexes of $\mathbf{L}^{3-}$. Then, the catalytic activities of **7**, **8**, and **9** in intramolecular C–H amination of trisylazide (2,4,6-triisopropylphenylsulfonyl azide) were examined. Toluene solutions (1 mL) containing trisylazide (35 μmol) and a catalytic amount of **7**, **8** or **9** (3.5 μmol, 10 mol%) were stirred under dark and dinitrogen atmosphere at 50°C. As seen in Table 2, the yield of intramolecular amination reaction catalyzed by **7** to give the aminated product **10** (5,7-di-isopropyl-2,3-dihydro-3,3-dimethyl-1,2-benzothiazole-1,1-dioxyde) was very low; the total turnover number was quite low (TON = 1.2, entry 1). On the other hand, complex **8** was found to act as a better catalyst as compared to **7** (TON = 3.4, entry 2). The turnover number of **8** increased by extending the reaction time from 24 h to 48 h, whereas that of **7** did not

significantly increase (entries 3 and 4). Further extension of the reaction time to 72 h did not increase the turnover number (entries 5 and 6). Though complex **9** had no catalytic activity (entry 7), the catalytic amination proceeded with complex **9**, when 1 equiv of a reductant, cobaltocene (Cp_2Co^{II}), was added to the system (entry 8). These results clearly indicate that the catalytic C–H amination requires complex **8** supported by **L'**$^{\bullet-}$ as the key reactive intermediate. When the amination reaction catalyzed by **8** was conducted in the presence of 5 equiv of $^{n}Bu_4NCN$, the product yield of **10** decreased to 24% (entry 9). This result may suggest that the initial stage of the amination reaction involves replacement of the CN^- ligand with trisylazide.

Table 2. Catalytic activity of **7**, **8**, and **9** in the C–H amination of trisylazide.

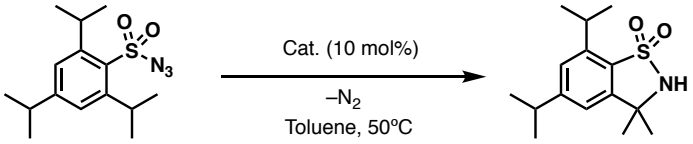

10

Entry	Cat.	Time (h)	Additive	Yields (%)[a,b]	TON
1	**7**	24	None	12	1.2
2	**8**	24	None	34	3.4
3	**7**	48	None	19	1.9
4	**8**	48	None	54	5.4
5	**7**	72	None	22	2.2
6	**8**	72	None	57	5.7
7	**9**	24	None	0	0
8	**9**	24	Cp_2Co^{II} [c]	27	2.7
9	**8**	24	5eq. CN^-	24	2.4

a) Based on trisylazide. b) ^{1}H NMR yield. c) 3.5 mM.

A possible mechanism for the catalytic amination reaction is presented in Scheme 2. First, the one-electron oxidized complex **8** reacts with trisylazide to give an azide adduct **A**, from which single electron transfer takes place from **L'**$^{\bullet-}$ to trisylazide, giving a nitrene radical species **B** via dinitrogen (N_2) release. From this intermediate, hydrogen atom abstraction (HAA) by the nitrene radical from one of the isopropyl methine carbon occurs to give intermediate **C**, from which the aminated product **10** is produced via intramolecular N–C bond formation. In this process, the oxidized ligand **L'**^{0} accepts one electron from the amido group (–NH-Rh) to induce the radical coupling reaction with the carbon center radical in **C**. In the final step, amine product **10** is released by ligand

substitution with cyanide ion, completing the catalytic cycle.

Scheme 2. Possible catalytic mechanism for the C–H amination of trisylazide.

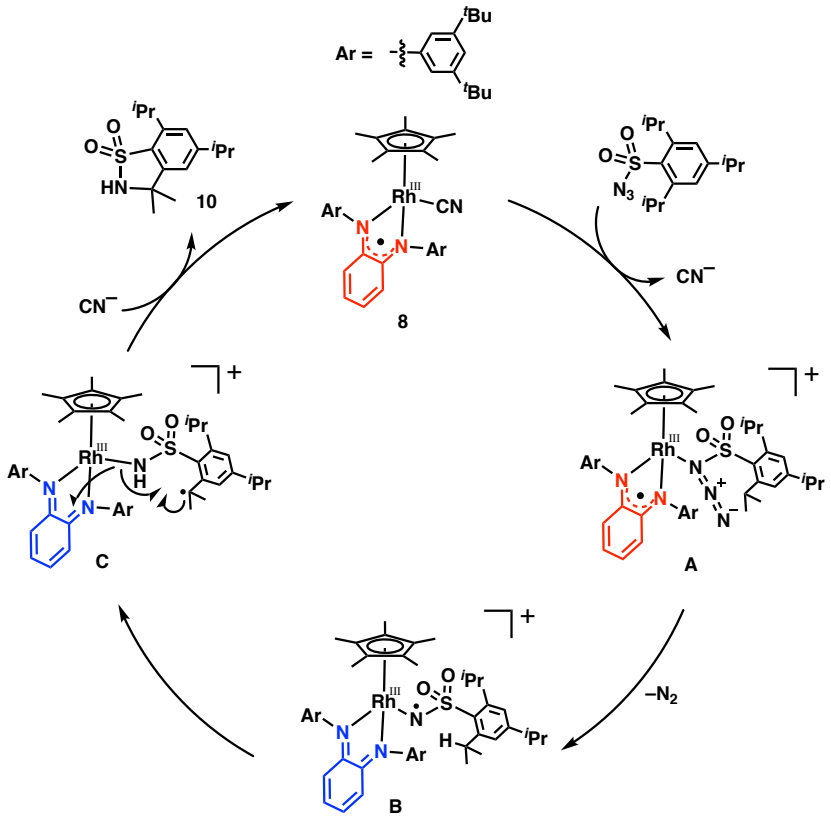

Conclusion

Half sandwich Cp^*Rh^{III} complexes **7**, **8**, and **9** with a redox-active *o*-phenylenediamine ligand were synthesized and characterized by the ^1H NMR, UV-vis, ESI-mass, and EPR spectra and cyclic voltammogram as well as the crystal structure analysis. The structural analysis showed that **7** ([Cp^*Rh^{III}(**L'**$^{2-}$)]) adopted a five-coordinate structure bearing the fully reduced *o*-phenylenediamido ligand **L'**$^{2-}$, whereas **9** [Cp^*Rh^{III}(**L'**^{0})(CN)]PF_6 had a six-coordinate structure bearing an additional cyanide ion and the two-electron oxidized *o*-diiminobenzoquinone ligand **L'**^{0}. The result of ESI-MS showed that complex **8** also had a cyanide ion to complete a six-coordinate rhodium(III) complex. The EPR spectrum and the DFT calculation indicated that **8** had the *o*-diiminobenzosemiquinone radical anion ligand **L'**$^{\bullet-}$. Among these complexes, complex **8** showed the highest activity in the catalytic amination of trisylazide. This study demonstrates that an amination can be controlled by oxidation states of redox-active

ligands, providing a rare example of C–H amination using half-sandwich complex bearing redox-active ligands.

References

(1) Kaim, W. *Inorg. Chem.* **2011,** *50*, 9752–9765.

(2) Luca, O. R.; Crabtree, R. H. *Chem. Soc. Rev.* **2013,** *42*, 1440–1459.

(3) Broere, D. L. J.; Plessius, R.; van der Vlugt, J. I. *Chem. Soc. Rev.* **2015,** *44*, 6886–6915.

(4) Broere, D. L. J.; de Bruin, B.; Reek, J. N. H.; Lutz, M.; Dechert, S.; van der Vlugt, J. I. *J. Am. Chem. Soc.* **2014,** *136*, 11574–11577.

(5) Broere, D. L. J.; van Leest, N. P.; de Bruin, B.; Siegler, M. A.; van der Vlugt, J. I. *Inorg. Chem.* **2016,** *55*, 8603–8611.

(6) Bagh, B.; Broere, D. L. J.; Sinha, V.; Kuijpers, P. F.; van Leest, N. P.; de Bruin, B.; Demeshko, S.; Siegler, M. A.; van der Vlugt, J. I. *J. Am. Chem. Soc.* **2017,** *139*, 5117–5124.

(7) Zhou, W.; Patrick, B. O.; Smith, K. M. *Chem. Commun.* **2014,** *50*, 9958–9960.

(8) Goswami, M.; Lyaskovskyy, V.; Domingos, S. R.; Buma, W. J.; Woutersen, S.; Troeppner, O.; Ivanović-Burmazović, I.; Lu, H.; Cui, X.; Zhang, X. P.; Reijerse, E. J.; DeBeer, S.; van Schooneveld, M. M.; Pfaff, F. F.; Ray, K.; de Bruin, B. *J. Am. Chem. Soc.* **2015,** *137*, 5468–5479.

(9) Fujita, D.; Sugimoto, H.; Shiota, Y.; Morimoto, Y.; Yoshizawa, K.; Itoh, S. *Chem. Commun.* **2017,** *53*, 4849–4852.

(10) Fujita, D.; Sugimoto, H.; Morimoto, Y.; Itoh, S. *Inorg. Chem.* **2018,** *57*, 9738-9747.

(11) Ren, Y.; Cheaib, K.; Jacquet, J.; Vezin, H.; Fensterbank, L.; Orio, M.; Blanchard, S.; Desage-El Murr, M. *Chem.–Eur. J.* **2018,** *24*, 5086–5090.

(12) Broere, D. L. J.; Metz, L. L.; de Bruin, B.; Reek, J. N. H.; Siegler, M. A.; van der Vlugt, J. I. *Angew. Chem., Int. Ed.* **2015,** *54*, 1516–1520.

(13) Jacquet, J.; Blanchard, S.; Derat, E.; Desage-El Murr, M.; Fensterbank, L. *Chem. Sci.* **2016,** *7*, 2030–2036.

(14) Jacquet, J.; Cheaib, K.; Ren, Y.; Vezin, H.; Orio, M.; Blanchard, S.; Fensterbank, L.; Desage-El Murr, M. *Chem.–Eur. J.* **2017,** *23*, 15030–15034.

(15) Abakumov, G. A.; Poddel'sky, A. I.; Grunova, E. V.; Cherkasov, V. K.; Fukin, G. K.; Kurskii, Y. A.; Abakumova, L. G. *Angew. Chem., Int. Ed.* **2005,** *44*, 2767–2771.

(16) Lippert, C. A.; Arnstein, S. A.; Sherrill, C. D.; Soper, J. D. *J. Am. Chem. Soc.* **2010,** *132*, 3879–3892.

(17) Chakraborty, B.; Paine, T. K. *Angew. Chem., Int. Ed.* **2013,** *52*, 920–924.

(18) Bittner, M. M.; Lindeman, S. V.; Popescu, C. V.; Fiedler, A. T. *Inorg. Chem.* **2014,** *53*, 4047–4061.
(19) Metzinger, R.; Demeshko, S.; Limberg, C. A. *Chem.–Eur. J.* **2014,** *20*, 4721–4735.
(20) Chatterjee, S.; Paine, T. K. *Inorg. Chem.* **2015,** *54*, 1720–1727.
(21) Lakshman, T. R.; Chatterjee, S.; Chakraborty, B.; Paine, T. K. *Dalton Trans.* **2016,** *45*, 8835–8844.
(22) Corcos, A. R.; Villanueva, O.; Walroth, R. C.; Sharma, S. K.; Bacsa, J.; Lancaster, K. M.; MacBeth, C. E.; Berry, J. F. *J. Am. Chem. Soc.* **2016,** *138*, 1796–1799.
(23) Paul, G. C.; Banerjee, S.; Mukherjee, C. *Inorg. Chem.* **2017,** *56*, 729–736.
(24) Pierpont, C. G. *Coord. Chem. Rev.* **2001,** *216-217*, 99–125.
(25) Chang, H.-C.; Kiriya, D. *Eur. J. Inorg. Chem.* **2013,** 2013, 642–652.
(26) Matsumoto, T.; Chang, H.-C.; Wakizaka, M.; Ueno, S.; Kobayashi, A.; Nakayama, A.; Taketsugu, T.; Kato, M. *J. Am. Chem. Soc.* **2013,** *135*, 8646–8654.
(27) Wakizaka, M.; Matsumoto, T.; Tanaka, R.; Chang, H.-C. *Nat. Commun.* **2016,** *7*, 12333.
(28) Noro, S.; Chang, H.-C.; Takenobu, T.; Murayama, Y.; Kanbara, T.; Aoyama, T.; Sassa, T.; Wada, T.; Tanaka, D.; Kitagawa, S.; Iwasa, Y.; Akutagawa, T.; Nakamura, T. *J. Am. Chem. Soc.* **2005,** *127*, 10012–10013.
(29) Que, L.; Ho, R. Y. N. *Chem. Rev.* **1996,** *96*, 2607–2624.
(30) Kaim, W.; Schwederski, B. *Coord. Chem. Rev.* **2010,** *254*, 1580–1588.
(31) Lyaskovskyy, V.; de Bruin, B. *ACS Catal.* **2012,** *2*, 270–279.
(32) van der Vlugt, J. I. *Chem.–Eur. J.* **2019,** *25*, 2651–2662.
(33) Perrin, D. D.; Armarego, W. L. F.; Perrin, D. R. *Purification of Laboratory Chemicals 4th Edition*. 4th ed.; Pergamon Press: Elmsford, NY, 1996.
(34) Hartwig, J. F. *Angew. Chem., Int. Ed.* **1998,** *37*, 2046–2067.
(35) Chłopek, K.; Bothe, E.; Neese, F.; Weyhermüller, T.; Wieghardt, K. *Inorg. Chem.* **2006,** *45*, 6298–6307.
(36) Mishra, V. K.; Ravikumar, P. C.; Maier, M. E. *Tetrahedron* **2016,** *72*, 6499–6509.
(37) Diethelm, S.; Schindler, C. S.; Carreira, E. M. *Chem.–Eur. J.* **2014,** *20*, 6071–6080.
(38) Ruppel, J. V.; Kamble, R. M.; Zhang, X. P. *Organic Letters* **2007,** 9, 4889–4892.
(39) Frisch, M. J.; Trucks, G. W.; Schlegel, H. B.; Scuseria, G. E.; Robb, M. A.; Cheeseman, J. R.; Scalmani, G.; Barone, V.; Mennucci, B.; Petersson, G. A.; Nakatsuji, H.; Caricato, M.; Li, X.; Hratchian, H. P.; Izmaylov, A. F.; Bloino, J.; Zheng, G.; Sonnenberg, J. L.; Hada, M.; Ehara, M.; Toyota, K.; Fukuda, R.; Hasegawa, J.; Ishida, M.; Nakajima, T.; Honda, Y.; Kitao, O.; Nakai, H.; Vreven, T.; Montgomery, J., J. A.; Peralta, J. E.; Ogliaro, F.; Bearpark, M.; Heyd, J. J.;

Brothers, E.; Kudin, K. N.; Staroverov, V. N.; Kobayashi, R.; Normand, J.; Raghavachari, K.; Rendell, A.; Burant, J. C.; Iyengar, S. S.; Tomasi, J.; Cossi, M.; Rega, N.; Millam, J. M.; Klene, M.; Knox, J. E.; Cross, J. B.; Bakken, V.; Adamo, C.; Jaramillo, J.; Gomperts, R.; Stratmann, R. E.; Yazyev, O.; Austin, A. J.; Cammi, R.; Pomelli, C.; Ochterski, J. W.; Martin, R. L.; Morokuma, K.; Zakrzewski, V. G.; Voth, G. A.; Salvador, P.; Dannenberg, J. J.; Dapprich, S.; Daniels, A. D.; Farkas, O.; Foresman, J. B.; Ortiz, J. V.; Cioslowski, J.; Fox, D. J. Gaussian 09, revision D.01, Gaussian, Inc.: Wallingford CT, 2009.

(40) Becke, A. D. *J. Chem. Phys.* **1993,** *98*, 5648–5652.

(41) Andrae, D.; Häußermann, U.; Dolg, M.; Stoll, H.; Preuß, H. *Theor. Chim. Acta* **1990,** *77*, 123–141.

(42) Hehre, W. J.; Ditchfield, R.; Pople, J. A. *J. Chem. Phys.* **1972,** *56*, 2257–2261.

(43) Hariharan, P. C.; Pople, J. A. *Theor. Chim. Acta* **1973,** *28*, 213–222.

(44) Dennington, I. R.; Keith, T.; Millam, J.; Eppinnett, K.; Hovell, W. L.; Gilliland, R. *GaussView, Semichem, Shawnee Mission, KS.* 2003.

(45) Weber, R. T. WIN-EPR SIMFONIA Manual; Bruker: Madison, WI, 1995.

(46) Sheldrick, G. *Acta Crystallogr. Sect. A* **2015,** *71*, 3–8.

(47) Crystal Structure Analysis Package, Rigaku Corporation (2000-2017). Tokyo 196-8666, Japan.

(48) Sheldrick, G. *Acta Crystallogr. Sect. A* **2008,** *64*, 112–122.

(49) van der Meer, M.; Manck, S.; Sobottka, S.; Plebst, S.; Sarkar, B. *Organometallics* **2015,** *34*, 5393–5400.

(50) Greulich, S.; Kaim, W.; Stange, A. F.; Stoll, H.; Fiedler, J.; Záliš, S. *Inorg. Chem.* **1996,** *35*, 3998–4002.

(51) Hübner, R.; Weber, S.; Strobel, S.; Sarkar, B.; Záliš, S.; Kaim, W. *Organometallics* **2011,** *30*, 1414–1418.

(52) Bubrin, M.; Schweinfurth, D.; Ehret, F.; Záliš, S.; Kvapilová, H.; Fiedler, J.; Zeng, Q.; Hartl, F.; Kaim, W. *Organometallics* **2014,** *33*, 4973–4985.

(53) Blacker, A. J.; Clot, E.; Duckett, S. B.; Eisenstein, O.; Grace, J.; Nova, A.; Perutz, R. N.; Taylor, D. J.; Whitwood, A. C. *Chem. Commun.* **2009**, 6801–6803.

(54) Saha, P.; Saha Roy, A.; Weyhermüller, T.; Ghosh, P. *Chem. Commun.* **2014,** *50*, 13073–13076.

Supporting Information for Chapter 3

(Table S1 and Figure S1–S4)

Table S1. Cartesian coordinate of the optimized structure of **8**.

Center Number	Coodinates (Å) X	Y	Z
1	-0.722211	1.510705	-1.429597
2	0.722221	1.510703	-1.429594
3	1.413742	2.385096	-2.314799
4	0.708816	3.234509	-3.149093
5	-0.708794	3.23451	-3.149097
6	-1.413726	2.385098	-2.314805
7	2.495843	2.367295	-2.337094
8	1.246324	3.893007	-3.82381
9	-1.246297	3.89301	-3.823816
10	-2.495827	2.3673	-2.337107
11	-1.307812	0.612161	-0.585122
12	1.307817	0.612154	-0.585121
13	2.7258	0.477215	-0.501237
14	3.507338	1.532934	0.000116
15	3.335418	-0.720676	-0.907669
16	4.901768	1.407796	0.098088
17	3.004002	2.441056	0.30643
18	4.728589	-0.874177	-0.825498
19	5.485941	0.197559	-0.316867
20	6.563085	0.088727	-0.24959
21	-2.725797	0.477223	-0.501249
22	-3.335413	-0.720671	-0.907675
23	-3.507337	1.532943	0.000096
24	-4.728583	-0.874176	-0.825499
25	-2.701154	-1.504094	-1.300192
26	-4.901767	1.407803	0.098069
27	-5.485937	0.197561	-0.316874
28	-6.56308	0.088725	-0.249592
29	-0.000002	-0.624425	0.434042
30	0.000014	-0.109318	2.726833
31	-1.166164	-0.915894	2.440449
32	1.166154	-0.915941	2.440445
33	-0.730924	-2.18428	1.922833
34	0.730859	-2.184311	1.922831
35	2.583066	-0.53151	2.736205
36	2.737604	0.547262	2.658812
37	2.84538	-0.834428	3.760027
38	3.288515	-1.012032	2.054383
39	1.598096	-3.368535	1.610589
40	2.609036	-3.061086	1.329072
41	1.681341	-4.031141	2.483913
42	1.189746	-3.95284	0.781683
43	-1.59822	-3.36846	1.610586
44	-1.189893	-3.952788	0.781684
45	-1.68151	-4.031061	2.483909
46	-2.60914	-3.060954	1.329056
47	-2.583056	-0.5314	2.736221
48	-3.288531	-1.011851	2.054376
49	-2.845389	-0.834352	3.760028
50	-2.737534	0.547384	2.658878
51	0.000045	1.24376	3.377276
52	-0.882145	1.825509	3.093445
53	0.000051	1.160359	4.473898
54	0.882254	1.825473	3.093433

55	2.701161	-1.504098	-1.300191
56	-3.004005	2.441069	0.306405
57	0.000005	-1.877855	-1.096662
58	0.000009	-2.685263	-1.961085
59	-5.445022	-2.16154	-1.292815
60	-5.799108	2.545569	0.636136
61	5.79911	2.545559	0.636159
62	5.445033	-2.161533	-1.29283
63	4.983092	3.791477	1.051061
64	4.427187	4.212381	0.205629
65	4.270781	3.561647	1.852121
66	5.662181	4.567244	1.422538
67	6.805452	2.974021	-0.467526
68	7.45398	3.777858	-0.097771
69	7.444283	2.140447	-0.777353
70	6.276015	3.340703	-1.354369
71	6.584754	2.046396	1.879808
72	5.897319	1.748767	2.680352
73	7.216595	1.184747	1.640543
74	7.232917	2.843843	2.263679
75	6.228211	-2.78257	-0.103511
76	6.750464	-3.69073	-0.42847
77	6.975399	-2.089658	0.29822
78	5.546991	-3.054944	0.711573
79	6.441041	-1.810658	-2.432973
80	6.958917	-2.715874	-2.772987
81	5.911915	-1.376843	-3.288927
82	7.199146	-1.091888	-2.103693
83	4.456401	-3.222117	-1.828803
84	3.737476	-3.535169	-1.063678
85	3.891356	-2.854129	-2.691705
86	5.012206	-4.111328	-2.147543
87	-4.456388	-3.222119	-1.828794
88	-3.891367	-2.854133	-2.691713
89	-3.73744	-3.535157	-1.063686
90	-5.012189	-4.11134	-2.147515
91	-6.228182	-2.782577	-0.103484
92	-6.97537	-2.089669	0.298253
93	-6.750434	-3.690741	-0.428433
94	-5.546951	-3.054945	0.711593
95	-6.441045	-1.81068	-2.43295
96	-6.958916	-2.715902	-2.772956
97	-7.199154	-1.091915	-2.103665
98	-5.911932	-1.376862	-3.28891
99	-6.584716	2.046423	1.879817
100	-7.232874	2.843872	2.263691
101	-7.216556	1.184764	1.640584
102	-5.897257	1.748813	2.680347
103	-6.805482	2.974	-0.467531
104	-7.454005	3.777841	-0.097776
105	-6.276071	3.340666	-1.354396
106	-7.444317	2.140416	-0.777323
107	-4.98309	3.791501	1.050991
108	-4.270762	3.561697	1.852043
109	-4.427204	4.212387	0.205537
110	-5.662177	4.567274	1.422462

E(UB3LYP) = –2025.98346109 a.u.

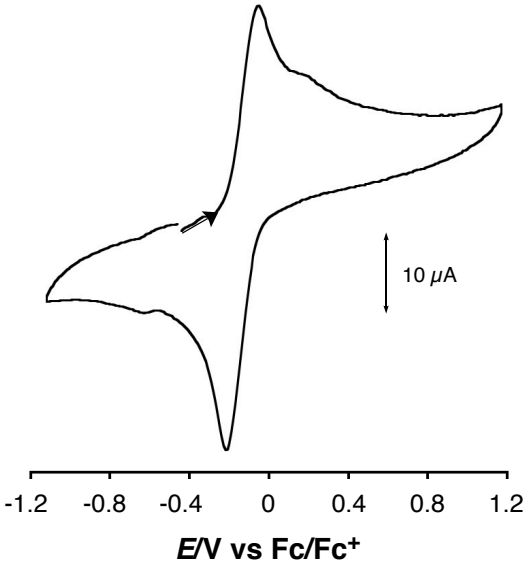

Figure S1. Cyclic voltammogram of **7** at room temperature in CH_2Cl_2 solution (1.0 mM) containing $^nBu_4PF_6$ (0.10 M). Working electrode: glassy carbon. Counter electrode: Pt wire. Scan rate: 100 mVs^{-1}.

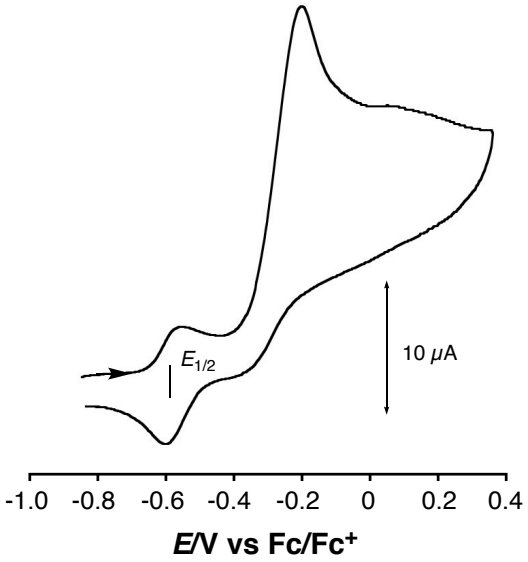

Figure S2. Cyclic voltammogram of **7** (1.0 mM) in the presence of $^nBu_4N(CN)$ (1.0 mM) at room temperature in CH_2Cl_2 solution containing $^nBu_4PF_6$ (0.10 M). Working electrode: glassy carbon. Counter electrode: Pt wire. Scan rate: 100 mVs^{-1}.

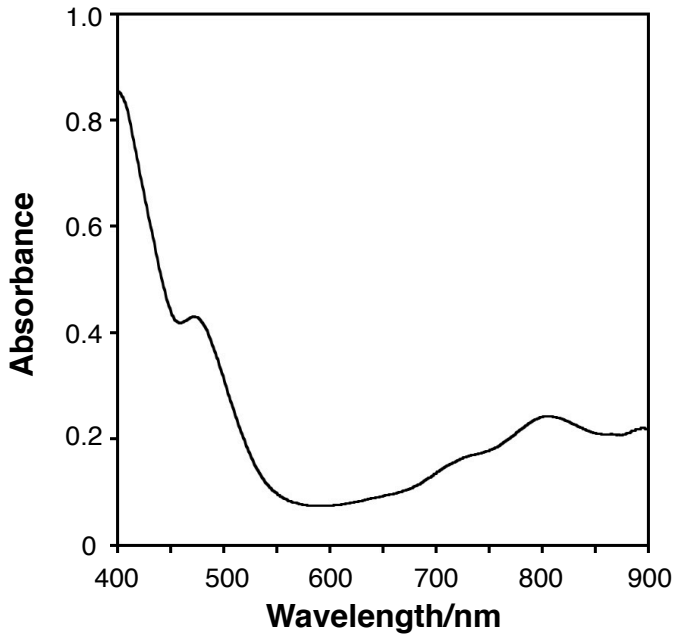

Figure S3. Absorption spectrum of **8** (0.100 mM) in toluene at 25 °C.

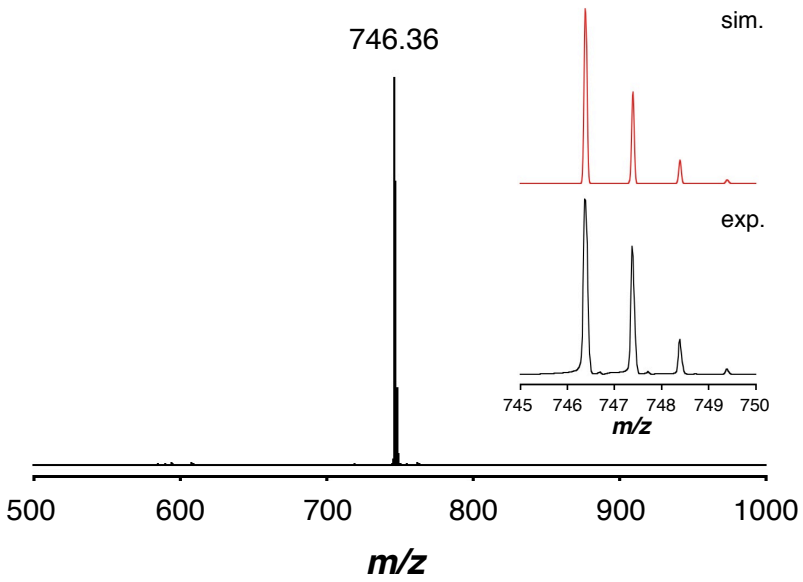

Figure S4. ESI-MS of **8** synthesized from AgCN. Simulated spectrum is calculated as $C_{45}H_{61}N_3Rh$ (inset).

List of Publications

1. Daiki Fujita, Hideki Sugimoto, Yoshihito Shiota, Yuma Morimoto, Kazunari Yoshizawa, and Shinobu Itoh
   Catalytic C–H amination driven by intramolecular ligand-to-nitrene one-electron transfer through a rhodium(III) centre.
   Chem. Commun., **2017**, *53*, 4849–4852.

2. Daiki Fujita, Hideki Sugimoto, Yuma Morimoto, and Shinobu Itoh
   Noninnocent Ligand in Rhodium(III)-Complex-Catalyzed C–H Bond Amination with Tosyl Azide.
   Inorg. Chem., **2018**, *57*, 9738–9747.

3. Daiki Fujita, Akira Kaga, Hideki Sugimoto, Yuma Morimoto, and Shinobu Itoh
   Controlling Coordination Number of Rhodium(III) Complex by Ligand-based Redox for Catalytic C–H Amination.
   Bull. Chem. Soc. Jpn., in press (doi:10.1246/bcsj.20190291).

4. Daiki Fujita, Hideki Sugimoto, and Shinobu Itoh
   C–H Iodination and Pseudo Oxidative Addition of Iodine at the Metal Center in the Rhodium(III) Complex with a Redox-active Ligand.
   Chem. Lett., in preparation.

Acknowledgements

The studies presented in this thesis have been carried out under the guidance of Professor Shinobu Itoh at Osaka University during 2014–2020.

The author would like to express his gratitude to Professor Shinobu Itoh for his kind guidance, invaluable suggestions and encouragement throughout his study.

His gratitude also goes to Associate Professor Hideki Sugimoto and Dr. Yuma Morimoto for their excellent suggestions and continuous encouragement throughout his study.

The author is deeply grateful to Professor Kazunari Yoshizawa and Associate Professor Yoshihito Shiota for their cooperation on DFT calculation in chapter 1.

Similarly, the author deeply appreciates Mr. Akira Kaga for his considerable cooperation on the experiments in chapter 3.

The author thanks all technicians in Analytical Division, Graduate School of Engineering, Osaka University for some kinds of analysis (^{1}H and ^{13}C NMR, Mass Spectroscopy, and Elemental Analysis).

Special thanks to all the members of Bio-Functional Chemistry (BFC) laboratory for their help, valuable suggestions, useful discussions and friendship.

The author acknowledges financial support from Japan Society for the Promotion of Science (JSPS Research Fellowships for Young Scientists).

Finally, the author acknowledges continuous encouragement and support given by his friends and family, Yoichi Fujita, Keiko Fujita, Natsuko Fujita, and Shohei Fujita.

Osaka, Japan
January, 2020

Daiki Fujita

Department of Material and Life Science
Division of Advanced Science and Biotechnology
Graduate School of Engineering
Osaka University